CHARLES UNIVERSITY IN PRAGUE

FACULTY OF SCIENCE

Study programme: Biology

Branch of study: Genetics, Molecular Biology and Virology

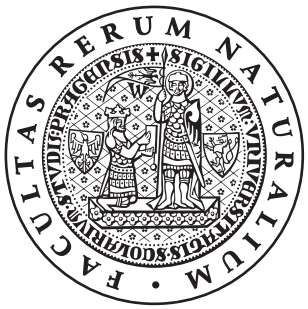

Jan Benada, B.Sc.

Dynamics of Selected DNA Damage Response Proteins

Dynamika vybraných proteinů buněčné odpovědi na poškození DNA

Master's Thesis

Supervisor: Zdeněk Hodný, M.D., Ph.D.

Prague, 2011

Declaration

I herewith declare that I have produced this paper without the prohibited assistance of third parties and without making use of aids other than those specified; notions taken over directly or indirectly from other sources have been identified as such. This paper has not previously been presented in identical or similar form to any other Czech or foreign examination board.

The thesis work was conducted from 2009 to 2011 under the supervision of Zdeněk Hodný, M.D., Ph.D. at the Institute of Molecular Genetics, ASCR, v.v.i.

Prohlášení

Prohlašuji, že jsem závěrečnou práci zpracoval samostatně a že jsem uvedl všechny použité informační zdroje a literaturu. Tato práce ani její podstatná část nebyla předložena k získání jiného nebo stejného akademického titulu.

V Praze, 28. 9. 2011 Podpis

Abstract

DNA damage response (DDR) represents a vital signaling network that protects genome integrity and prevents development of cancer. Therefore the study of DDR is of a crucial clinical importance and DDR proteins are promising therapeutic targets. Although the great advances have been made mapping out interactions between individual DDR proteins, better understanding of complex behavior of this network is still needed. One approach, which might help us in this task, is to describe the dynamics of key proteins under different conditions. The first objective of this study was to investigate whether the temporal dynamics of selected DDR proteins differ upon different genotoxic insults, particularly upon γ-irradiation and UV-C irradiation. We showed that under certain insult some DDR proteins exhibit a monotone continuous activation pulse, while the activation of others triggers a series of pulses. We observed a previously described pulsative dynamics of p53 after γ-irradiation in MCF7 cells. Interestingly, we detected a monotone increase of p53 in U2OS after γ-irradiation and similar dynamics upon UV-C irradiation. We suggest that p53 dynamics depends on the presence or absence of effective negative feedback loops between the upstream p53-activating kinases and Wip1 phosphatase. In the second part of this work, we focused on the dynamics and regulation of Wip1 upon genotoxic stress and during the cell cycle progression. We validated current and developed new tools, including new expression vectors and stable monoclonal cell lines expressing the Wip1 fusion proteins. We showed that Wip1 undergoes phosphorylation after UV-C irradiation. Additionally, we identified a new phosphorylation of Wip1 that occurs exclusively in mitosis, implicating that Wip1 is distinctly regulated during the cell cycle progression. Our findings contribute to the knowledge of DDR behavior and will be followed up in our future studies.

Keywords:

DNA damage response, Wip1, *PPM1D*, p53, p21, p38MAPK, cell cycle, temporal protein dynamics, UV-C irradiation, γ-irradiation

Abstrakt

Buněčná odpověď na poškození DNA (DNA damage response) představuje kriticky důležitou signalizační síť, která ochraňuje celistvost genomu a brání vzniku rakoviny. Studium odpovědi na poškození DNA má tudíž zásadní klinický význam a proteiny účastnící se této signalizace jsou slibnými cíli léčiv. Ačkoliv byly dosaženy značné pokroky v popisu interakcí jednotlivých proteinů této signalizace, stále potřebujeme lépe porozumět komplexnímu chování celé signální sítě. Jedním z přístupů, který nám v tomto může pomoci, je popsání dynamiky klíčových proteinů této signalizace v různých podmínkách. Prvním cílem této práce bylo popsat časovou dynamiku vybraných proteinů odpovědi na poškození DNA po různých genotoxických insultech, konkrétně po γ-ozáření a UV-C ozáření. Ukázali jsme, že zatímco určité proteiny jsou aktivovány v jednom spojitém pulzu, jiné vykazují aktivaci v sérii pulzů. Na buněčné linii MCF7 jsme po γ-ozáření pozorovali již dříve popsané pulzy p53. Nicméně, na buněčné linii U2OS jsme po γ-ozáření detekovali spojitý nárůst hladin p53. Stejnou dynamiku p53 jsme pozorovali i po UV-C ozáření. Navrhujeme, že dynamika p53 závisí na účinném zapojení negativní zpětné vazby mezi kinázami aktivujícími p53 a fosfatázou Wip1. V druhé části této práce jsme se zaměřili na studium dynamiky Wip1 po UV-C ozáření a v průběhu buněčného cyklu. Ověřili jsme stávající a vytvořili nové nástroje pro studium Wip1; tyto zahrnují nové expresní vektory a stabilní monoklonální buněčné linie, exprimující fúzní protein Wip1. Ukázali jsme, že Wip1 je fosforylována po UV-C ozáření. Dále jsme identifikovali novou fosforylaci Wip1, která se vyskytuje pouze v mitóze. Toto naznačuje, že Wip1 je během mitózy odlišně regulována. Naše zjištění přispívají ke znalostem o chování buněčné odpovědi na poškození DNA a budou dále rozvíjena v budoucích studiích.

Klíčová slova:

Odpověď na poškození DNA, Wip1, *PPM1D*, p53, p21, p38MAPK, buněčný cyklus, časová dynamika proteinů, UV-C záření, γ záření

Acknowledgements

I would like to express my gratitude to all those who gave me the possibility to complete this thesis. I would like to thank my supervisor, Zdeněk Hodný, M.D. Ph.D., for the opportunity to work at Department of Genome Integrity, Institute of Molecular Genetics, ASCR and for the help I have received in making of this thesis. I would like to thank to Libor Macůrek, M.D., Ph.D. for allowing me to collaborate with him on Wip1 phosphatase, introducing me to many laboratory techniques and for valuable consultations. I am indebted to Markéta Vančurová, M.Sc. for language correction of this thesis and for introducing me to the world of cell culture. My thank goes to Katka Krejčíková, M.Sc. for the inestimable help with quantitative PCR analyses. I would also like to thank to Hanka Hanzlíková, Ph.D. for sharing her experience with immunoprecipitations and for her healthy critical point of view. All my lab colleagues thank you for providing me help whenever I needed and for being such a great bunch of people to be around. Last but not least, I would like to thank Prof. Jiří Bartek, M.D., D.Sc. for support.

I would like to acknowledge the Laboratory of Ladislav Anděra, Ph.D. at IMG, ASCR for providing us with Z-VAD-FMK and Anti-PARP antibody, Zdeněk Cimbůrek, from IMG Flow Cytometry and Light Microscopy Facility, for cell sorting and Roman Liška, from X-ray Radiation Facility, IMG/Department of Radiometry, Institute of Physiology, ASCR, for operating the orthovoltage X-ray instrument T-200.

I would also like to extend my deepest gratitude to my family for their continuous support during my studies and this thesis in particular.

My work was partially supported by P301/10/1525 (J. Bartek) and P305/10/P420 (L. Macůrek) grants of the Grant Agency of the Czech Republic.

Abbreviations

β-TrCP1	β-transducin repeat containing; F-box and WD repeats protein β-TrCP
βTrCP-SCF	β-transducin repeat-containing protein-Skp1-Cullin-F-box
14-3-3	14-3-3 protein family; a large family of signal-transducing adaptor proteins present in wide variety of eukaryotes, phosphoserine and phosphothreonine binding proteins involved in important cellular processes including signal transduction, cell-cycle control, apoptosis, and cellular stress responses;
14-3-3γ	14-3-3γ protein; protein of the 14-3-3 family; Adapter protein implicated in the regulation of a large spectrum of both general and specialized signaling pathways
53BP1	tumor suppressor p53-binding protein 1; enhances p53-mediated activation, plays a role in the response to DNA damage
9-1-1	Rad9-Rad1-Hus1 complex; cell-cycle checkpoint response complex, plays a major role in DNA repair
ddH_2O	double distilled water
ERBB2	a proto-oncogene that codes for the erbB-2 receptor
ERBB2	avian erythroblastic leukemia viral oncogene homolog 2; encodes a member of the epidermal growth factor (EGF) receptor family of receptor tyrosine kinases
MYC	family of retrovirus-associated DNA sequences (myc) originally isolated from an avian myelocytomatosis virus
PPM1D	a gene coding for protein of the PP2C family of Ser/Thr protein phosphatases; Wip1
RAS	rat sarcoma, oncogene, encodes a single-subunit small GTPase
A	adenine; a purine base; 9H-purin-6-amine
aa	amino acid
APAF-1	apoptotic protease-activating factor 1; oligomeric Apaf-1 mediates the cytochrome c-dependent autocatalytic activation of pro-caspase-9 (Apaf-3), leading to the activation of caspase-3 and apoptosis
APS	ammonium persulfate; $(NH_4)_2S_2O_8$
ASCR	the Academy of Sciences of the Czech Republic

ATM	ataxia telangiectasia mutated; serine-protein kinase; serine/threonine protein kinase which activates checkpoint signaling upon double strand breaks
ATM-Chk2-p53	ataxia telangiectasia mutated-checkpoint kinase 2-p53
ATM-pS1981	ATM phoshpo-serine-1981
ATM-S1987A	mouse homologue of human ATM with mutated serine 1987 residue to alanine
ATP	adenosine triphosphate; an adenine nucleotide containing three phosphate groups esterified to the sugar moiety
ATR	ataxia telangiectasia and Rad3-related protein; serine/threonine-protein kinase; serine/threonine protein kinase which activates checkpoint signaling upon genotoxic stresses such as ionizing radiation, ultraviolet light, or DNA replication stalling, thereby acting as a DNA damage sensor
ATR-Chk1-p53	ataxia telangiectasia and Rad3 related-checkpoint kinase 1-p53
ATRIP	ATR interacting protein; required for checkpoint signaling after DNA damage; required for ATR expression, possibly by stabilizing the protein
BAX	apoptosis regulator; accelerates programmed cell death by binding to, and antagonizing the apoptosis repressor BCL2 or its adenovirus homolog E1B 19k protein
Bcl-2	apoptosis regulator; suppresses apoptosis in a variety of cell systems including factor-dependent lymphohematopoietic and neural cells
BER	base excision repair
BRCA1	breast cancer type 1 susceptibility protein; E3 ubiquitin-protein ligase that specifically mediates the formation of 'lysine-6'-linked polyubiquitin chains and plays a central role in DNA repair by facilitating cellular responses to DNA damage
C	cytosine; a pyrimidine base; 4-aminopyrimidin-2(1H)-one
C-teminal	end of the protein (peptide) terminated by a free carboxyl group
CDC25A	M-phase inducer phosphatase 1; functions as a dosage-dependent inducer of mitotic progression; directly dephosphorylates CDK1 and stimulates its kinase activity; dephosphorylates CDK2 in complex with cyclin E, in vitro.
CDC25B	M-phase inducer phosphatase 2; tyrosine protein phosphatase, functions as a dosage-dependent inducer of mitotic progression, directly dephosphorylates CDK1 and stimulates its kinase activity
CDC25C	M-phase inducer phosphatase 3; functions as a dosage-dependent inducer in mitotic control; a tyrosine protein phosphatase; required for progression of the cell cycle; directly dephosphorylates CDK1 and activate its kinase activity
CDK(s)	mammalian cyclin-dependent kinases; cyclin-dependent kinases (CDKs) are activated by the binding to a cyclin and mediate the progression through the cell cycle; each different complex controls a specific transition between two subsequent phases in the cell cycle

cdk5	cyclin-dependent kinase 5; interacts with D1 and D3-type G1 cyclins; can phosphorylate histone H1, tau, MAP2 and NF-H and NF-M; interacts with p35
Chk1	serine/threonine-protein kinase; required for checkpoint mediated cell cycle arrest in response to DNA damage or the presence of unreplicated DNA; may negatively regulate cell cycle progression during unperturbed cell cycles
Chk1-pS317	Chk1 phospho-serine-317
Chk2	serine/threonine-protein kinase; regulates cell cycle checkpoints and apoptosis in response to DNA damage, particularly to DNA double-strand breaks
Chk2-pT68	Chk2 phospho-threonine-68
CtIP	CtBP-interacting protein, DNA endonuclease, synonym RBBP8; endonuclease that cooperates with the MRN complex in processing meiotic and mitotic double-strand breaks by ensuring both resection and intrachromosomal association of the broken ends
D	Asp; aspartic acid
DAXX	death domain-associated protein 6; acts as an adapter protein in a MDM2-DAXX-USP7 complex by regulating the RING-finger E3 ligase MDM2 ubiquitination activity
DBSs	DNA double strand breaks
DDR	DNA Damage Response Pathways
DH5a	
DMEM	Dulbecco's Modified Eagle's Medium
DMSO	dimethyl sulfoxide, $(CH_3)_2SO$
DNA	deoxiribonucleic acid
DNA-PK	DNA-dependent protein kinase; serine/threonine-protein kinase; acts as a molecular sensor for DNA damage; involved in DNA nonhomologous end joining (NHEJ); required for double-strand break (DSB) repair and V(D)J recombination
dNTPs	deoxyribonucleotide triphosphates
dpi	dot per inch; a measure of spatial printing; indirectly correlate with image resolution
DSB(s)	DNA double-strand break(s)
E1	ubiquitin-activating enzyme; activates ubiquitin by first adenylating its C-terminal glycine residue with ATP
E1A	early E1A 32 kDa protein; has both transforming and trans-activating activities; plays a role in viral genome replication by driving entry of quiescent cells into the cell cycle
E2	ubiquitin-conjugating enzyme; accepts ubiquitin from the E1 complex and catalyzes its covalent attachment to other proteins

E3	ubiquitin-protein ligase; accepts ubiquitin from the E1 complex and catalyzes its covalent attachment to other proteins
E4F1	transcription factor; E3 ubiquitin-protein ligase; may function as a transcriptional repressor
EDTA	ethylene-diamine-tetraacetic acid; 2,2',2",2"'-(Ethane-1,2-diyldinitrilo)tetraacetic acid; a chelating agent
EGFP	enhanced GFP
EGTA	ethylene glycol tetraacetic acid; ethylene glycol-bis(2-aminoethylether)-N,N,N',N'-tetraacetic acid; a chelating agent with higher affinity for calcium ions than for magnesium ions
ELM	eukaryotic linear motif; a computational biology resource for investigating candidate functional sites in eukarytic proteins
ERK	extracellular-signal-regulated kinase 1; involved in both the initiation and regulation of meiosis, mitosis, and postmitotic functions in differentiated cells by phosphorylating a number of transcription factors such as ELK-1
EYA1	eyes absent homolog 1 (Drosophila); in human, a tyrosine phosphatase that specifically dephosphorylates 'tyrosine-142' of histone H2AX
EYA3	eyes absent homolog 3 (Drosophila); in human, a tyrosine phosphatase that specifically dephosphorylates 'tyrosine-142' of histone H2AX
FACS	fluorescence-activated cell sorting
FAS	tumor necrosis factor receptor superfamily member 6; receptor for TNFSF6/FASLG; adapter molecule FADD recruits caspase-8 to the activated receptor, resulting death-inducing signaling complex (DISC) performs caspase-8 proteolytic activation which initiates the subsequent cascade of caspases (aspartate-specific cysteine proteases) mediating apoptosis
FAT	RAP-ATM-TRRAP (FAT) domain; nteracts with ATM's kinase domain to stabilize the C-terminus region of ATM itself
FBS	fetal bovine serum
FHA	forkhead-associated; mediates phospho-peptide interactions with proteins phosphorylated by serine/threonine kinases
FLAG	DYKDDDDK peptide; extensively used as a general epitope tag
FRAXA	folate-sensitive fragile site originally discovered in patients with X-linked mental retardation; Fragile X syndrome
G	guanine; a purine base; 2-amino-1H-purin-6(9H)-one
G1	cell cycle growth phase 1
G2	cell cycle growth phase 2
G418	geneticin sulphate; an aminoglycoside related to Gentamicin and is used as a selective agent in molecular genetics experiments; is toxic to both prokaryotic and eukaryotic cells
Gadd45	growth arrest and DNA damage-inducible protein GADD45 alpha; DNA damage-inducible transcript 1 protein; binds to proliferating cell nuclear antigen

GAPDH	glyceraldehyde-3-phosphate dehydrogenase; has glyceraldehyde-3-phosphate dehydrogenase and nitrosylase activities; plays a role in glycolysis and nuclear functions
GFP	green fluorescent protein
H2A	a type of histone; a part of nucleosome core particle
H2AX	histone that replaces conventional H2A in a subset of nucleosomes
H4	a type of histone; a part of nucleosome core particle
HAUSP	ubiquitin carboxyl-terminal hydrolase; hydrolase that deubiquitinates target proteins such as FOXO4, p53/TP53, MDM2, PTEN and DAXX
HEPES	4-(2-hydroxyethyl)-1-piperazineethanesulfonic acid; a zwitterionic organic chemical buffering agent; one of the twelve Good's buffers
HRP	Horseradish Peroxidase; enzyme used in immunoblotting and immunocytochemistry applications; used as the reporter enzyme for SuperSignal-Chemiluminescent substrates
HTC116	human colorectal carcinoma cell line
HUS1	checkpoint protein; component of the 9-1-1 cell-cycle checkpoint response complex, plays a major role in DNA repair
IGFBP3	insulin-like growth factor-binding protein-3; IGF-binding proteins prolong the half-life of the IGFs and have been shown to either inhibit or stimulate the growth promoting effects of the IGFs on cell culture
IgG	immunoglobulin G
IMG	Institute of Molecular Genetics of the ASCR, v.v.i.
IP	immunoprecipitation
JNK	c-Jun Nterminal kinases; responds to activation by environmental stress and pro-inflammatory cytokines by phosphorylating a number of transcription factors, primarily components of AP-1 such as JUN, JDP2 and ATF2 and thus regulates AP-1 transcriptional activity
K	Lys; an amino acid lysine
L	Leu; an amino acid leucine
LAP	LAP tag; facilitate cell biological analysis and proteomics in higher eukaryotes; combines the advantages of generating a fluorescent protein fusion (GFP or mRFP) with flexibility of the tandem affinity purification
LB	Lysogeny broth; Luria broth; a nutritionally rich medium, used for the growth of bacteria
M	mitosis
MAP	mitogenactivated protein kinases
MAPKAP-K2	MAP kinase-activated protein kinase 2; MK2; its physiological substrate seems to be the small heat shock protein (HSP27/HSP25); *in vitro* can phosphorylate glycogen synthase at 'serine-7' and tyrosine hydroxylase (on 'serine-19' and 'serine-40'); phosphorylates Ser in the peptide sequence, Hyd-X-R-X(2)-S, where Hyd is a large hydrophobic residue

MAPKAP-K2-pS334	MAPKAP-K2 phospho-serine-334
MCF7	human breast adenocarcinoma cell line
MDC1	mediator of DNA damage checkpoint protein 1; required for checkpoint mediated cell cycle arrest in response to DNA damage within both the S phase and G2/M phases of the cell cycle
Mdm2	E3 ubiquitin-protein ligase; mediates ubiquitination of p53/TP53, leading to its degradation by the proteasome; inhibits p53/TP53- and p73/TP73-mediated cell cycle arrest and apoptosis by binding its transcriptional activation domain. Also acts as an ubiquitin ligase E3 toward itself and ARRB1; permits the nuclear export of p53/TP53; promotes proteasome-dependent ubiquitin-independent degradation of retinoblastoma RB1 protein; inhibits DAXX-mediated apoptosis by inducing its ubiquitination and degradation; component of the TRIM28/KAP1-MDM2-p53/TP53 complex involved in stabilizing p53/TP53; component of the TRIM28/KAP1-ERBB4-MDM2 complex which links growth factor and DNA damage response pathways
Mdm2-YFP	Mdm2 fused to yellow fluorescent protein (YFP)
MdmX	murine double minute, an important negative regulator of the p53 tumor suppressor, homolog Mdm2
MEFs	murine embryonic fibroblasts
MIU	motif interacting with ubiquitin; mediate the interaction with ubiquitin and the localization at sites of DNA damage
MIUs	motifs interacting with ubiquitin
MK2	MAP kinase-activated protein kinase 2, MAPKAP-K2
MKK3	dual specificity mitogen-activated protein kinase kinase 3; activated by cytokines and environmental stress in vivo; catalyzes the concomitant phosphorylation of a threonine and a tyrosine residue in the MAP kinase p38
MKK4	dual specificity mitogen-activated protein kinase kinase 4; activates the JUN kinases MAPK8 (JNK1), MAPK9 (JNK2), MAPK14 (p38MAPK) but not MAPK1 (ERK2) or MAPK3 (ERK1)
MKK6	dual specificity mitogen-activated protein kinase kinase 6; catalyzes the concomitant phosphorylation of a threonine and a tyrosine residue in MAP kinase p38 exclusively
MMSET	probable histone-lysine N-methyltransferase NSD2; probable histone methyltransferase; may act as a transcription regulator that binds DNA and suppresses IL5 transcription
MRE11	meiotic recombination 11; double-strand break repair protein; component of the MRN complex, which plays a central role in double-strand break (DSB) repair, DNA recombination, maintenance of telomere integrity and meiosis
MRN	heterotrimeric protein complex consisting of Mre11, Rad50 and Nbs1
mRNA	messenger ribonucleic acid

Myt1	myelin transcription factor 1; binds to the promoter regions of proteolipid proteins of the central nervous system
N-terminal	end of the protein (peptide) terminated by a free amino group
NBS1	nibrin; cell cycle regulatory protein p95; Nijmegen breakage syndrome protein 1; component of the MRE11/RAD50/NBN (MRN complex); plays a critical role in the cellular response to DNA damage and the maintenance of chromosome integrity; complex is involved in double-strand break (DSB) repair, DNA recombination, maintenance of telomere integrity, cell cycle checkpoint control and meiosis
Nek11	serine/threonine-protein kinase Nek11; never in mitosis A-related kinase 11; possible role in S-phase checkpoint mechanism
NEM	N-ethylmaleimide; 1-ethylpyrrole-2,5-dione; a small compound that forms stable, covalent thioether bonds with sulfhydryls, enabling them to be permanently blocked to prevent disulfide bond formation
NF-κB	nuclear factor of κ light polypeptide gene enhancer in B-cells 1; a pleiotropic transcription factor which is present in almost all cell types
NIH-3T3	mouse embryonic fibroblasts cell line
NLS	nuclear localization signal; an amino acid sequence tagging a protein for import into the cell nucleus
NOXA	phorbol-12-myristate-13-acetate-induced protein 1; promotes activation of caspases and apoptosis; promotes mitochondrial membrane changes and efflux of apoptogenic proteins from the mitochondria; contributes to p53/TP53-dependent apoptosis after radiation exposure; promotes proteasomal degradation of MCL1; competes with BAK1 for binding to MCL1 and can displace BAK1 from its binding site on MCL1 By similarity; competes with BIM/BCL2L11 for binding to MCL1 and can displace BIM/BCL2L11 from its binding site on MCL1
p16^{INK4A}	cyclin-dependent kinase inhibitor 2A; a negative regulator of the proliferation of normal cells by interacting strongly with CDK4 and CDK6
p19^{ARF}	cyclin-dependent kinase inhibitor 2A isoform 3; capable of inducing cell cycle arrest in G1 and G2 phases
p21	cyclin-dependent kinase inhibitor 1; CDK-interacting protein 1; may be the important intermediate by which p53/TP53 mediates its role as an inhibitor of cellular proliferation in response to DNA damage; binds to and inhibits cyclin-dependent kinase activity, preventing phosphorylation of critical cyclin-dependent kinase substrates and blocking cell cycle progression
p300	histone acetyltransferase p300; regulates transcription via chromatin remodeling; acetylates all four core histones in nucleosomes
p38MAPK	mitogen-activated protein kinase 14; mitogen-activated protein kinase p38 alpha; responds to activation by environmental stress, pro-inflammatory cytokines and lipopolysaccharide (LPS) by phosphorylating a number of transcription factors (ELK1, ATF2) and several downstream kinases (MAPKAPK2 and MAPKAPK5)

p38MAPK-MAPKAP-K2 p38 mitogen-activated protein kinasemitogen- activated protein kinase-activated protein kinase-2

p38MAPK-pT180p/pY182 p38MAPK phospho-treonine-180 and phospho-tyrosine-182

p53 cellular tumor antigen; acts as a tumor suppressor in many tumor types; induces growth arrest or apoptosis depending on the physiological circumstances and cell type; involved in cell cycle regulation as a trans-activator that acts to negatively regulate cell division by controlling a set of genes required for this process

p53-CFP p53 fused to cyan fluorescent protein (CFP)

p53pS15 p53 phospho-serine-15

p65 human transcription factor 65; nuclear factor NF-κB p65 subunit; a pleiotropic transcription factor, present in almost all cell types,involved in many biological processed such as inflammation, immunity, differentiation, cell growth, tumorigenesis and apoptosis

PARN poly(A)-specific ribonuclease; 3'-exoribonuclease that has a preference for poly(A) tails of mRNAs, thereby efficiently degrading poly(A) tails

PARP poly ADP ribose polymerase

PBS phosphate buffered saline; commonly used biological buffer

PCAF histone acetyltransferase KAT2B; functions as a histone acetyltransferase (HAT) to promote transcriptional activation

PCNA proliferating cell nuclear antigen; an auxiliary protein of DNA polymerase delta, involved in the control of eukaryotic DNA replication

PCR Polymerase Chain Reaction

PIKK phosphoinositide three-kinase-related kinase; a family of kinases includes ATM (ataxia-telangiectasia mutated), ATR (ATM- and Rad3-related), DNA-PKcs (DNA-dependent protein kinase catalytic subunit), mTOR (mammalian target of rapamycin), and SMG1 (suppressor with morphological effect on genitalia family member)

Plk-1 polo-like kinase 1; serine/threonine-protein kinase Plk-1; performs several important functions throughout M phase of the cell cycle, including the regulation of centrosome maturation and spindle assembly, the removal of cohesins from chromosome arms, the inactivation of APC/C inhibitors, and the regulation of mitotic exit and cytokinesis

PP1 serine/threonine protein phosphatase 1

PP2 serine/threonine protein phosphatase 2

PP2A serine/threonine-protein phosphatase 2A

PP2C serine/threonine-protein phosphatase 2C

PP5 serine/threonine-protein phosphatase 5; may play a role in the regulation of RNA biogenesis and/or mitosis; *in vitro* dephosphorylates serine residues of skeletal muscle phosphorylase and histone H1

pSQ/pTQ ATM/R phosphorylable serine or threonine residues with glutamine (Q) at the +1 position; the so-called SQ/TQ motif

PTEN	phosphatidylinositol-3,4,5-trisphosphate 3-phosphatase and dual-specificity protein phosphatase; tumor suppressor, acts as a dual-specificity protein phosphatase, dephosphorylating tyrosine-, serine- and threonine-phosphorylated proteins
pTXpY	phosphorylation motif, e.g. in active loop of p38MAPK
PUMA	JFY-1; Bcl-2-binding component 3; essential mediator of p53-dependent and p53-independent apoptosis
qPCT	Real-Time quantitative Polymerase Chain Reaction
qRT-PCR	Real Time quantitative Reverse Transcription Polynucleoide Chain Reaction
RAD1	cell cycle checkpoint protein; component of the 9-1-1 cell-cycle checkpoint response complex, plays a major role in DNA repair
Rad17-RFC	Rad17-replication factor C; component of the 9-1-1 cell-cycle checkpoint response complex that plays a major role in DNA repair
RAD50	DNA repair protein; component of the MRN complex, which plays a central role in double-strand break (DSB) repair, DNA recombination, maintenance of telomere integrity and meiosis
Rad50	DNA repair protein; component of the MRN complex, which plays a central role in double-strand break (DSB) repair, DNA recombination, maintenance of telomere integrity and meiosis
RAD9	cell cycle checkpoint control protein RAD9A; component of the 9-1-1 cell-cycle checkpoint response complex that plays a major role in DNA repair
RAP80	receptor-associated protein 80; an acidic nuclear protein of 719 amino acids that contains two Cys-X2-Cys-X11-His-X3-Cys zinc finger-like motifs and two ubiquitin interacting motifs (UIMs) at its amino terminus.
RHINO	Rad9, Rad1, Hus1 interacting nuclear orphan
RING	Really Interesting New Gene; protein structural domain of zinc finger type
RNF168	E3 ubiquitin-protein ligase; RING finger protein 168; E3 ubiquitin-protein ligase required for accumulation of repair proteins to sites of DNA damage
RNF8	E3 ubiquitin-protein ligase; required for assembly of repair proteins to sites of DNA damage; catalyzes the 'lysine-63'-linked ubiquitination of histone H2A and H2AX; following DNA double-strand breaks (DSBs), it is recruited to the sites of damage by ATM-phosphorylated MDC1, mediates the ubiquitination of histones H2A and H2AX, thereby promoting the formation of TP53BP1 and BRCA1 ionizing radiation-induced foci (IRIF); promotes the formation of 'lysine-63'-linked polyubiquitin chains and functions with the specific ubiquitin-conjugating UBE2N/UBC13
RO3066	CDK1 inhibitor
ROS	reactive oxygen species; chemically-reactive molecules containing oxygen
RPA	replication protein A; required for DNA recombination, repair and replication; its activity is mediated by single-stranded DNA binding and protein interactions; required for the efficient recruitment of the DNA double-strand break repair factor RAD51 to chromatin in response to DNA damage

RT-PCR	Reverse Transcription Polymerase Chain Reaction
S	cell cycle synthetic phase
S-protein	a product of the limited digestion of ribonuclease A by subtilisin (residues 21-124); used in affinity chromatography and sodium dodecyl sulfate-polyacrylamide gel electrophoresis
SCF	ubiquitin ligase; SCF(β-TrCP) ubiquitin ligase, SKP1 Cullin Ubiquitin Ligase, Cullin-F-box protein
SDS	sodium dodecyl sulfate; sodium lauryl sulfate; $NaC_{12}H_{25}SO_4$; an anionic surfactant-detergent
SDS-PAGE	Sodium Dodecyl Sulfate Polyacrylamide Gel Electrophoresis
siRNA	small interfering RNA; double-stranded RNA, about 21 nucleotides long, with 3' overhangs (2 nucleotides) at each end; is used to interfere with the translation of proteins by binding to and promoting the degradation of messenger RNA at specific sequences
ssDNA	single stranded DNA
ssDNA-RPA	single-stranded DNA-binding protein replication protein A; essential for both DNA replication and recombination
SYBRGreen	SYBRGreen 1; N',N'-dimethyl-N-[4-[(E)-(3-methyl-1,3-benzothiazol-2-ylidene) methyl]-1-phenylquinolin-1-ium-2-yl]-N-propylpropane-1,3-diamine; a cyanine dye used as a nucleic acid stain in molecular biology
T	Thr; an amino acid threonine
T	thymine,a pyrimidine base; 5-Methylpyrimidine-2,4(1H,3H)-dione
TAO	thousand and one amino acid kinases; kinases family that mediate activation of p38MAPK in response to DNA damage
TAP	tandem affinity purification, a general procedure of protein complex purification
TEMED	tetramethylethylenediamine; N,N,N',N'-tetramethylethane-1,2-diamine; an essential catalyst for polyacrylamide gel polymerization
TEV-protease	tobacco etch virus protease; used to cleave affinity tags from recombinant proteins
TIAR	nucleolysin; TIA-1-related protein; RNA-binding protein; possesses nucleolytic activity against cytotoxic lymphocyte target cells; may be involved in apoptosis
TIFF	Tagged Image File Format; a lossless raster file format for digital images; standard graphics format for high color depth and b/w graphics
Tip60	histone acetyltransferase KAT5; catalytic subunit of the NuA4 histone acetyltransferase complex which is involved in transcriptional activation of select genes principally by acetylation of nucleosomal histones H4 and H2A
TopBP1	DNA topoisomerase 2-binding protein 1; required for DNA replication; plays a role in the rescue of stalled replication forks and checkpoint control; binds double-stranded DNA breaks and nicks as well as single-stranded DNA

Tris	tris(hydroxymethyl)aminomethane; 2-Amino-2-hydroxymethyl-propane-1,3-diol; a component of buffer solutions
Triton-X-100	polyethylene glycol p-(1,1,3,3-tetramethylbutyl)-phenyl ether; a nonionic surfactant-detergent
Tween20	polyoxyethylene (20) sorbitan monolaurate; a common detergent used in biology, in cell lysis and membrane protein solubilisation
U2OS	human osteosarcoma cell line
U2OS-D7	monoclonal cell line derived from U2OS
U2OS-GFP-Wip1	monoclonal cell line derived from U2OS
UBC1	ubiquitin-conjugating enzyme; catalyzes the covalent attachment of ubiquitin to other proteins
UBC13	ubiquitin-conjugating enzyme E2 13; accepts the ubiquitin from the E1 complex and catalyzes its covalent attachment to other proteins; involved in the formation of multiubiquitin chains; signals the protein for selective degradation
UNG2	uracil-DNA glycosylase 2; removes uracil near replication forks and in non-replicating DNA
UV-A	ultraviolet, electromagnetic radiation subtype A, 315 - 400 nm
UV-B	ultraviolet, electromagnetic radiation subtype B, 280 - 315 nm
UV-C	ultraviolet, electromagnetic radiation subtype C, 100 - 280 nm
V(D)J	Variable, Diverse, and Joining gene segments of vertebrates; a type of somatic recombination
WB	western blot; used for identification proteins with specific antibodies that were separated by gel electrophoresis
Wee1	Wee1-like protein kinase; acts as a negative regulator of entry into mitosis (G2 to M transition) by protecting the nucleus from cytoplasmically activated cyclin B1-complexed CDK1 before the onset of mitosis by mediating phosphorylation of CDK1 on 'tyrosine-15'
Wip1	wild-type p53-induced phosphatase 1; required for the relief of p53-dependent checkpoint mediated cell cycle arrest
WSTF	Williams–Beuren syndrome transcription factor
Y	Tyr; an amino acid tyrosine
Z-VAD-FMK	carbobenzoxy-valyl-alanyl-aspartyl-[O-methyl]- fluoromethylketone; caspase Inhibitor

Definitions of terms were taken from following databases: UniProt (2011); NCBI (2011); thesignalinggateway (2011) and Reference.MD (2011)

Contents

List of Figures

List of Tables

1

Introduction

DNA damage response (DDR) represents a vitally important signaling network that protects genome integrity. On one hand, deficiency in the DDR leads to an increased genomic instability and possibly to cancer development. On the other hand, DNA damage targeted in genetically unstable cancerous cells represents underlying mechanism of most cancer treatments, such as radiotherapy and chemotherapy. Yet due to limited selectivity of these therapies, the DNA damage occurring in healthy cells is also a culprit of most undesired side effects of cancer treatment. Therefore, the study of cellular response to DNA damage is of potential clinical importance. With increased understanding of molecular mechanisms of DNA damage response, we might hope for developing the targeted drugs that would effectively eradicate tumor cells, while sparing healthy ones. From academic point of view, the DNA damage response represents an intriguing model of cellular signaling network. The interconnected network of DNA damage response is able to react to quantitatively and qualitatively diverse stimuli, integrate them with actual state of the cell and choose the most convenient output from plethora of variants. The unraveling of control mechanisms in DNA damage response network would greatly improve our understanding of cell decision making in general.

Great advances have been made by mapping interactions between the individual proteins and describing the architecture of DNA damage response network. Nevertheless, we are still facing the challenge to understand how network structure determines the functional behavior of DNA damage response and what the

decisive network nodules in response to particular stresses are. One approach which might help to understand this complex regulation is to describe the dynamics of key proteins after different genotoxic insults.

Galit Lahav's group demonstrated that γ-irradiation triggers a series of discrete undamped p53 pulses. These pulses exhibit fixed amplitude, which do not increase with irradiation dose. On the other hand, the number of pulses positively correlated with the irradiation dose. This implies that p53 response to γ-irradiation behaves in a "digital" rather than "analog" way. It was suggested that this remarkable dynamics of p53 may have a decisive role for cell fate, e.g. whether the cell will trigger apoptotic response or whether will stay arrested at the cell cycle checkpoint. The negative feedback loop between p53 and Mdm2 (murine double minute 2) ubiquitin ligase has been suggested as a main controller responsible for the generation of p53 pulses. Later, the negative feedback between the ATM (ataxia telangiectasia mutated) kinase and p53-inducible phosphatase Wip1 (wild-type p53-induced phosphatase 1) has been shown to be essential for maintenance of the pulses uniformity.

To explore the possibility that such dynamics is elicited not exclusively after γ-irradiation-induced double-strand breaks, we decided to investigate the temporal dynamics of DNA damage response to different insults, particularly to the UV-C irradiation. This type of genotoxic insult for was chosen for two reasons. Firstly, the UV light induces exposure of single-stranded DNA, which leads to activation of the ATR-Chk1-p53 pathway (ataxia telangiectasia and Rad3 related-checkpoint kinase 1- p53 pathway) as opposed to double-strand breaks that trigger mainly the ATM-Chk2-p53 pathway (ataxia telangiectasia mutated-checkpoint kinase 2-p53 pathway). Thus we were interested whether this different circuitry will provide the same p53 dynamics or not. Secondly, using UV-C irradiation we were able to deliver the damaging insult at one particular moment, contrary to the continuous damage caused by prolonged treatment by chemical drugs. This was important since we investigated the dynamics at cell population level and we thus needed to strike all cells simultaneously. Although we had in mind the limitations of studying the protein dynamics at population level, western blotting was method of choice since it enabled us to investigate several proteins in one experiment and, even

more importantly, it also allowed us to look for posttranslation modifications.

In the next part of our work we focused on Wip1 phosphatase. Wip1 phosphatase is induced in p53-dependent manner and in turn negatively regulates DNA damage response at most of its levels, most prominently counteracting the activation of p53. We examined Wip1 dynamics and regulation upon DNA damage and also through cell cycle progression. We were particularly interested in its regulation by posttranslational modifications, since this issue represents currently unmapped ground. The understanding of Wip1 regulation will provide additional insight to field of DNA damage response. With respect to the fact that Wip1 can act as an oncoprotein, this has also important clinical significance. For the purpose of studying the Wip1 regulation, we validated current and developed new tools, including stable monoclonal cell lines expressing Wip1 fusion proteins.

2

Aims of the thesis

1. To validate current and to develop novel tools for study of Wip1 dynamics and regulation. This includes the preparation of stable monoclonal U2OS cell lines expressing fluorescent tagged Wip1 and cloning of new expression vectors.

2. To describe dynamics of selected key DNA damage response proteins upon γ-irradiation and UV-C irradiation.

3. To investigate dynamics and regulation of Wip1 during the cell cycle progression.

3

Literature review

3.1 DNA damage response

Cells constantly face numerous endogenous and exogenous genotoxic insults. The insults affecting the DNA's sugar-phosphate backbone represent the most serious form of DNA damage since they directly affect the chromosomal stability and thus disrupt the genomic integrity. As maintenance of genomic integrity is crucial for survival at both cellular and organism level, eukaryota have evolved specialized mechanisms to cope with genotoxic stress. This sophisticated network of sensing and executive molecules is termed DNA damage response.

The initiation of DNA damage response depends on members of phosphoinositide 3-kinase-like kinase (PIKK) family, which includes ATR (ataxia telangiectasia and Rad3 related), ATM (ataxia telangiectasia mutated) and DNA-PK kinases (DNA-dependent protein kinase, (Yang *et al.*, 2003). In general, DNA damage response can be divided into two main branches. DNA double strand breaks trigger mainly ATM-Chk2-p53 (ataxia telangiectasia mutated-checkpoint kinase 2-p53) pathway, while single-stranded lesions activate ATR-Chk1-p53 (ataxia telangiectasia and Rad3 related-checkpoint kinase 1-p53) pathway. Yet this view is very simplified and there are possible crosstalks between these pathways. Both pathway, although consisting of different proteins, share a similar structure of signal transmission (Figure 3.1). Firstly, a site of damage is detected by DNA damage sensors, which in turn recruit upstream kinases ATM and ATR. Recruitment and

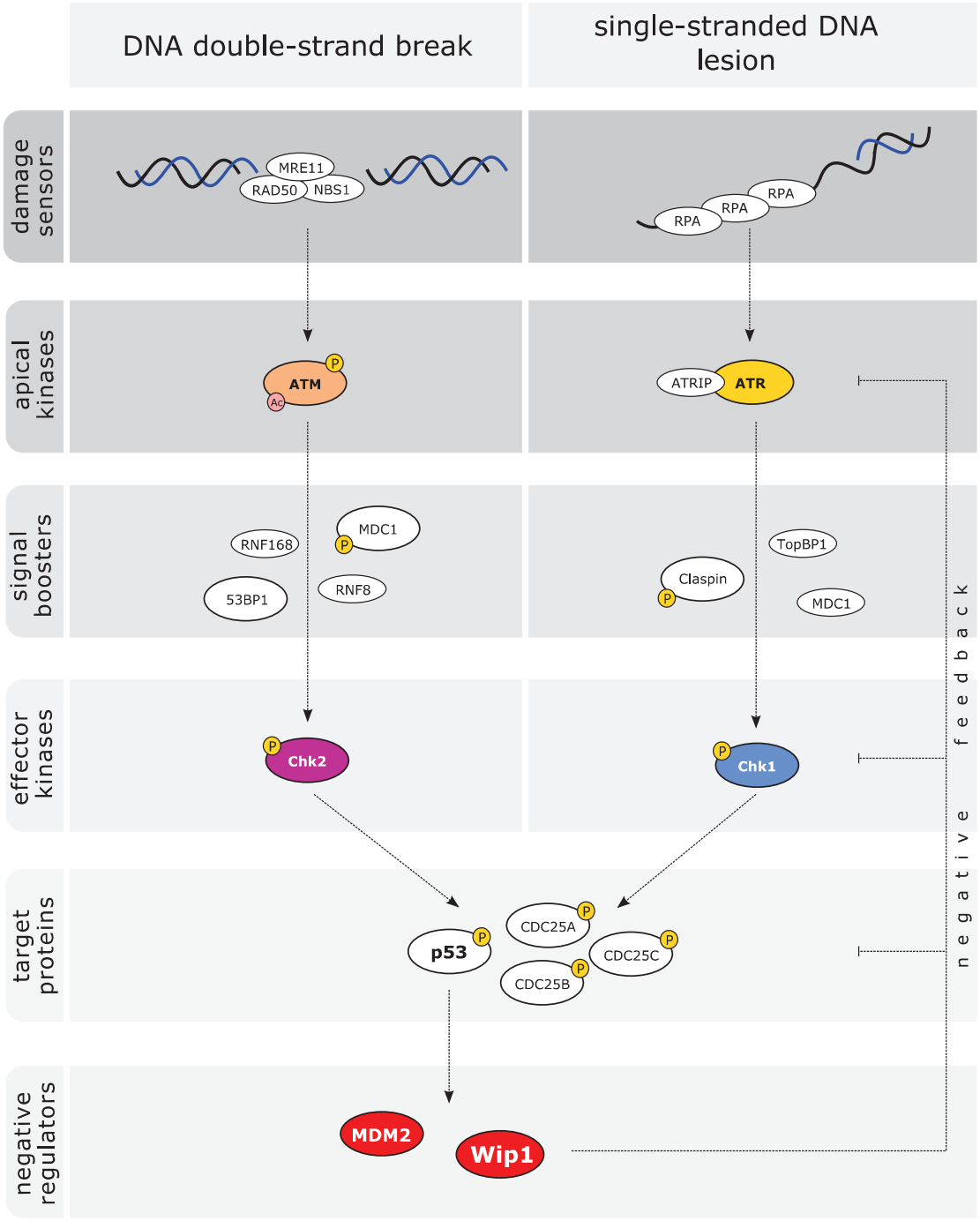

Figure 3.1: The structure of signal transmission in DNA damage response cascades - note that only selected representatives are depicted on most levels of cascade, concept is discussed in the text above, in greater detail then described in following chapters; (loosely based on diagrams from (Bartek and Lukas, 2003; Campisi and d'Adda di Fagagna, 2007; d'Adda di Fagagna, 2008)

activation of upstream kinases is potentiated by several mediator proteins, which often act in positive feedback loops (Chapters 3.1.1.2 and 3.1.2.2). Activated upstream kinases then pass on the signal to diffusible effector kinases Chk2 and Chk1, which subsequently spread the signal to their numerous targets (Bartek and Lukas, 2007) (Chapter 3.1.3). DNA-PK kinase is triggered also by DNA double strand breaks and except its role in initiation of DNA damage response, it is particularly important for DNA repair through non-homologous end-joining (Burma *et al.*, 2006).

Except canonical DNA damage response mentioned above, DNA damage can induce also more general stress response pathway of MAP kinases (mitogen-activated protein kinases), including ERK (extracellular-signal-regulated kinase), JNK (c-Jun N-terminal kinase) and p38MAPK-MAPKAP-K2 (p38 mitogen-activated protein kinase mitogen- activated protein kinase-activated protein kinase-2) pathway. The p38MAPK-MAPKAP- K2 pathway was recently reported to be involved in checkpoint control (Reinhardt *et al.*, 2010). The exact mechanism which couples activation of this pathway and DNA damage still remains unclear. Possibly, different genotoxic insults differ in the way how they activate p38MAPK-MAPKAP-K2 pathway (Reinhardt and Yaffe, 2009) (Chapter 3.2).

In most cases, DNA damage response (DDR) and stress response pathways lead to activation of cell cycle checkpoints. For the rapid arrest of cell cycle, it is crucial to inactivate CDC25 phosphatases. CDC25 phosphatases are able to remove inhibitory phosphorylations on CDK-cyclin complexes. Therefore, without active CDC25 phosphatases, CDKs cannot be fully activated and cell cycle progression is stopped (Bartek and Lukas, 2007); (Chapter 3.1.3). Both DDR pathways and p38MAPK-MAPKAP-K2 pathways converge to deactivate CDC25 phosphatases (Reinhardt and Yaffe, 2009) (Chapter 3.1.3 and 3.2). In addition, these pathways activate p53 tumor suppressor. One of the p53 transcriptional targets, $p21^{WAF1/Cip1}$ (hereafter referred to as p21), further sustains the cell cycle arrest by inhibition of CDKs-cyclins complexes (Meek, 2009); (Chapter 3.1.3).

The cell cycle checkpoints prevent proliferation of cells with damaged DNA. These cells are prone to genomic instability and thus at increased risk of malignant transformation. During this proliferative arrest, the cells are given time to

repair the damaged DNA. DNA repair is tightly coupled with DDR signaling and recruitment of many repair factors directly depends on activation of DDR cascades. If DNA lesions are repaired, cells are then able to recover from checkpoint and re-entry the cell cycle (Bartek and Lukas, 2007).

How cells attenuate checkpoint signaling is not completely clear. Multiple lines of evidence suggest an important role for Wip1 phosphatase (wild-type p53-induced phosphatase 1) in checkpoint recovery (Chapter 3.5.2). Wip1 phosphatase is induced in p53 dependent manner and dephosphorylates many of the components of activated DDR and inhibits through the negative feedback DDR signaling on most of its levels (Medema and Macurek, 2011) (Chapters 3.5.2). Interestingly, it is the regulation through negative feedbacks that most probably give rise to sustained pulsative dynamics in activation of particular DNA damage response proteins (p53 most prominently) upon γ-irradiation (Batchelor *et al.*, 2009) (Chapters 3.6).

However, in case of unrepairable damage, the DNA damage response can trigger apoptotic pathway. Alternatively, persistent activation of DNA damage response can result in permanent cell cycle arrest termed cellular senescence. Both of these DDR outcomes represent important tumorsuppressive barriers (Bartek and Lukas, 2007).

3.1.1 DNA double strand breaks activate ATM-Chk2-p53 pathway

3.1.1.1 The DNA double strand breaks and their causes

DNA double strand breaks (DSBs) represent the most dangerous DNA lesions since they directly disrupt the structural stability of chromosomes. Broken chromosomes are prone to chromosomal rearrangements, which may eventually lead to malignant transformation and cancer development. DBSs can be caused by oxidative stress, ionizing radiation, such as γ-irradiation, radiomimetic drugs, such as etoposide (Hande, 1998) or doxorubicin (Schwartz, 1975) and even by bacterial toxins, such as cytolethal distending toxins (Blazkova *et al.*, 2010).

It is estimated that during mitochondrial oxidative phosphorylation around

one percent of inhaled oxygen is converted into reactive oxygen species (ROS) of total amount more than 3×10^6 ROS per person every hour (Lieber and Karanjawala, 2004). Hence, oxidative stress represents the most common insult to cellular molecules. Oxidation of DNA sugar-phosphate backbone directly gives rise to DNA breaks, mainly to single-strand nicks, yet in lesser extent also to DSBs. Single strand nicks, if unrepaired, can be transformed to DSBs during DNA replication (Lieber and Karanjawala, 2004). In addition, certain chemicals, such a hydrogen peroxide (Konat, 2003) or bacterial antibiotics bleomycin (Ackland *et al.*, 1988) and its analogue phleomycin D1 (Robles *et al.*, 1999) can further contribute to ROS production and oxidative damage.

Ionizing radiation is capable of ionizing the molecules of matter through which it propagates and this can result in a breakage of chemical bonds. Thus, ionizing radiation can cause DSBs when passing through chromatin. The standard unit used to measure absorbed dose of ionizing radiation is the gray (Gy), defined absorption of one joule of ionizing radiation by one kilogram of matter. The exposure to ionizing radiation from both natural and manmade sources is commonly very low. Nevertheless, in case of exceptionally exposed groups such as underground miners of uraniferous coal deposits or atomic bomb survivors the ionizing radiation stochastic effects were connected to cancer development (reviewed by Little (2003). On the other hand, the capacity of ionizing radiation to induce DSBs is employed in radiotherapeutic cancer treatments, since induction of DSBs can lead to apoptosis or stress-induced senescence of cancer cells (Suzuki and Boothman, 2008).

Radiomimetic drugs etoposide and doxorubicin (also called adriamycin) cause DSBs through inhibition of topoisomerase II (Hande, 1998). Topoisomerase II is able to transiently cut both strands of DNA and allows the DNA strands to pass through each other and unwind or unknot tangled DNA. Finally, it again religates both strands. Inhibiton of the religation step by etoposide and doxorubicin and similar drugs leads to induction of DSBs (reviewed by Chikamori *et al.* (2010).

Furthermore, DSBs naturally occur during strictly orchestrated physiological processes such as V(D)J recombination, class switch recombination (reviewed by Tsai and Lieber (2010) and meiotic recombination (Longhese *et al.*, 2009).

3.1.1.2 Initiation of ATM-Chk2-p53 pathway

Cellular response to DSBs is mainly controlled by ATM kinase (Figure 3.2). Firstly, DBS is recognized by MRN complex, composed of MRE11 (meiotic recombination 11), Rad50 and NBS1 (Nijmegen breakage syndrome) subunits (Grenon *et al.*, 2001; Nelms *et al.*, 1998). NBS1 can subsequently recruit ATM kinase to the site of the break (Lee and Paull, 2004). In unstressed cells, ATM is present in form of homodimers with the kinase domain tightly bound to FAT domain, which prevents its activity (Bakkenist and Kastan, 2003). According to observations of Bakkenist and Kastan (2003) that extensive amount of ATM can be rapidly activated even by few DSBs, it seems that its activation is not dependent on its binding to foci of damage. It has been suggested that the initiating activatory stimulus may be induced by chromatin alterations spreading in long range from DSBs, yet the exact mechanism remains to be clarified (Bakkenist and Kastan, 2003). The ATM homodimers undergo autophoshorylation on serine 1981 (S1981) within the FAT domain. This leads to the dissociation of ATM into active monomers (Bakkenist and Kastan, 2003). Even though this phosphorylation is thought to be directly linked to ATM activation, it has been shown that, at least in mice, it is not essential for activation of ATM-dependent response. Pellegrini *et al.* (2006) demonstrated that the non-phoshorylatable S1981A ATM mutant was still able to dissociate into active monomers.

Protein phosphatase 5 (PP5) has indispensable role for ATM activation, since its deficiency leads to the abrogation of ATM-mediated cell cycle arrest (Ali *et al.*, 2004; Yong *et al.*, 2007). However, its direct action on ATM remains unknown. Speculatively, PP5 may eliminate putative inhibitory phosphates from ATM and therefore promotes its activation (Ali *et al.*, 2004). Cyclin dependent kinase 5 (cdk5) phosphorylates ATM on serine 794. It has been suggested that this phosphorylation precedes, and is required for, ATM autophosphorylation at S1981 (Tian *et al.*, 2009).

Parallel to S1981 phosphorylation, ATM is acetylated on lysine 3016 by Tip60 acetyltransferase (Sun *et al.*, 2007, 2005). Tip60 is targeted to the site of damage by MRN complex. At the site of break, Tip60 interacts with trimethylated histone

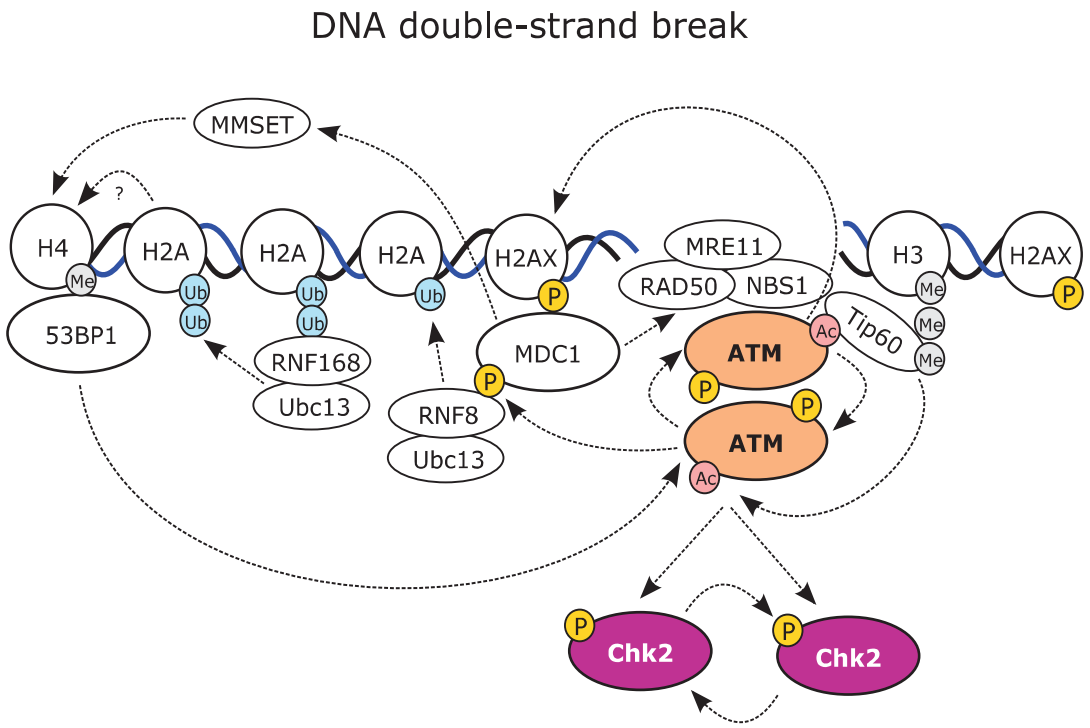

Figure 3.2: DNA double strand breaks initiate the ATM-Chk2-p53 pathway - The molecular mechanisms are described in text above. Figure is based on articles cited in the text above.

H3, which greatly increases its catalytic activity (Sun *et al.*, 2009). Importantly, the expression of a dominant negative mutant of Tip60 (Ikura *et al.*, 2000), as well as depletion of Tip60 by siRNA (Jiang *et al.*, 2006), resulted in the inhibition of ATM dependent signaling. Lavin and Kozlov (2007) proposed that acetylation of lysine 3016 functionally precedes and is required for ATM S1981 autophosphorylation and activation.

Activated ATM phosphorylates histone variant H2AX on serine 139 (Burma *et al.*, 2001). In absence of DNA damage, H2AX is phosphorylated on tyrosine 142 by WSTF (Williams–Beuren syndrome transcription factor; (Xiao *et al.*, 2009)). This phosphorylation must be removed by Eya1/3 phosphatases prior to ATM dependent serine 139 phosphorylation can occur (Cook *et al.*, 2009). H2AX phosphorylated on serine 139, also termed, γH2AX, is commonly used as DNA damage marker (Mah *et al.*, 2010). γH2AX attracts adaptor protein MDC1 (mediator of DNA damage checkpoint protein 1; (Stommel and Wahl, 2004), which in turn binds NBS1 (Melander *et al.*, 2008). This results in further accumulation of MRN

complexes at the site of DNA damage. Subsequently, more MRN complexes recruit more ATM, which phosphorylate more H2AX. Hence a positive feedback loop is set up to amplify the signal.

Phosphorylated MDC1 is also recognized by E3 ubiquitin ligase RNF8 (RING finger protein 8). In cooperation with E2 conjugating enzyme UBC13 (Ubiquitin-conjugating enzyme E2 13), RNF8 ubiquitinates histone variants H2A and H2AX (Mailand *et al.*, 2007). Notably, UBC13 catalyzes the ubiquitination of lysines 63. Lysine 63-linked ubiquitination does not trigger proteasomal degradation as opposed to canonical lysine 48-linked polyubiquitination (Thrower *et al.*, 2000), but rather serves as platforms for proteins containing so called motifs interacting with ubiquitin (MIUs). Otherwise from differential lysine linkage, the lysine 63-linked ubiquitination share the same canonical sequence of events leading to ubiquitination of targeted protein. Firstly, ubiquitin activating enzyme E1 activates the ubiquitin in ATPdependent manner. This involves the transient formation of ubiquitin-adenylate intermediate. Subsequently, ubiquitin is transferred onto cysteine residue in active site of E1, with simultaneous release of adenosine monophosphate. In the second step, the activated ubiquitin is transferred from E1 to cysteine of active site of ubiquitinconjugating enzyme E2 through the transesterification reaction. Finally, the E3 ubiquitin-protein ligase catalyzes the formation of isopeptide bond between ubiquitin and targeted protein or another ubiquitin (Hershko *et al.*, 1983). Notably, the E3 ubiquitin-protein ligase determines the specifity of ubiquitination to the targeted protein. Lysine 63-linked monoubiquitination of histone serves as a docking site for another E3 ubiquitin ligase RNF168 (RING finger protein 168). RNF168, again in cooperation with UBC13, further increases Lys63-linked ubiquitination of chromatin in the vicinity of DSBs (Doil *et al.*, 2009). This modification of chromatin is essential for recruitment of DNA damage mediator protein 53BP1 (p53-binding protein 1) and DNA repair factor BRCA1 (breast cancer type 1 susceptibility protein; (Doil *et al.*, 2009).

Even though BRCA1 itself does not contain any MIUs, it is able to associate with ubiquitinated chromatin through interaction with its adaptor proteins Abraxas and RAP80, as RAP80 provides MIUs for the whole complex (Wang *et al.*, 2007). The mechanism of BRCA1 accumulation demonstrates the tight connection of DDR

with DNA repair. As DNA repair lies beyond the scope of this diploma thesis we refer to the review of Kass and Jasin (2010) for further details.

Although 53PB1 recruitment to DNA damage foci is also dependent on RNF8 and RNF168 (Doil *et al.*, 2009), 53BP1 itself does not interact with ubiquitinated Lys63 or any adaptor mediating this interaction. Based on observations that 53PB1 binds to methylated lysine 20 residue on histone H4 (Botuyan *et al.*, 2006; Sanders *et al.*, 2004), it has been proposed that ubiquitination of nearby chromatin might be needed to expose this methylated motif on histones (Bekker-Jensen and Mailand, 2011). Recently, it was described that histone methyltransferase MMSET, which is responsible for H4 methylation, is recruited to DNA damage foci through binding to MDC1 (Pei *et al.*, 2011). 53BP1 also amplifies ATM activation by facilitating the direct interaction between MRN and ATM (Lee *et al.*, 2010).

Finally, fully active ATM phosphorylates Chk2 kinase on threonine 86 (T86, (Ahn *et al.*, 2000). This phosphorylation triggers sequence of Chk2 autophosphorylation events on threonine 383 and threonine 387, within the Chk2 activation loop and additionally on serine 516. All these modifications result in activation of Chk2. The autophosphorylation of Chk2 can also happen, both in cis and in trans, proposing that oligomerization of Chk2 may promote its activation (Schwarz *et al.*, 2003). Activated Chk2 then passes the signal downstream to its targets. Importantly, ATM can also directly phosphorylate p53 on serine 15 (S15), which contributes to its stabilization and activation after DNA damage (Canman *et al.*, 1998; Khanna *et al.*, 1998). ATM and Chk2 are not essential for cell viability, however their deficiency results in severe hereditary disorders. The deficiency in ATM causes neurodegenerative disease, known as ataxia telangiectasia. Ataxia telangiectasia patients suffer from difficulty with control of movement, immunodeficiency and are hypersensitive to DNA damaging agents (reviewed in Ball and Xiao (2005). The deficiency in Chk2 partially mimics the loss of p53 function and is responsible for development of Li-Fraumeni-like syndrome. Similarly to Li-Fraumeni syndrome, this deficiency is also demonstrated by increased risk of development of wide range of malignancies at early age (Bell *et al.*, 1999).

3.1.2 Single-stranded DNA lesions trigger ATR-Chk1-p53 pathway

3.1.2.1 Occurrence and causes of single-stranded DNA lesions

The most harmful environmental agent that causes single-stranded DNA (ssDNA) lesions is ultraviolet (UV) radiation. The UV-light induces cross-linking between consecutive pyrimidine bases, which leads to exposure of single-stranded DNA. This can happen in two ways. Firstly, UV-induced lessions cause distortions in the DNA helix, which interfere with progession of transcription (Donahue *et al.*, 1994) and replication machinery (Batista *et al.*, 2006), revealing the ssDNA. Secondly, the ssDNA is also exposed during the repair of UV-induced lessions through the nucleotide excision repair (O'Driscoll *et al.*, 2003).

The UV light spectrum emitted by the Sun can be divided based on its wavelength into three main categories: UV-C (100-280 nm), UV-B (280-315nm) and UV-A (315-400nm) according to ISO 21348 Definitions of Solar Irradiance Spectral Categories; 2007. Even though the ozone layer absorbs the most hazardous UV-C, the residual UV-A and UV-B can induce in direct sunlight over 100 000 DNA lesions per exposed cell per hour (Jackson and Bartek, 2009).

The DNA single-strand regions are also naturally exposed during DNA replication. Progression of the replication fork itself represents a hazardous event to DNA integrity. Moreover, several pathological conditions may interfere with replication progression. These conditions that lead to halt or collapse of DNA replication forks are broadly referred to as replicative stress. Replicative stress can be caused by depletion of deoxynucleotide pool, e.g. by inhibition of ribonucleotide reductase by hydroxyurea (Krakoff *et al.*, 1968) or by folate deficiency (Duthie and Hawdon, 1998). DNA binding agents, such as actinomycin D (Hou *et al.*, 2002) or distamycin A (Luck *et al.*, 1977), block proper progression of replication fork. In addition, activation of oncogenes has been described to results in increased replicative stress (Bartkova *et al.*, 2005; Gorgoulis *et al.*, 2005).

Interestingly, distribution of lesions caused by replicative stress is not random. Spots in genome, preferentially prone to replicative stress are termed chromosomal fragile sites (Durkin *et al.*, 2008; Magenis *et al.*, 1970); for extensive review

see Durkin and Glover (2007). Based on their incidence proportion, chromosomal fragile sites can be divided into two groups. Common fragile sites can be found in every individual, whereas rare fragile sites occur with incidence less than 5% and are frequently associated with certain human disorders. Comprehensive summary of known fragile sites in human genome can be found in Lukusa and Fryns (2008). Probably the best characterized example is represented by the FRAXA site which is causally linked to the development of Fragile X syndrome, one of the most frequent hereditary causes of mental retardation in men (Verkerk *et al.*, 1991).

The mechanism of chromosomal fragile sites susceptibility to replicative stress is not known. Nevertheless, chromosomal fragile sites contain in common repetitive sequences (Kremer *et al.*, 1991; Yu *et al.*, 1997), which have been described to form secondary structures. These secondary structures possibly further hinder replication fork progression and thus potentiate effects of replication stress (Gacy *et al.*, 1995; Zlotorynski *et al.*, 2003).

3.1.2.2 Initiation of the ATR-Chk1-p53 pathway

The ATR-Chk1-p53 pathway is primary activated by single-stranded DNA lesions (Figure 3.3). Single-stranded DNA (ssDNA) is immediately and constantly coated by replication protein A (RPA) to prevent forming of secondary structures and to protect DNA integrity (Wold, 1997). RPA directly binds ATRIP, the ATR interacting partner (Zou and Elledge, 2003). As ATR and ATRIP are constitutively bound in complex (Cortez *et al.*, 2001), this results in ATR localization to ssDNA lesions. Although ATRIP-RPA interaction is believed to be the crucial step in ATR activation, splice variant of ATRIP, which is not able to bind RPA, had been reported to still support ATR activation (Ball *et al.*, 2005).

To fully activate the ATR-Chk1-p53 pathway, ATR requires interaction with its activator TopBP1 (topoisomerase II-binding protein 1, (Kumagai *et al.*, 2006) and adaptor protein Claspin (Kumagai and Dunphy, 2003). TopBP1 is recruited to the site of lesion by PCNA-related 9-1-1 complex, consisting of RAD9, RAD1 and HUS1 (Delacroix *et al.*, 2007; Lee *et al.*, 2007). 9-1-1 complex is loaded onto ssDNA-RPA by a clamp loader RAD17-RFC (Rad17-replication factor C, (Zou *et al.*, 2002). Recently, a novel protein, called RHINO (Rad9, Rad1, Hus1 interacting nuclear

orphan), was identified as an ATR activator. RHINO independently binds both 9-1-1 complex and TopBP1, possibly acting as a scaffold that facilitates TopBP1 recruitment (Cotta-Ramusino *et al.*, 2011). TopBP1 directly associates with ATR in ATRIP-dependent manner and greatly potentiates its kinase activity (Kumagai *et al.*, 2006). Contrary to ATM, ATR does not undergo autophosphorylation upon its activation.

Moreover, MDC1 was recently described to interact with γH2AX on chromatin flanking the ssDNA region. MDC1 can bind TopBP1 and further enhance its accumulation at site of the lesion (Wang *et al.*, 2011). As H2AX can be phosphorylated by ATR (Ward and Chen, 2001), MDC1 thus sets up a positive feedback loop to amplify the activation of ATR. This situation is similar to the role of MDC1 at doublestrand breaks foci.

The recruitment of RNF8 and UBC13 was observed also in case of UV-irradiation induced lesions; however it seems that this event acts downstream of nucleotide excision repair. On the contrary in response to DSBs, the RNF8 and UBC13 are recruited before initiation of DNA repair (Huen *et al.*, 2007; Mailand *et al.*, 2007).

In addition to 9-1-1 complex, RAD17 also recruits Claspin to the proximity of ATR (Wang *et al.*, 2006). Subsequently, Claspin undergoes ATR-dependent phosphorylation within its Chk1 interacting domain. Modified in this way, Claspin can in turn mediate interaction between ATR and Chk1 (Jeong *et al.*, 2003; Kumagai and Dunphy, 2003), enabling ATR to phosphorylate pSQ/pTQ motifs in Chk1 C-terminal regulatory domain. Among phosphorylated pSQ/pTQ motifs, the phosphorylation of serine 345 is thought to be indispensable for activation of Chk1 (Liu *et al.*, 2000). In addition to ATR phosphorylation, Chk1 undergoes autophosphorylation, which further enhances its activity. Finally, the fully activated Chk1 dissociates from chromatin (Liu *et al.*, 2000). Similarly to ATM, ATR can directly phosphorylate p53 on S15 (Lakin *et al.*, 1999).

Notably, ATR was described to phosphorylate ATM on S1981, suggesting that ATR-Chk1-p53 pathway can be activated also upon UV-C irradiation or replicative stress (Stiff *et al.*, 2006). Similarly, the ATR-Chk1-p53 pathway can be activated, to lesser extent, by DSBs. Mre11 of MRN complex in cooperation with CtIP endonuclease is able to generate stretches of ssDNA at the site of DSB. These single

stranded regions can in turn lead to activation of the ATR-Chk1-p53 pathway. The activation of ATR-Chk1- p53 pathway by DSBs seems to be restricted to S and G2 cell cycle phases and to be depended on CDK kinase activity (Jazayeri *et al.*, 2006; Sartori *et al.*, 2007).

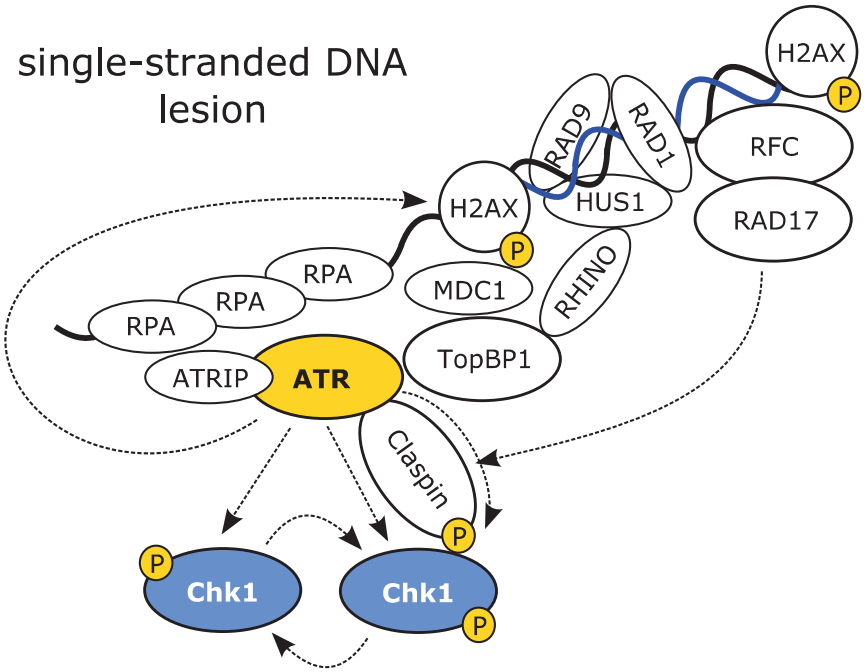

Figure 3.3: Single-stranded DNA lesions initiate the ATR-Chk1-p53 pathway - The molecular mechanisms are described in text above. Figure is based on articles cited in the text above.

3.1.3 DNA damage response activates the cell cycle checkpoints

Cellular proliferation is organized into series of phases, namely - G1 (growth phase 1), S (synthetic phase, during which DNA replication occurs), G2 (growth phase 2) and M-phase (consisting of mitosis, during which nuclear division happens and cytokinesis, during which cell division happens), collectively termed the cell cycle (Figure 3.4). Progression through the cell cycle is controlled by complexes of CDK kinases and their cofactors, cyclins. While levels of CDKs remain constant, levels of cyclins oscillate during the cell cycle. This restricts the function of the CDK-cyclin complexes only to particular cell cycle phase. In addition, activity of CDKs is regulated by phosphorylation on threonine 14 and tyrosine 15. The

Wee1 and Myt1 kinases are able to phosphorylate these sites and thus inhibit the CDKs, whereas the CDC25 phosphatases remove the inhibitory phoshorylations and therefore contribute to CDK activation (Perry and Kornbluth, 2007).

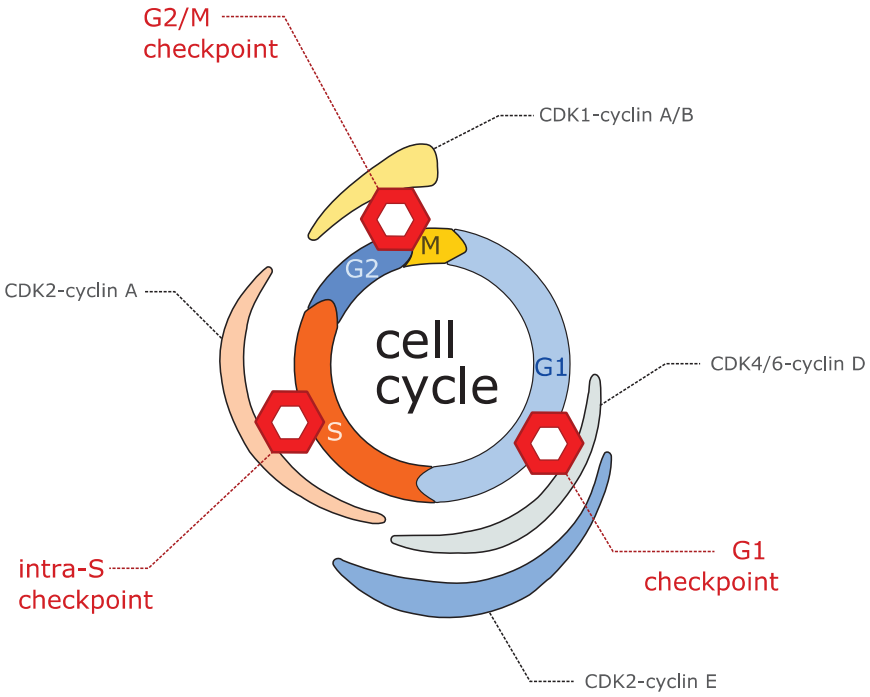

Figure 3.4: Cell cycle progression is controlled by CDK-cyclin complexes - activity of major CDK-cyclins is denoted; DNA damage triggers cell cycle checkpoints in G1, S and on G2/M transition. Adapted with modifications from Lodish *et al.* (1995)

The DNA damage can lead to genomic instability and consequently to mitotic catastrophe or to malignant transformation of the cell. Therefore it is mostly desired to stop the proliferation of cells with damaged DNA and, if possible, to repair the damage before the cells can continue their progress through the cell cycle. The DNA damage signaling converges to stop the cell cycle progression through the series of actions, called the cell cycle checkpoints. Cell cycle checkpoints can be divided into G1, intra-S, and G2/M checkpoints, according to the phase which they affect (Figure 3.4). Generally, the DDR firstly targets CDC25 phosphatases and Wee1 kinase (Figure 3.5). The activation or deactivation of these regulatory molecules is executed very quickly through the posttranslation modifications, thus the cell cycle arrest can be established very promptly. Secondly, DDR triggers the transcription of p21, which acts as an inhibitor of CDKs (Figure 3.5). This hap-

pens lately in p53-dependent manner. The role of p53 is particularly important for the maintenance of checkpoints. Aside from induction of p21, p53 contributes to the G2/M checkpoint maintenance also through transcriptional repression of genes, that are indispensable for checkpoint recovery - cyclin B and Plk-1, Polo-like kinase 1 (Ikura *et al.*, 2000; McKenzie *et al.*, 2010). Regulation of p53 will be discussed in separate Chapter 3.3.

As described above, DNA damage leads to activation of checkpoint kinases Chk1 and Chk2. Active Chk1 autophosphorylates itself on serine 296. Upon this phosphorylation it can be recognized by 14-3-3γ, which mediates its interaction with CDC25A (Kasahara *et al.*, 2010). Consequently, Chk1 phosphorylates CDC25A on serine 76. Moreover, Chk1 phosphorylates and thus activates Nek11 (Never in mitosis gene A-related kinase 11). Nek11 further contribute to CDC25A phosphorylation (Melixetian *et al.*, 2009). Phosphorylated CDC25A is then recognized by βTrCP-SCF (β-transducin repeat-containing protein-Skp1-Cullin-F-box) ubiquitin ligase complex and targeted to proteasomal degradation (Busino *et al.*, 2003; Jin *et al.*, 2003). CDC25B and CDC25C are phosphorylated in Chk1-dependent manner on serine 323 (Forrest and Gabrielli, 2001) and serine 216, respectively (Peng *et al.*, 1997; Sanchez *et al.*, 1997). Both phosphatases are in turn recognized by 14-3-3 proteins. Binding of 14-3-3 to the CDC25B blocks it catalytic site and thus inhibits its activity (Forrest and Gabrielli, 2001). CDC25C interaction with 14-3-3 results in its sequestration into cytoplasm, which prevents its actions toward nuclear CDKs (Graves *et al.*, 2001). Additionally, Chk1 also phosphorylates Wee1 kinase, which potentiates its negative regulatory activity toward CDKs (O'Connell *et al.*, 1997).

Chk2 is able to phosphorylate CDC25A/B/C in the same manner as Chk1, suggesting that their roles in checkpoint activation are mostly overlapping (Bartek and Lukas, 2003). Nevertheless, they are not mutually interchangeable. Chk1 is indispensable for the regulation of CDC25A basal turnover during non-stressed S phase progression. Balanced CDC25A activity is needed to restrain the proliferative activity of CDK2- cyclin E within physiological range (Sørensen *et al.*, 2003). The overexpression of CDC25A leads to unscheduled DNA replication, premature mitotic entry and consequent cell death (Molinari *et al.*, 2000). The physiological

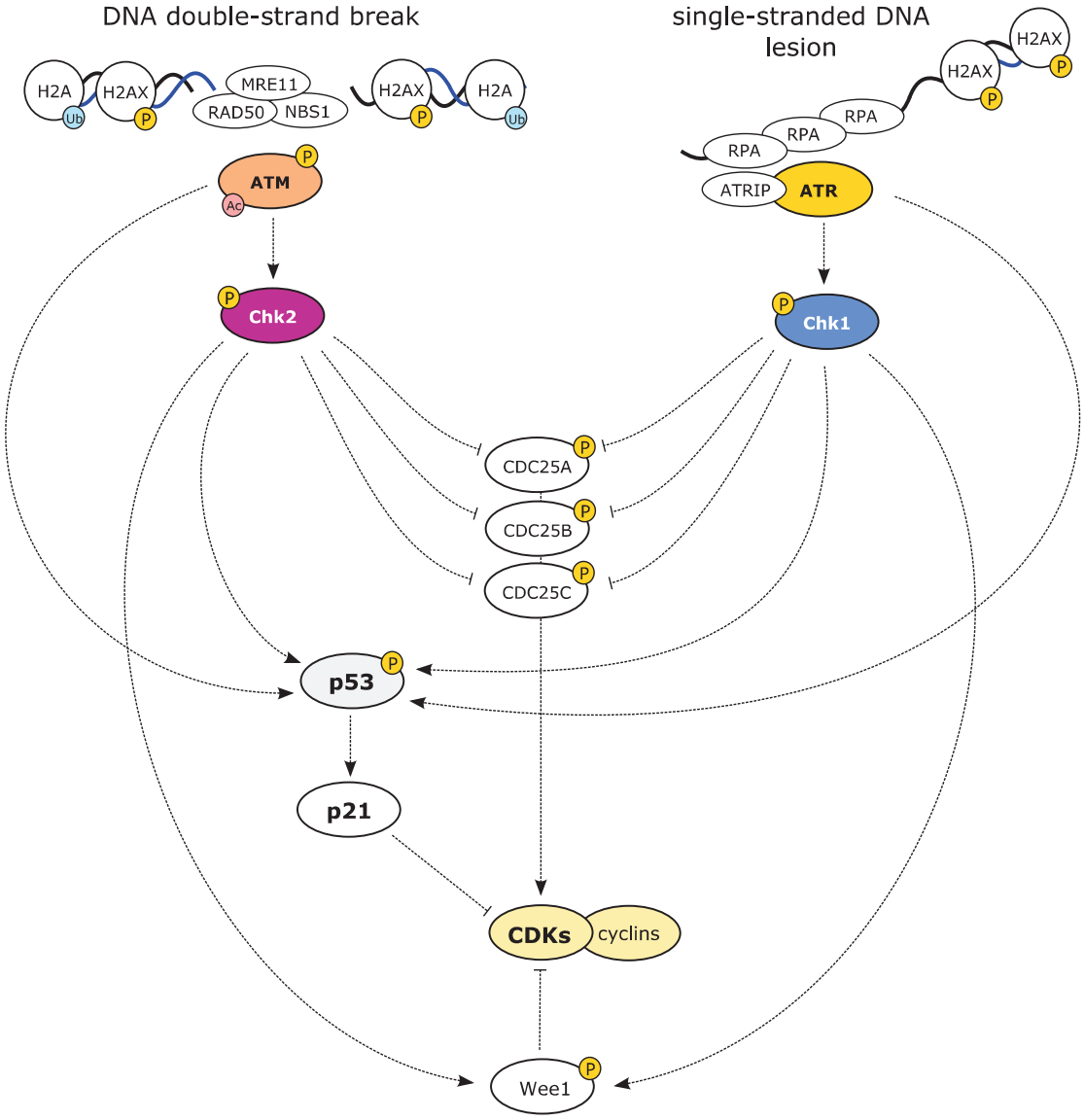

Figure 3.5: DNA damage response activates the cell cycle checkpoint - The effector kinases Chk2 and Chk1 cooperate with ATM and ATR in downstream DDR signal transduction. Together, they promote establishment of cell cycle checkpoint by inhibiting CDC25 phosphatases and activating the Wee1 kinase and p53. Figure is based on articles cited in the text above.

importance of Chk1 is well reflected in Chk1 knockout mice, which exhibits peri-implantation embryonic lethality (Liu *et al.*, 2000). In contrast, Chk2 knockout mice are viable and do not exhibit excessive tumor development, unless they are exposed to carcinogens (Hirao *et al.*, 2002; Takai *et al.*, 2002). Upon γ-irradiadion, Chk2 knockout mice showed increased radioresistance, which was attributed particularly to defective apoptotic response. Notably, Chk2 role in checkpoint activations seems to be at least under certain conditions redundant. Jack *et al.* (2002), demonstrated that Chk2-/- mouse embryo fibroblasts (MEFs) were able to fully activate the G1 arrest in response to γ-irradiation. On the contrary, p53-mediated apoptosis was abrogated in these cells. This suggests that Chk2 represent a key p53 activator in apoptotic response to DSBs. In addition to the ATR-Chk1 and ATM-Chk2 pathways, the p38MAPKMAPKAPK- 2 pathway has been recently described to contribute to the checkpoint activation and maintenance (Bulavin *et al.*, 2001; Manke *et al.*, 2005; Reinhardt *et al.*, 2010).

3.2 p38MAPK-MAPKAP-K2 pathway contributes to the activation of cell cycle checkpoint

The p38MAPK-MAPKAP-K2 pathway responds to a wide range of extrinsic and intrinsic stresses, including DNA damaging insults like UV and γ-irradiation, oxidative stress, osmotic stress, heat shock and inflammatory cytokines. As actions of p38MAPK are excessively pleiotropic, we stay focused solely on their contribution to the activation of cell cycle checkpoints. For p38MAPK roles in cellular differentiation, inflammation and cell migration we recommend a review of Cuenda and Rousseau (2007).

In mammals, there are four p38MAPK isoforms described – p38α, p38β , p38γ and p38δ. Isoforms α and β give rise to two additional splice variants. p38α isoform is ubiquitously expressed, whereas p38β is expressed mostly in brain and heart and p38γ in skeletal muscles, lung, kidney, gut and endocrine organs (Reinhardt and Yaffe, 2009).

The exact mechanism, which couples activation of the p38MAPK-MAPKAP-K2

pathway and DNA damage, is not completely clear. It seems that different insults can activate this pathway in different ways (Figure 3.6). The MKK3 and MKK6 kinases are considered as main activators of p38MAPK in response to osmotic stress, inflammatory cytokines and UV-irradiation (Brancho *et al.*, 2003; Enslen *et al.*, 1998). Additionally, in response to UV-irradiation, p38MAPK can be activated also by MKK4 kinase (Brancho *et al.*, 2003). TAO kinase has been shown to activate p38MAPK in response to γ and UV irradiation and hydroxyurea treatment. Interestingly, TAOs actions were reported to be dependent on ATM/ATR activity (Raman *et al.*, 2007). All these upstream kinases activate the p38MAPK through its dual phosphorylation on pTXpY motif in its active loop. While phosphorylation of threonine 180 (T180) is indispensable for p38MAPK catalytic function, phosphorylated tyrosine 182 (Y182) is necessary for its autoactivation and substrate recognition (Askari *et al.*, 2009).

p38MAPKα is associated in complex with MAPKAP-K2 kinase (ter Haar *et al.*, 2007; White *et al.*, 2007), also known as MK2. MAPKAP-K2 is activated directly by MAPKp38a-dependent phosphorylation on threonine 222, serine 272, and threonine 334 (Ben-Levy *et al.*, 1995). Whether other p38MAPK isoforms associate with MAPKAP-K2, is not elucidated. Activated complex of p38MAPKα (hereafter referred to as p38MAPK) and MAPKAP-K2 contributes to establishment of the checkpoint in two ways. Firstly, MAPKAP-K2 phosphorylates CDC25B/C phosphatases (Lemaire *et al.*, 2006; Manke *et al.*, 2005; Uchida *et al.*, 2011). Phosphorylated CDC25 phosphatases are consequently recognized by 14-3-3 proteins and prevented from activating CDK kinases, as described in previous chapter. Secondly, p38 phoshorylates p53 on Ser15 (Kim *et al.*, 2002), Ser33 (Sanchez-Prieto *et al.*, 2000) and Ser46 (Bulavin *et al.*, 1999) and thus promotes its activation. Hence p38MAPK-MAPKAP-K2 promotes checkpoint activation in very similar manner to Chk2 and Chk2 kinase (Figure 3.6). It is crucial that these pathways contribute to checkpoint activation in different extent dependent upon primary stress stimulus and are not mutually substitutable.

The p38MAPK-MAPKAP-K2 pathway has been proposed to be indispensable particularly for effective cellular stress response and cell cycle checkpoint activation upon UV-irradiation (Bulavin *et al.*, 2001; Manke *et al.*, 2005). It was

demonstrated that inhibition of p38MAPK by its specific inhibitor SB202190 or by antisense nucleotides resulted in cell cycle checkpoint abrogation after UV-irradiation (Bulavin *et al.*, 2001). Importantly, activation p38MAPK-MAPKAP-K2 upon UV irradiation does not depend on ATR-Chk1 signaling, or vice versa. Hence it suggests that these pathway act in parallel way in cellular response to UV irradiation. On the contrary, response of the p38MAPK-MAPKAP-K2 pathway to radiomimetic drugs such as cisplatin, camptothecin and doxorubicin was described to be ATM/ATR dependent, since without active ATM/ATR the p38MAPK-MAPKAP-K2 pathway was not triggered (Reinhardt *et al.*, 2007).

The findings of Reinhardt *et al.* (2010) further imply that the p38MAPK-MAPKAP-K2 pathway is crucial particularly for prolonged maintenance of checkpoint. The activated complex of p38MAPK-MAPKAP-K2 can translocate to the cytoplasm. Afterward, the MAPKAP-K2 phosphorylates RNA-binding protein hnRNPA0, which leads to stabilization of Gadd45α (Growth Arrest and DNA Damage 45 α) mRNA. Additionally, MAPKAP-K2 also phosphorylates PARN (Poly(A)-specific ribonuclease) that blocks Gadd45a mRNA degradation. p38MAPK contributes to Gadd45α upregulation via phosphorylation and consequent releases of the translational inhibitor TIAR (TIA-1-related protein). Consequently, Gadd45α interacts with p38 and notably potentiates p38-mediated MK2 activation. Hence, p38-MAPKAP-K2-Gadd45α circuit acts in double-positive feedback loop, which promotes maintenance of checkpoint.

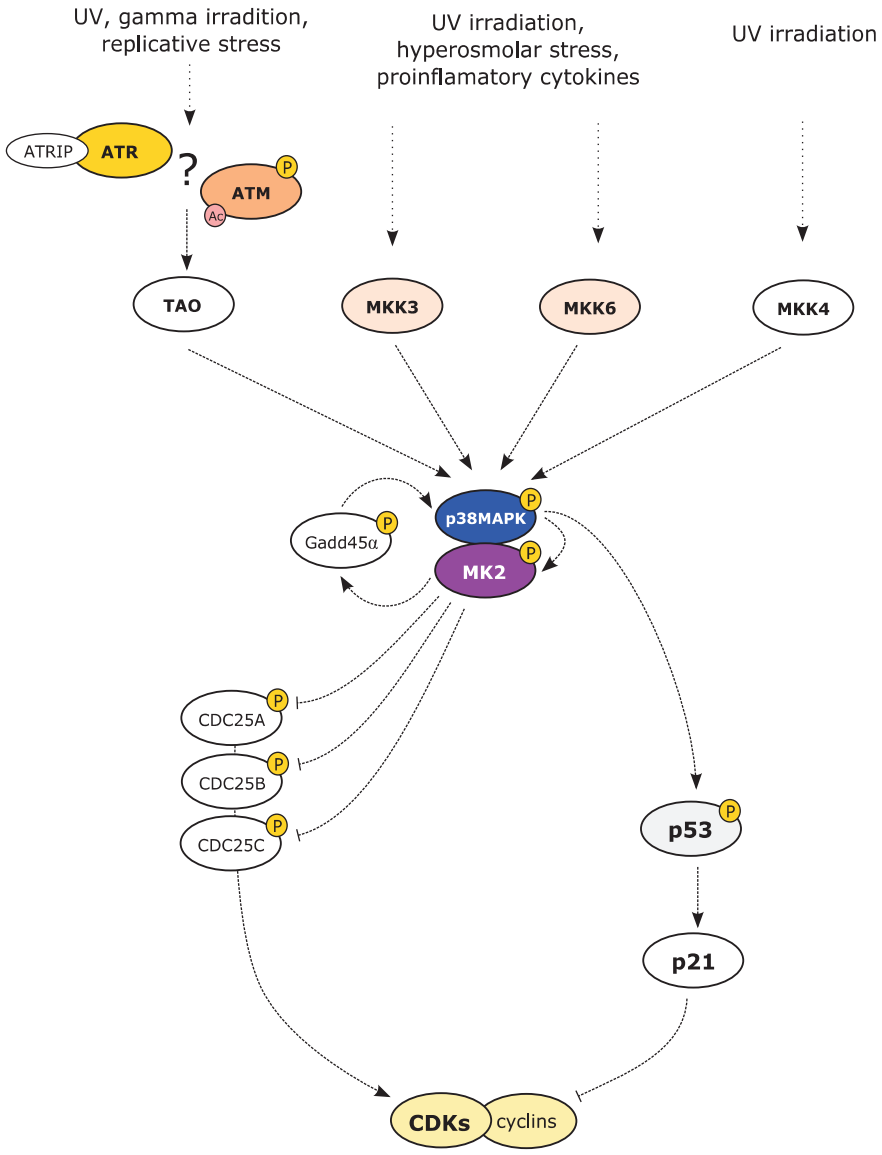

Figure 3.6: p38MAPK-MAPKAP-K2 pathway - Various stresses activate the p38MAPK-MAPKAP-K2 pathway, which in turn contributes to cell cycle checkpoint establishment by inhibiting CDC25 phosphatases and activating p53. Figure is based on articles cited in the text above.

3.3 p53 – the integrative hub of stress signaling

p53 transcription factor, often denoted as the guardian of genome or cellular gatekeeper, represents a crucial integrative hub of stress signaling. All previously described stress signaling pathways converge at some points to the activation of p53. The transcriptional targets of p53 are mostly pleiotropic and hence the outcomes of p53 signaling greatly vary. p53 can trigger transcription of p21, which serves as an inhibitor of CDK-cyclin complexes and thus contributes to establishment of the cell cycle checkpoint (el Deiry *et al.*, 1993; Harper *et al.*, 1993). Although the p53 is not essential for the checkpoint activation, its function is indispensable for the long-term checkpoint maintenance (Bunz *et al.*, 1998). In addition to p21 induction, p53 facilitates the checkpoint maintenance also by repression of mitotic inducers, such as cyclin B and Plk1 (Polo-like kinase 1; (Imbriano *et al.*, 2005; McKenzie *et al.*, 2010). In presence of persisting stress signaling, p53 can even mediate an establishment of permanent cell cycle arrest, termed as cellular senescence (Gorbunova *et al.*, 2002; Leonardo *et al.*, 1994; von Zglinicki *et al.*, 2005). Alternatively, excessive stress signaling can lead to induction of apoptosis through pro-apoptotic p53 targets such a Fas, BAX, PUMA, NOXA, and APAF-1. In addition, p53 also represses antiapoptotic genes, e.g. Bcl-2, PTEN, IGF-BP3 (thoroughly reviewed by Vousden and Lu 2002). Despite the intensive research in this field it is still not clear how cells choose the appropriate response from plethora of variants. Nevertheless in all cases, the p53-mediated response represents a crucial tumor-suppressive barrier. This significance of p53 functions is well demonstrated by the fact that p53 is the most frequently mutated gene in human cancer (reviewed by Goh *et al.* (2011). In addition, p53+/- heterozygotes suffer from condition, termed as Li-Fraumeni syndrome, characterized by increased risk for development of wide range of malignancies at early age (reviewed by Malkin (2011).

3.3.1 Regulation of p53 turnover and its stabilization upon stress

Under unstressed conditions, the p53 half-life is very short and p53 does not accumulate at high levels (Maltzman and Czyzyk, 1984). The p53 turnover is

regulated mainly by Mdm2 E3 ubiquitin ligase (Fang *et al.*, 2000; Honda *et al.*, 1997; Momand *et al.*, 1992). Since Mdm2 is a transcriptional target of p53, these two proteins operate together in a negative feedback loop (Barak *et al.*, 1993). p53 activates Mdm2 transcription and Mdm2 in turn targets p53 to proteasomal degradation, keeping the p53-Mdm2 circuit in balance. Additionally, p53 transcription activity is negatively regulated by MdmX. Recently it was demonstrated that MdmX potentiates also actions of Mdm2 (Wang *et al.*, 2011). Interestingly, Mdm2 can also ubiquitinylate also itself and MdmX (de Graaf *et al.*, 2003; Fang *et al.*, 2000; Pan and Chen, 2003). Which of the Mdm2 actions will prevail is controlled by HAUSP (herpesvirus-associated ubiquitinspecific protease) and DAXX (death domain-associated protein). In the absence of stress signaling, DAXX mediates formation of complex consisting of HAUSP, Mdm2 and MdmX and thus directs HAUSP deubiquitination activity toward mentioned negative p53 regulators. On the contrary, when stress signaling is triggered, phosphorylation mediated by upstream DDR kinases leads to disruption of HAUSP-DAXX-Mdm2-MdmX complex, which promotes Mdm2 self-ubiquitination (Meulmeester *et al.*, 2005; Stommel and Wahl, 2004; Tang *et al.*, 2006). Surprisingly, it seems that at least under some stress conditions, the DAXX can potentiate p53 actions, particularly the activation of apoptotic response (Li *et al.*, 2007).

In addition to promoting Mdm2 degradation, the stress signaling contributes to p53 stabilization also through disruption of p53 and Mdm2 interaction. In unstressed conditions p53 and Mdm2 interact via their N-termini. While upon stress, the p53 N-terminus undergoes several phosphorylation events, which interfere with Mdm2 binding and thus prevents p53 ubiquitination. Most prominent role among these phosphorylations belongs to the phosphorylation of serine 15 (S15) that acts as a priming phosphorylation permitting modification of several others sites, in particular serine 9, serine 20 and serine 46. S15 is phosphorylated upon DNA damage by ATM (Canman *et al.*, 1998; Khanna *et al.*, 1998), ATR (Lakin *et al.*, 1999), DNA-PK (Lees-Miller *et al.*, 1992) and p38MAPK (Kim *et al.*, 2002). In addition, ATR phosphorylates serine 37 (Tibbetts *et al.*, 1999). Effector kinase Chk2 contributes to N-terminus phosphorylation on threonine 18 and serine 20 (Shieh *et al.*, 2000). Chk1 was described to phosphorylate serine 20 (Shieh *et al.*,

2000), while p38 phosphorylates serine 33 (Sanchez-Prieto *et al.*, 2000) and serine 46 (Bulavin *et al.*, 1999). ATM can also phosphorylate Mdm2 on serine 395, which inhibits its activity toward p53 (Khosravi *et al.*, 1999; Maya *et al.*, 2001). For further stabilization, p53 undergoes several CBP/p300–dependent acetylations within its C-terminus. Since acetylation and ubiquitination are considered mutually exclusive, acetylations within C-terminus prevent p53 from being targeted to proteasomal degradation (Gu and Roeder, 1997). Together, all these modifications essentially cut off the Mdm2 feedback from p53 and thus enable its stabilization and accumulation (Figure 3.7).

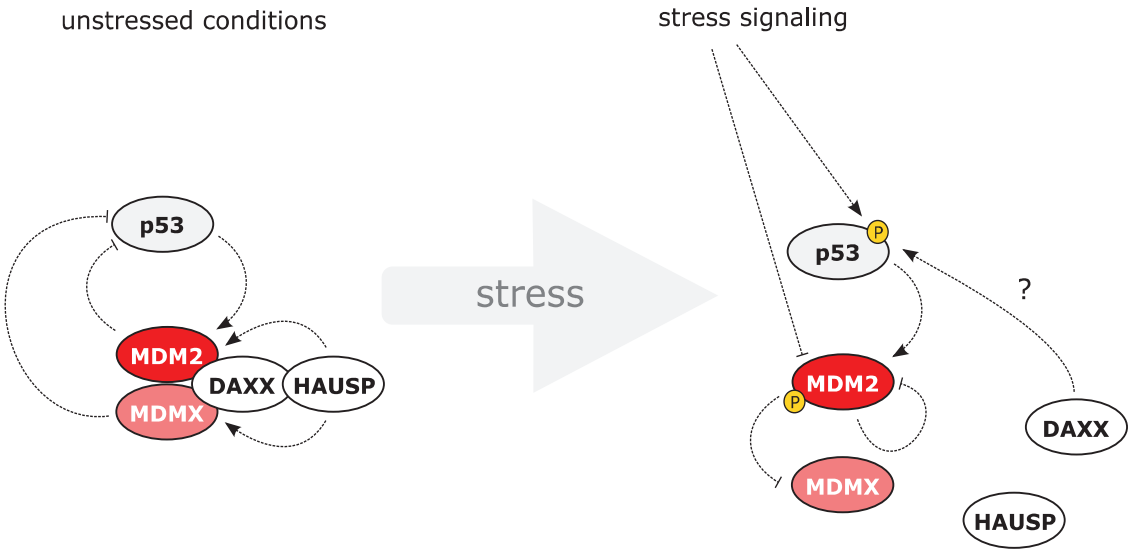

Figure 3.7: Regulation of p53 turnover and its stabilization upon stress - Under unstressed conditions, the levels of p53 are kept low mainly by Mdm2 E3 ligase. Upon stress, the actions of upstream modifiers essentially cut off the Mdm2 feedback loop from p53 and thus enable its stabilization and accumulation. (figure is based on Ronai (2006)

3.3.2 p53 post-translational modification can affect its transcriptional specificity

Intriguingly, several post-translational modifications were described to influence p53 transcriptional specificity. The E4F1 E3 ubiquitin ligase induces lysine 48-linked oligo-ubiquitination within lysine cluster lysine 319 to lysine 321 of p53.

As opposed to canonical role of lysine 48-linked ubiquitination, E4F1-dependent modifications do not target p53 for proteasomal degradation. Unexpectedly, E4F1-dependent ubiquitination stimulates the recruitment of p53 to the p21 promoter. On the contrary, it prevents p53 binding to promoters of pro-apoptotic genes, such as NOXA. In addition, the E4F1- mediated ubiquitination was shown to compete with acetylation of lysine 320 by PCAF. Interestingly, PCAF overexpression sensitizes cells to apoptosis. Moreover, acetylation of p53 on lysine 120 by Tip60 was showed to be essential for induction of p53- dependent apoptosis, but expendable for growth arrest (Tang *et al.*, 2006). Taken together, it might suggest that balance between these modifications contributes to the cell decision between cell cycle arrest and apoptosis (Cam *et al.*, 2006).

3.4 Checkpoint recovery

If DNA damage is successfully repaired, cells need to attenuate the DNA damage response signaling and terminate the checkpoint. Processes organizing the cell cycle re-entry, termed the checkpoint recovery, are dependent mostly on actions of Plk- 1 (Polo-like kinase 1) and Wip1 (wild-type p53-induced phosphatase 1; (Medema and Macurek, 2011). The Plk-1 is activated during checkpoint recovery by the complex of Aurora-A kinase and its cofactor hBora (Macůrek *et al.*, 2008). Active Plk-1 downregulates several key checkpoint mediators - Claspin, Chk2, Wee1 and CDC25C. Claspin phosphorylated by Plk-1 is recognized by β-TrCP1/2-SCF (Skp1-Cullin-F-boxprotein) ubiquitin ligase complex and targeted to proteasomal degradation (Mamely *et al.*, 2006; Peschiaroli *et al.*, 2006). The destruction of Wee1 is controlled by Plk-1 in the same manner ((Watanabe *et al.*, 2004). CDC25C is phosphorylated by Plk-1 in a nuclear export sequence, which promotes its nuclear localization (Toyoshima-Morimoto *et al.*, 2002). Importantly, Plk-1 also downregulates Chk2 by direct phoshorylation within its FHA domain, which inhibits the catalytic function of Chk2. Most likely, 53BP1 phosphorylated by Plk-1 and CDK1-cyclin B, serves as scaffold, that brings Plk-1 to the proximity of Chk2 (van Vugt *et al.*, 2010). Wip1 phosphatase opposes actions of DDR kinases and thus negatively regulates DDR on most of its levels, the most prominently

counteracting the activation of p53. As significant part of this master's thesis is dedicated to Wip1 phosphatase, it will be discussed in greater detail in the following section.

3.5 Wip1 phosphatase

Wip1 (wild-type p53-induced phosphatase 1, alternatively PP2C delta or PPM1D; EC 3.1.3.16) was identified in 1997 by Fiscella *et al.* (1997). They demonstrated that Wip1 expression is induced in response to γ-irradiation in a p53-dependent manner. Additionally, using immunoprecipitation of Wip1 from nuclear and cytosolic cell fractions and indirect immunofluorescence of fusion Wip1-proteins, they showed that Wip1 is localized exclusively to the cell nucleus. Recent studies further specified that Wip1 is bound to chromatin (Macůrek *et al.*, 2010).

3.5.1 Wip1 phosphatase overview

Wip1 is a magnesium-dependent serine/threonine phosphatase that belongs to the protein phosphatase 2C (PPC2) family. Unlike PP1 and PP2A phosphatases, it is not inhibited by okadaic acid (Fiscella *et al.*, 1997). In human, Wip1 is coded by *PPM1D* gene at locus 17q23.2. Three different protein coding transcripts produced from this locus are annotated. The *PPM1D-201* encodes full-length Wip1 protein of 605 aminoacids (aa), *PPM1D-202* encodes Wip1 isoform of 430 aa and *PPM1D-203* encodes Wip1 isoform of 282 aa (Ensembl release 62 - April 2011).

The *PPM1D-202* (also called PPM1D430) alternative splicing variant comprises the common 420 residues of the full-length Wip1 (PPM1D605) and in addition a stretch of PPM1D430-specific 10 amino acids (Figure 3.8). Same as full-length Wip1, *PPM1D-202* is also induced in p53-dependent manner upon γ-irradiation and possesses phosphatase activity. Unlike full-length Wip1, *PPM1D-202* is not expressed ubiquitously, but almost exclusively occurs in testes and in leucocytes (Chuman *et al.*, 2009). The *PPM1D-203* isoform, although predicted *in silico*, has not been identified *in vivo* yet.

The full length Wip1 protein comprises two major domains – N-terminal do-

main, which contains a putative PP2C catalytic domain (18-372 aa) and non-catalytic C-terminal domain (376-605; (Lu *et al.*, 2008a; Yoda *et al.*, 2006).

The C-terminal domain seems to be crucial for nuclear localization of Wip1. The Wip1 mutant missing this domain does not exhibit exclusively nuclear localization in contrast to wild-type or mutants deficient in N-terminal domains. Two putative nuclear localization signals (NLS) were identified in the C-terminal domain at 535–552 aa, 581–589 aa, respectively. However, mutants lacking one or both of these regions still localized to cell nucleus (Yoda *et al.*, 2006). Therefore regulation of Wip1 nuclear transport remains to be elucidated.

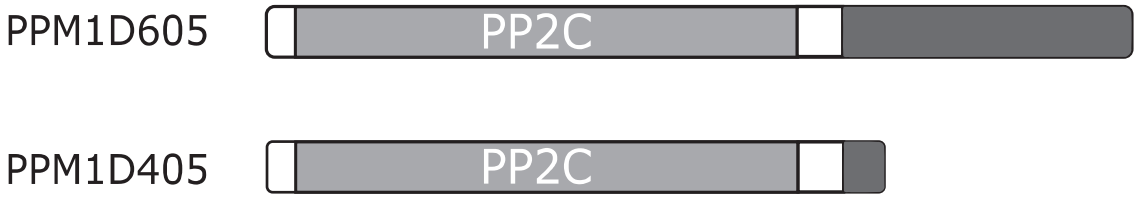

Figure 3.8: Schematic representation of the Wip1 splice variants, PPM1D605 and PPM1D430 - light grey denotes the PP2C catalytic domain, dark grey denotes variant-specific C-terminal sequences (adapted with modification from Chuman *et al.* (2009)

3.5.2 Wip1 substrates and its role in checkpoint recovery

Based on their specific recognition motifs, Wip1 substrates can be divided into two groups. Firstly, Wip1 exhibits specificity towards phoshorylated pSQ/pTQ motif, the same pSQ/pTQ motif is phosphorylated by DDR kinases (ATM, ATR), that play a major role in initiation and propagation DNA damage response, as described above (Chapters 3.1.1.2 and 3.1.2.2). Secondly, Wip1 has been shown to dephosphorylate pTXpY motif in p38MAPK (Takekawa *et al.*, 2000) and in nuclear uracil DNA glycosylase, UNG2 (Lu *et al.*, 2004). Wip1 substrates are summarized in Table 1.

3.5.2.1 Wip1 dephosphorylates pSQ/pTQ motif and counteracts p53 actions to enable checkpoint recovery

Wip1 shares the consensus pSQ/pTQ motif with ATM and ATR (Yamaguchi *et al.*, 2007). Hence, Wip1 is able to remove activating phosphorylations from ATM, checkpoint kinases Chk1, Chk2 and p53 to turn off the checkpoint signal (Figure 3.9) (Fujimoto *et al.*, 2006; Lu *et al.*, 2005; Shreeram *et al.*, 2006; Yamaguchi *et al.*, 2007). In addition to a direct dephosphorylation of p53, Wip1 inhibits ATM, an upstream regulator of ATM, and it also activates Mdm2 ubiquitin ligase (Lu *et al.*, 2007). Taken together, Wip1 can be viewed as a vital antagonist of p53.

Importantly, Lindqvist *et al.* (2009) showed that Wip1 activity is not needed solely for checkpoint inactivation, but it is crucial also in early stages of the checkpoint response for maintenance of cell competence for further proliferation. The depletion of Wip1 during unperturbed cell cycle has very little effect on the cell cycle progression. On the contrary, when Wip1-depleted cells were subjected to genotoxic insult leading to checkpoint activation, the later checkpoint recovery was strongly inhibited. Notably, the inhibition of upstream DDR kinases did not lead to checkpoint abrogation in Wip1- depleted cells, as opposed to the cells with active Wip1. It suggests therefore that the essential role of Wip1 in recovery

Table 3.1: Summary of identified Wip1 substrates

Protein	Site	Motif	Protein function	References
p38 MAPK	T180	TXY	stress response	(Takekawa *et al.*, 2000)
UNG2	T6	TXY	base excision repair	(Lu *et al.*, 2004)
ATM	S1981; S365	SQ/TQ	DDR	(Shreeram *et al.*, 2006)
Chk2	S19; S33/35; T68; T432	SQ/TQ	DDR	(Fujimoto *et al.*, 2006)
Chk1	S345	SQ/TQ	DDR	(Lu *et al.*, 2005)
H2AX	S139	SQ/TQ	DDR	(Macůrek *et al.*, 2010)
p53	S15	SQ/TQ	DDR	(Lu *et al.*, 2005)
MDM2	S395	SQ/TQ	regulator of p53	(Lu *et al.*, 2007)
MDMX	S403	SQ/TQ	regulator of p53	(Zhang *et al.*, 2009)
p65	S536	-	subunit NF-KB	(Chew *et al.*, 2009)

Adapted with modification from (Lu *et al.*, 2008b)

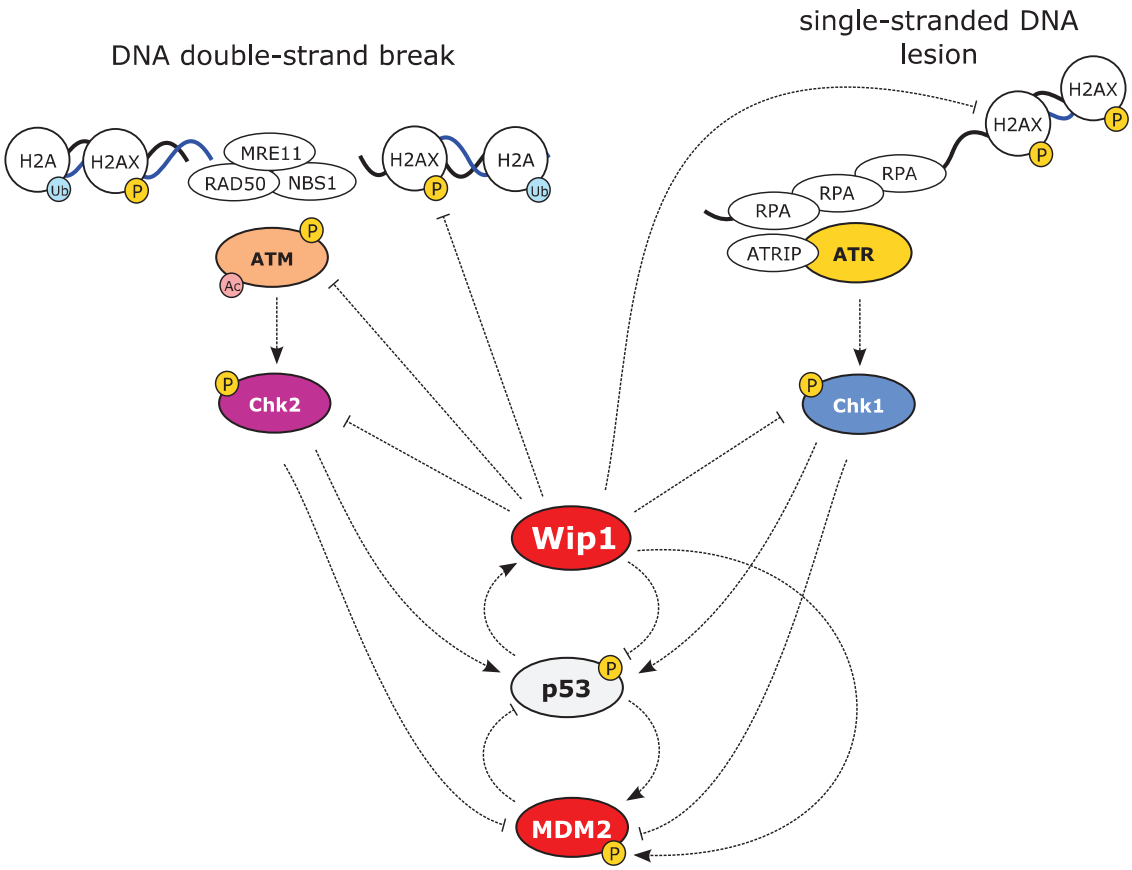

Figure 3.9: Wip1 opposes the actions of DDR kinases - thus negatively regulates DDR and enables the checkpoint recovery. Most importantly, Wip1 balances the p53 actions, which is essential for maintenance of checkpoint recovery competence. Figure is based on articles cited in the text above

competence does not consist in mere reversion of DDR induced phosphorylation sites. The insight into the Wip1 actions has been obtained using HCT116 and derived HCT116 p53-/- cell lines. The HCT116 p53+/+ depleted of Wip1 did not enter mitosis, confirming the previous observations. On the contrary, HCT116 p53-/- depleted of Wip1 were able to enter mitosis with no difficulties. Therefore, it demonstrates that Wip1 is required for maintenance of recovery competence by counteracting activity of p53. As described above, p53 facilitates checkpoint maintenance by upregulation of CDK inhibitor p21 and downregulation of mitotic inducers, including cyclin B (Imbriano *et al.*, 2005). It was shown that in Wip1-depleted background, p53 downregulates cyclin B levels below a threshold needed for preserving the minimal CDK1-cyclin B1 activity (Lindqvist *et al.*, 2009). Since the residual CDK1-cyclin B activity is required for possible checkpoint recovery (Alvarez-Fernández *et al.*, 2010), the lack of cyclin B results in a loss of recovery competence. In conclusion, Wip1 enables the checkpoint recovery competence by balancing the p53-mediated transcriptional repression of mitotic inducers.

3.5.2.2 Wip1 exhibits specifity toward pTXpY motif

There are two substrates with pTXpY motif described to be recognized by Wip1, p38MAPK kinase (Takekawa *et al.*, 2000) and nuclear uracil DNA glycosylase, UNG2 (Lu *et al.*, 2004).

Takekawa *et al.* (2000) described that Wip1 is able to directly inhibit p38MAPK through dephosphorylation of T180 in regulatory pTXpY motif of p38MAPK activation loop. The p38MAPK inhibition attenuates activatory phosphorylation of p53 on serine 33 and serine 34. As Wip1 is a transcriptional target of p53, it is conceived that Wip1 mediates a negative feedback loop in the p38MAPK-p53 pathway (Figure 3.10). With respect to recently described role of p38MAPK-MK2 pathway in the establishment of the checkpoint, Wip1 may contribute to checkpoint recovery also through p38MAPK inhibition.

Except the targets directly involved in DDR, Wip1 can also dephosphorylate nuclear uracil DNA glycosylase, UNG2 (Lu *et al.*, 2004). UGN2 initiates base excision repair (BER) through creation of apyrimidic sites. Wip1 dephosphorylates UGN2 on threonine 6, which results in significant reduction of its activity and sub-

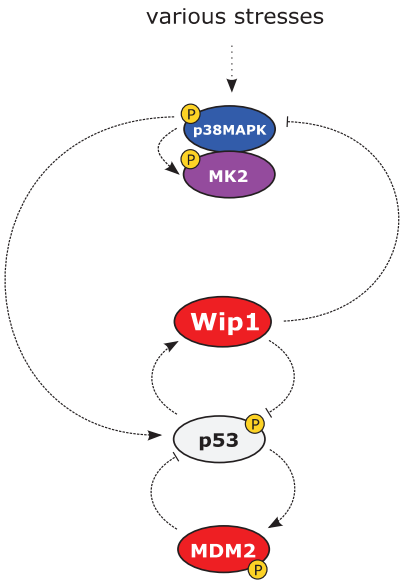

Figure 3.10: Wip1 mediates a negative feedback loop in p38MAPK-p53 pathway - therefore may contribute to checkpoint recovery also through p38MAPK inhibition. Figure is based on articles cited in the text above

sequently in decline of BER (Lu *et al.*, 2004). As BER lies beyond the scope of this thesis, we refer to review of Dalhus *et al.* (2009) for further reading.

3.5.2.3 Beyond the canonical motifs of Wip1

Wip1 was also shown to dephosphorylate serine 536 of p65 subunit of NF-κB transcription factor. The serine 536 surroundings correspond neither to the pSQ/pTQ nor to the pTXpY, suggesting that Wip1 specificity may be wider than originally thought. The phosphorylation of serine 536 is required for interaction with transcriptional co-activator p300, therefore Wip1 directly downregulates NF-κB signaling (Chew *et al.*, 2009). Interestingly, the p65 NF-κB subunit was described to bind to the *PPM1D* promoter region and to promote Wip1 transcription (Lowe *et al.*, 2010). Therefore, it is likely that NF-κB-Wip1 signaling circuit is regulated in negative feedback loop, similarly to p53-Wip1 circuit.

3.5.3 Wip1 in murine model

Wip1 shows 83% overall sequence identity at the amino acid level between human and mice (Choi *et al.*, 2000). Studies on murine model revealed that Wip1 is

ubiquitously expressed in all adult and embryonic tissues, with a very high level of expression in testis, specifically in the postmeiotic round spermatid compartment of the seminiferous tubules (Choi *et al.*, 2000, 2002). Wip1 expression during spermatogenesis correlates with the final stages of meiosis, thus it is possible that Wip1 plays regulatory role in meiotic division.

3.5.3.1 Characteristics of Wip1 knockout mice stress Wip1 importance in development

Wip1 knockout mice, although viable, exhibit several organ system defects. The main deficiencies were reported for male reproductive organs, immune system and cell proliferative and renewal capacity. Wip1-/- males were significantly smaller compared to wildtype, while Wip1-/- females did not exhibit decrease in size. Wip1-/- males had also notably smaller testes and reduced fertility. This finding further strengthened the importance of Wip1 for proper spermatogenesis, yet the exact mechanism of its action remains to be elucidated (Choi *et al.*, 2002).

In Wip1-/- mice, the proliferative response of T and B cells to antigenic and mitogenic stimulation was reduced, resulting in immune defects (Choi et al. 2001). It could be hypothesized that this could be attributed to defects in general cell cycle progression and checkpoint recovery. Alternatively, taking in account Wip1 role in DNA damage response signaling, its deficiency might influence also V(D)J recombination during which DBSs occurs.

Murine embryonic fibroblasts (MEFs) derived from Wip1 knockouts had decreased proliferation rate and entered cellular senescence earlier than their wild type counterparts. FACS (fluorescence-activated cell sorting) analysis of Wip1-/- MEFs revealed threefold increase in G2/M ratio compared to wildtype cells, suggesting defects in G2/M transition (Choi *et al.*, 2002) Importantly, Wip1-/- MEFs were resistant to transformation by *E1A*, *RAS*, *ERBB2* and *MYC*, suggesting that Wip1 can act as oncoprotein (Bulavin *et al.*, 2004).

3.5.4 Wip1 acts as oncoprotein

The gene locus of Wip1 is amplified approximately in 15% of breast adenocarcinomas and derived cell lines (e.g. MCF7; (Li *et al.*, 2002). Same amplification was demonstrated also in ovarian clear cell adenocarcinomas (Hirasawa *et al.*, 2003) and neuroblastomas (Saito-Ohara *et al.*, 2003). Moreover, in these tumors high Wip1 levels correlate with poor patient prognosis. Overexpression of Wip1 was also reported in latestage prostate cancers, even in the absence of Wip1 gene locus amplification (Li *et al.*, 2002).

Experimental overexpression of sole Wip1 in NIH-3T3 did not led to malignant transformation. However, overexpression of Wip1 in *RAS/E1A* transformed primary fibroblasts resulted in significant decrease in serum starvation-induced apoptosis (Bulavin *et al.*, 2002; Li *et al.*, 2002).

The oncogenic role of Wip1 apparently reflects its action as a negative regulator of stress responses, particularly of p53. The fact that Wip1 overexpression is usually found in tumors with functional p53 supports this view (Bulavin *et al.*, 2002). Since overexpressed Wip1 efficiently inhibits p53 function, there is no selection pressure for p53 functional loss during tumorigenesis. Moreover, transformed Wip1-deficient cells exhibit upregulation of CDK inhibitors $p16^{INK4A}$ and $p19^{ARF}$. This proposes that Wip1 may contribute to tumorigenesis also by counteracting their activation (Bulavin *et al.*, 2004). Notably, treatment of neuroblastoma–derived cell lines with Wip1 antisense oligonucleotide suppressed cell growth and induced apoptosis (Saito-Ohara *et al.*, 2003). Hence it suggests that developing the Wip1 inhibitors, might have significant clinical relevance for treatment of p53 wild-type tumors.

3.6 Temporal dynamics of DNA damage response

Bar-Or *et al.* (2000) observed that dynamics of p53 expression pattern upon γ-irradiation was not monotone but rather corresponded to damped oscillations. In addition to p53 levels, the levels of its negative regulator Mdm2 exhibit similar, phase-delayed oscillatory behavior, that was attributed to the p53-Mdm2 negative

feedback loop. Notably, these observations were based on studies of whole cell populations using western-blot technique.

Lahav *et al.* (2004) used p53-CFP and Mdm2-YFP fusion proteins and timelapse fluorescence microscopy approach to demonstrate that the damped oscillatory behavior is an artifact caused by averaging the response at the population level. Single cell observation showed that cells exhibit upon γ-irradiation a series of discrete undamped pulses (Figure 3.11). Nevertheless, even in genetically identical population and after the identical dose of irradiation, the number of pulses differs between cells. While some cells do not elicit any pulse during their response, other exhibit one, two or even more pulses. Hence when the response of whole population is averaged it seems as the cells exhibit a number of damped oscillations (Figure 3.11).

Geva-Zatorsky *et al.* (2006) further examined the behavior of p53 in longer timescale and showed that sustained undamped oscillations of p53 lasted for at least 3 days following γ-irradiation. Interestingly, the number of pulses correlated with the increase of γ-irradiation dose, whereas the pulse amplitude remained almost constant. This suggests that p53 response to γ-irradiation behaves in a digital rather than analog way. However, according to theoretical models of simple negative feedback loop, the p53-Mdm2 circuit should result in damped oscillations, therefore additional contributions to this circuit were expected (Lahav *et al.*, 2004).

Batchelor *et al.* (2008) demonstrated that p53 and Mdm2 pulses are controlled by upstream kinases ATM and Chk2 and identified Wip1 phosphatase as essential regulator for maintenance of the uniformity of pulses. In the proposed model the p53 pulses result from repeated activation of the ATM-Chk2-p53 pathway, which is in turn attenuated by Wip1. The presence of persistent DNA damage leads again to ATM-Chk2- p53 reactivation and therefore results in pulsative behavior of DDR. It was shown that activation of ATM and Chk2 upon γ-irradiation really exhibits pulsative dynamics similar to p53. The activation of ATM and Chk2 was measured as the level of their phosphorylated forems (ATM-pS1981 and Chk2-pT68, respectively) using western-blot technique. Interestingly, the pulsative dynamics of upstream kinases was dependent on presence of functional p53, since p53

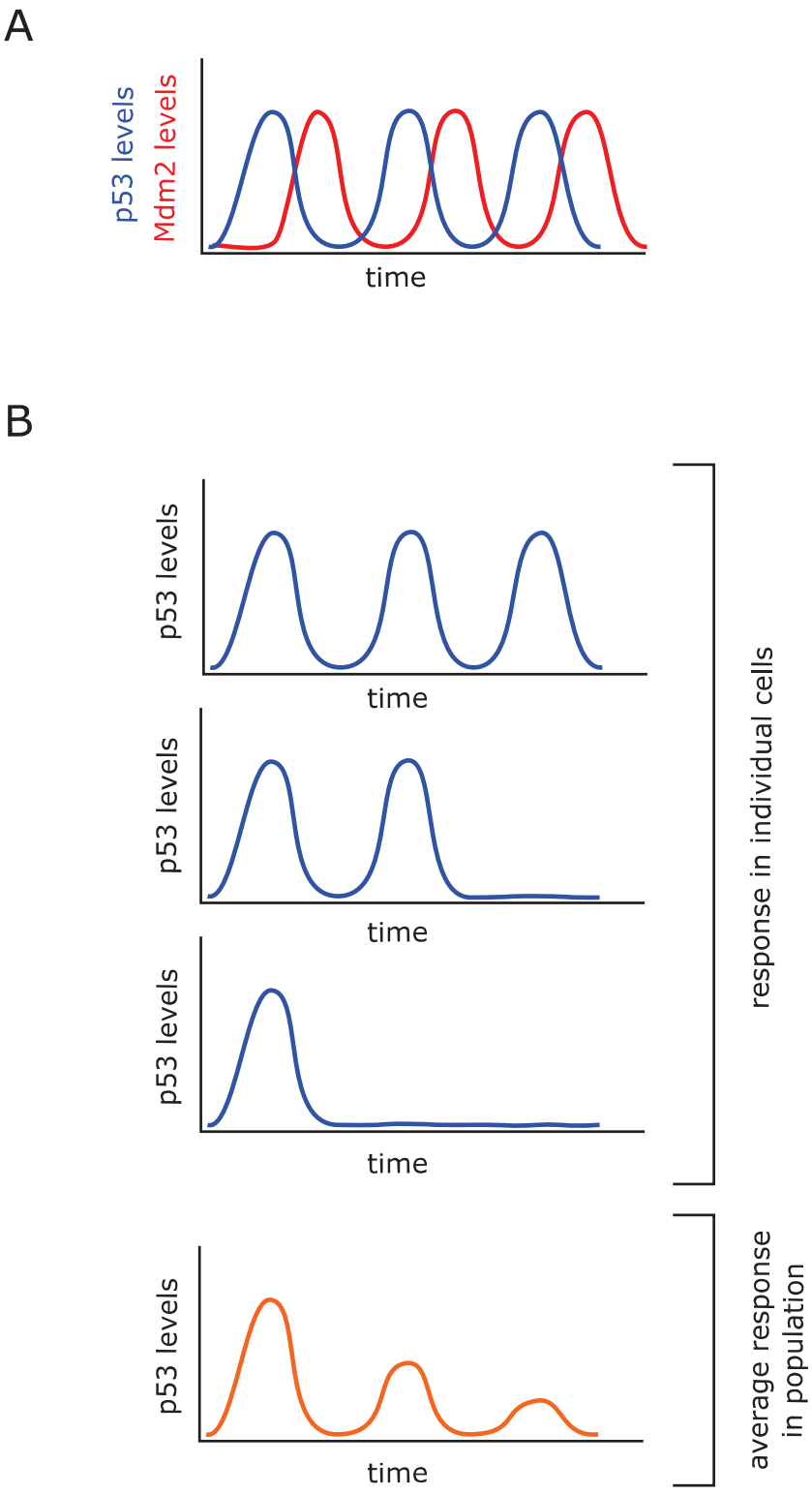

Figure 3.11: p53 dynamics upon γ-irradiation - **A:** p53 and Mdm2 exhibit pulsative dynamics upon γ-irradiation. **B:** Individual cells show variable number of undamped pulses at population level that appear as damped pulses. Figure is based on (Batchelor *et al.*, 2009; Geva-Zatorsky *et al.*, 2006)

depletion by RNA silencing led to attenuation of pulses. It suggested the existence of negative feedback mechanism connecting p53 with the upstream kinases. With respect to described features of Wip1 phosphatase, it represented the most prominent candidate for proving such a feedback mechanism. This assumption was proven by Wip1 depletion via RNA silencing which led to increased activation of ATM and Chk2, which did not exhibit the pulsative dynamics any longer. The p53 and Mdm2 pulses were not attenuated by Wip1 downregulation but exhibit deviations from the stereotypical pulse amplitude and the increased dose of γ-irradiation results in increased duration of each pulse. Thus Wip downregulation seriously disrupts otherwise digital behavior of p53 pulses. Taken together, although the p53-Mdm2 negative feedback loop seems to be sufficient to give rise of p53 pulsative dynamic behavior, the additional contribution of the p53-Wip1-ATM/Chk2 circuit is essential for maintenance of the uniformity of pulses.

The importance of the p53-Wip1-ATM/Chk2 circuit was further emphasized by Toettcher *et al.* (2010), who constructed a synthetic–natural hybrid of p53-Mdm2 oscillator. In this system the induction of p53-CFP (p53-cyan fluorescent protein) expression was controlled by zinc inducible metallothionein promoter. When p53-CFP expression was induced by zinc ions and not by DNA damage, the upper levels of DDR cascade were basically cut off from the circuit. Therefore, this system enables to investigate features of sole p53-Mdm2 negative feedback loop. It was confirmed that the sole p53-Mdm2 negative feedback loop gives rise to damped pulses upon zinc stimulation as opposed to undamped dynamics of full DDR circuit in the presence DNA damage.

Interestingly, the occurrence of p53 pulses is not restricted to the response to exogenous genotoxic insult such as γ-irradiation. Loewer *et al.* (2010) showed that p53 pulses can be detected also in cells proliferating under unstressed conditions. They observed that over 90% of proliferating cells induced up to three p53 pulses during one cell cycle. The inhibition of ATR and Chk1 had no noteworthy effect on induction of these pulses. Conversely, the inhibition of ATM and Chk2 resulted in significant reduction of p53 pulses. This suggests that spontaneous p53 pulses are caused by response to DSBs and not by response to ssDNA. The p53 pulses were not detected in cells with halted cell cycle progression. It seems that these

spontaneous p53 pulses can be attributed to the intrinsic DNA damage connected with cell cycle progression. Notably, these spontaneous p53 pulses do not lead to upregulation of p21, or to the cell cycle arrest. Therefore, it suggests that although the DDR exhibits a high sensitivity, the cells do not activate the full checkpoint response until the persistence of DNA damage exceeds a certain threshold.

3.6.1 Functional purpose of pulsative dynamics in DNA damage response

While the purpose of oscillations in controlling processes with cyclic pattern is apparent (e.g. oscillations of cyclins levels regulate cell cycle progression), the role of oscillatory behavior in DNA damage response is still waiting for its explanation.

One possibility is that repetitive degradation of p53 serves as "master reset" of its numerous posttranslational modifications. The complete degradation of p53 is probably preferred as a more efficient approach to reversing extensive modification pattern step by step. As described above, modification pattern greatly influences p53 actions, not only in terms of its stability but also of its specificity as a transcription factor (Cam *et al.*, 2006; Tang *et al.*, 2006). Thus cycles of p53 degradation and de novo synthesis provide cell a chance for reevaluation of DNA damage persistence and to choose the response appropriate for its current state (Lahav *et al.*, 2004). Furthermore, it is possible that p53 pulses encode information in a digital way. In other words, what really matters in cell's decision-making is the number of pulses, rather than the increase in p53 concentration. The striking uniformity in p53 pulses amplitude and wavelength might support this view, but otherwise it still remains highly speculative.

From different point of view, the main role of oscillatory behavior in DDR might occur at upper level of this cascade. The oscillations in ATM kinase activity may be necessary for a proper repair of DSBs. Batchelor *et al.* (2009) proposed that inhibition of ATM activity could lead to its dissociation from the DSB foci, which subsequently allow DNA damage repair factors to associate with the foci and take their actions. In case of successful repair, DDR signaling is terminated, otherwise ATM again relocates to the DSB foci and another pulse is triggered.

4

Materials & methods

4.1 Material

4.1.1 Chemicals and material

Table 4.1: List of chemicals and material

Chemical	Source
10 mM dNTPs (deoxynucleotide triphosphates)	Fermentas International Inc., Burligton, USA
10 × BamHI buffer	Fermentas International Inc., Burligton, USA
10 × Blue buffer	Fermentas International Inc., Burligton, USA
10 × Cfr9I buffer	Fermentas International Inc., Burligton, USA
10 × KpnI buffer	Fermentas International Inc., Burligton, USA
10 × Lambda Protein Phosphatase buffer	New England Biolabs, Ipswich,USA
10 × $MnCl_2$	New England Biolabs, Ipswich,USA
10 × Red buffer	Fermentas International Inc., Burligton, USA
10 × T4 ligase buffer	Fermentas International Inc., Burligton, USA
10 × TG buffer	Bio Rad; Hercules, USA
10 × TGS buffer	Bio Rad; Hercules, USA
5 × Phusion HF buffer	Thermo Fisher Scientific Inc., Waltham, USA
Acrylamid/Bis 30%	Serva Electrophoresis GmbH, Heidelberg, Germany
Agarose	Serva Electrophoresis GmbH, Heidelberg, Germany
APS (ammonium persulfate)	Sigma Aldrich, St. Louis, USA
Aqua pro injection	Braun GmbH, Frankfurt am Main, Germany
BamHI	Fermentas International Inc., Burligton, USA
BCA assay kit (Bicinchoninic acid kit)	Pierce, Rockford, IL, USA
Bromphenol blue	Pliva – Lachema a.s., Brno, Czech Republic
Cell culture plasticware	TPP Techno Plastic Products AG, Trasadingen, Switzerland
Cfr9I	Fermentas International Inc., Burligton, USA
Chloroform	Sigma Aldrich, St. Louis, USA
Cycloheximid	Calbiochem, Beeston Nottingham, United Kingdom

Continued on next page

Table 4.1 – continued from previous page

Chemical	Source
Dithiothreitol	Fluka, St. Gallen, Switzerland
DMEM (Dulbecco's Modified Eagle's Medium) Biochrom AG	Media preparation unit, IMG ASCR, v.v.i., Prague, CR
DMSO (dimethylsulfoxide)	Sigma Aldrich, St. Louis, USA
Double-distilled sterile H_2O	Media preparation unit, IMG ASCR, v.v.i., Prague, CR
Doxycycline hydrochloride	Sigma Aldrich, St. Louis, USA
EDTA (Ethylenediaminetetraacetic acid)	Sigma Aldrich, St. Louis, USA
EGTA (Ethyleneglycoltetraacetic acid)	Sigma Aldrich, St. Louis, USA
Ethanol 96%	Penta, Prague, CR
Ethidium bromide	Sigma Aldrich, St. Louis, USA
Foetal bovine serum	PAA Laboratories GmbH, Pasching, Austria
Foetal Bovine Serum TET system approved	Biological Industries, Kibbutz Beit Haemek, Israel
FuGENE 6 Transfection Reagent	Roche Diagnostics GmbH, Mannheim, Germany
G418 (geneticin sulfate)	Gibco/Invitrogen, Carlsbad, USA
GeneRuler™ 1 kb DNA Ladder	Fermentas International Inc., Burligton, USA
Glycerol	Sigma Aldrich, St. Louis, USA
HEPES (4-(2-hydroxyethyl)-1-piperazineethanesulfonic acid)	Sigma Aldrich, St. Louis, USA
HindIII	Fermentas International Inc., Burligton, USA
JETSTAR 2.0 Plasmid Miniprep Kit	GENOMED GmbH, Löhne, Germany
Kanamycine sulfate	Fluka, St. Gallen, Switzerland
KpnI	Fermentas International Inc., Burligton, USA
Lambda Protein Phosphatase	New England Biolabs, Ipswich,USA
LB (Lysogeny broth) agar solid growth media	Media preparation unit, IMG ASCR, v.v.i., Prague, CR
LB medium (Lysogeny broth)	Media preparation unit, IMG ASCR, v.v.i., Prague, CR
Lipofectamine RNAiMAX Transfection Reagent	Invitrogen, Carlsbad, USA
Loading Dye Solution 6 ×	Fermentas International Inc., Burligton, USA
Medical X-ray film	Foma Bohemia, Hradec Králové, Czech Republic
Methanol	Penta, Prague, CR
MG132	Sigma Aldrich, St. Louis, USA
Multiscribe reverse transcriptase	Applied Biosystems, Foster City, USA
NaCl (Sodium chloride) 99%	Pliva – Lachema a.s., Brno, Czech Republic
NEM (N-Ethylmaleimide)	Sigma Aldrich, St. Louis, USA
Nocodazol	Sigma Aldrich, St. Louis, USA
Nonfat dry milk	Migros, Zurich, Switzerland
Nonidet P40	Fluka, St. Gallen, Switzerland
Opti-MEM	Gibco/Invitrogen, Carlsbad, USA
PageRuler prestained protein ladder	Fermentas International Inc., Burligton, USA
PBS (Phosphate buffered saline)	Media preparation unit, IMG ASCR, v.v.i., Prague, CR
Penicillin-Streptomycin solution 100 ×	Sigma Aldrich, St. Louis, USA
Phusion DNA polymerase	Thermo Fisher Scientific Inc., Waltham, USA
Ponceau S	Bio-Rad Laboratories, Hercules, USA
Protease inhibitor coctail tablets	Roche Diagnostics GmbH, Mannheim, Germany
Protein A/G UltraLink ResinS-protein beads	Thermo Fisher Scientific Inc., Waltham, USA
Protein Assay Bredford, Dye Reagent concentrate	Bio-Rad Laboratories, Hercules, USA
QIAquick® Gel Extraction Kit	Qiagen, Venlo, Netherlands
RNase inhibitor	Applied Biosystems, Foster City, USA
RO3066	GeneTiCA, Prague, Czech Republic

Continued on next page

Table 4.1 – continued from previous page

Chemical	Source
SacII	Fermentas International Inc., Burligton, USA
SDS (sodium dodecyl sulfate)	Serva Electrophoresis GmbH, Heidelberg, Germany
Shrimp alkaline phosphatase	Fermentas International Inc., Burligton, USA
S-protein-agarose	Novagen, Madison, USA
SuperSignal West Substrates Trial Kit	Thermo Fisher Scientific Inc., Waltham, USA
SYBRGreen PCR master mix	Applied Biosystems, Foster City, USA
T4 DNA ligase	Fermentas International Inc., Burligton, USA
TaqMan reverse transcription reagent	Applied Biosystems, Foster City, USA
TEMED (N,N,N',N'-tetramethylethylendiamine)	Fluka, St. Gallen, Switzerland
Thymidine	Sigma Aldrich, St. Louis, USA
Tri Reagent	Sigma Aldrich, St. Louis, USA
Tris (Tris(hydroxymethyl)aminomethane)	Fluka, St. Gallen, Switzerland
Triton X-100	Fluka, St. Gallen, Switzerland
Trypsin/EDTA (Ethylenediaminetetraacetic acid)	Media preparation unit, IMG ASCR, v.v.i., Prague, CR
Tween20	Fluka, St. Gallen, Switzerland
Whatman Protran® nitrocellulose membrane	Whatman plc, Maidstone, Kent, United Kingdom

Mammalian cell lines

- **MCF7**, human breast adenocarcinoma cell line; cell line was obtained from Jiří Bartek; Institute of Cancer Biology, Copenhagen, Denmark
- **U2OS**, human osteosarcoma cell line; cell line was obtained from Jiří Bartek; Institute of Cancer Biology, Copenhagen, Denmark
- **U2OS-D7**, monoclonal cell line derived from U2OS, expressing Tet-inducible Wip1-FLAG; cell line was obtained from Libor Macůrek; described in Lindqvist *et al.* (2009)
- **U2OS-GFP-Wip1**, monoclonal cell line derived from U2OS, stably expressing GFP-Wip1; cell line was prepared during this thesis; property of Department of Genome Integrity, Institute of Molecular Genetics, ASCR
- **U2OS-LAP-Wip1-D314A**, monoclonal cell line derived from U2OS, stably expressing phosphatase dead mutant (D314A) of Wip1, fused with LAP tag; cell line was prepared during this thesis; property of Department of Genome Integrity, Institute of Molecular Genetics, ASCR

Bacterial strains

- DH5α, *Escherichia coli strain*; property of Department of Genome Integrity, Institute of Molecular Genetics, ASCR

Table 4.2: List of used primary antibodies

Antibody	Host	Source	Cat. No.	WD
Chk1-pS317	rb/poly	Cell Signalling Technology Inc., Denvers, USA	#2344	1000 ×
Chk2-pT68	rb/poly	Cell Signalling Technology Inc., Denvers, USA	#2661	700 ×
Cyclin A	m/mono	Santa Cruz Biotechnology,Inc., Santa Cruz, USA	sc-53230	500 ×
Cyclin B	rb/poly	Abcam Inc., Cambridge, USA	ab7957	500 ×
FLAG	m/mono	Sigma Aldrich, St. Louis, USA	F 1804	1000 ×
GAPDH	m/mono	GeneTex, Irvine, USA / from Exbio, Vestec, CR	GTX30666	10000 ×
H3-pS10	rb/poly	Millipore-Upstate, Billerica, USA	06-570	1000 ×
MAPKAPK-2 pT334	rb/mono	Cell Signalling Technology Inc., Denvers, USA	#3007	1000 ×
MKK3-pS189/ MKK6 pS207	rb/mono	Cell Signalling Technology Inc., Denvers, USA	#9236	1000x
p21	m/mono	Santa Cruz Biotechnology,Inc., Santa Cruz, USA	sc-56335	500 ×
p38 MAPK	rb/poly	Cell Signalling Technology, Inc., Denvers, USA	#9212	1000 ×
p38 MAPK-pT180/ pY182	m/mono	Cell Signalling Technology Inc., Denvers, USA	#9216S	2000x
p53	m/mono	Cell Signalling Technology, Inc., Denvers, USA	sc-126	1000 ×
p53-pS15	rb/poly	Cell Signalling Technology Inc., Denvers, USA	#9284S	1000 ×
PARP	rb/poly	Cell Signalling Technology Inc., Denvers, USA	#9542	1000 ×
pSQ/pTQ	rb/poly	Cell Signalling Technology Inc., Denvers, USA	#2851	1000 ×
WIP1	rb/poly	Santa Cruz Biotechnology Inc., Santa Cruz, USA	sc-20712	3000 ×
WIP1	rb/poly	Bethyl Laboratories, Inc.,Montgomery,USA	A300-664A	3000 ×
γ-H2AX	rb/poly	Cell Signalling Technology Inc., Denvers, USA.	#2577	1000 ×
α-tubuline	m/mono	Sigma Aldrich, St. Louis, USA	T5168	10 000 ×

Abbreviations: rb- rabbit; m - mouse; poly – polyclonal; mono – monoclonal;
WD - working dilution for western blot from original stock

Table 4.3: List of used secondary antibodies

Antibody	Host	Source	Cat. No.	WD
Goat Anti-Mouse IgG (H + L)-HRP Conjugate	goat	Bio Rad; Hercules, USA	#170-6516	5 000 ×
Goat Anti-Rabbit IgG (H + L)-HRP Conjugate	goat	Bio Rad; Hercules, USA	#172-1019	5 000 ×

Abbreviations: HRP - horseradish peroxidase; IgG – immunoglobin G, H + L - heavy + light chain
WD - working dilution for western blot from original stock

Table 4.4: List of vectors

Vector	Obtained from
pcdnaTO-Wip1-D314A	Libor Macůrek
pcdnaTO-Wip1-S40A	Libor Macůrek
pcdnaTO-Wip1-S40D	Libor Macůrek
pEGFP-N3	Promega, Medison, USA
pEGFP-Wip1	Libor Macůrek
pGEM®-T Easy	Promega, Medison, USA
pLAP-Wip1-D314A	Libor Macůrek

4.1.2 List of used instruments and other equipment

Table 4.5: List of used instruments and other equipment

Instrument	Manufacturer
BioSafety Cabinet (laminar hood) Bio-II-A	Telstar, Barcelona, Spain
Bürker counting chamber	Fuchs-Rosenthal, Laboroptik, Friedrichsdorf, Germany
Centrifuge 5415R Eppendorf	Eppendorf,Hamburg, Germany
Centrifuge 5424 Eppendorf	Eppendorf,Hamburg, Germany
Centrifuge Nüve NF400	Nüve Inc., Ankara,Turkey
CO_2 Incubator FORMA Series II Water Jacket	Thermo Fisher Scientific Inc., Waltham, USA
Gilson PIPETMANs Neo® Set	Gilson, Inc., Middleton, USA
Kodak developing machine for X-ray film	Eastman Kodak Company, New York, USA
MACROMAN Gilson	Gilson, Inc., Middleton, USA
Microplate photometer Multiskan® EX	Thermo Fisher Scientific Inc., Waltham, USA
Microscope Leica DMIL	Leica Microsystems GmbH, Wetzlar, Germany
Microscope Nikon Eclipse T100	Nikon Instruments Europe B.V, Amstelveen, The Netherlands
Multi-Spin MSC-3000	Biosan, Riga, Latvia
NALGENE Cryo Freezing Container “Mr. Frosty”	Thermo Fisher Scientific Inc., Waltham, USA
NanoDrop® ND-1000 Spectrophotometer	Thermo Fisher Scientific Inc., Waltham, USA
Orthovoltage X-ray instrument T-200	WOLF-Medizintechnik GmbH, St.Gangloff / Thür, Germany
PTC-200 DNA Engine Cycler	Bio Rad; Hercules, USA
Safe Aspiration Kit Gilson	Gilson, Inc., Middleton, USA
SDS-PAGE Apparatus Mini-PROTEAN Tetra Cell	Bio Rad; Hercules, USA
Sonicator SONIPREP MSE 150	AL.BRA. Srl, Milano, Italy
Spectrophotometer DU® SERIES 700	Beckman Coulter, Inc., Fullerton, USA
The LightCycler® 480 System	Roche Diagnostics GmbH, Mannheim, Germany
Thermomixer comfort	Eppendorf,Hamburg, Germany
UltraLum Crosslinker series 800	UltraLum, Claremont, USA
UV-C light meter, model UVC-254	Lutron Electronic Enterprise Co., Ltd., Taipei, Taiwan
Vortex Lab dancer	VWR, Darmstadt, Germany
Water bath Nüve BM402	Nüve Inc., Ankara,Turkey
Western blot apparatus TE22 small transphor unit	Hoefer, Inc., San Francisco, USA
UV Transilluminator	East Port, Prague, Czech Republic
EC320 Primo Minicell Horizontal Gel System	Thermo Fisher Scientific Inc., Waltham, USA
Wide Mini-Sub Cell GT Cell	Bio Rad; Hercules, USA

4.2 Methods

4.2.1 Cell culture techniques

4.2.1.1 Propagation of mammalian cells

Mammalian cells were manipulated according to the standard cell culture protocols Freshney (2005). Cells were cultivated in D-MEM (Dulbecco's modified Eagle's medium), supplemented with 10% fetal bovine serum and Penicillin (100 U/ml) – Streptomycin (100 ng/ml). Tet-inducible cell line U2OS-D7 was cultivated in D-MEM supplemented with 10% foetal bovine Serum TET system approved and Penicillin (100 U/ml) – Streptomycin (100 ng/ml). Cells were kept at 37 °C under 5% CO_2 atmosphere.

4.2.1.2 Cryopreservation of cell lines

Cells were trypsinized, pelleted by centrifugation and then resuspended in 1 ml of cryopreservation medium containing 90% FBS and 10% DMSO (approximately 2×10^6 cells per 1 ml of medium per cryovial). Cryovials were transferred to Mr. Frosty cooling device, containing a propane-1,2,-diol filled bath, and in -80 °C freezer. After 24 hours cryovials were moved to liquid nitrogen, for long-term storage.

4.2.1.3 Thawing cell lines

Cryovials were transferred from liquid nitrogen storage on dry-ice and then promptly thawed in 37 °C water bath. Cells were centrifuged and resuspended in fresh medium.

4.2.1.4 Cell counting

Cells were counted using Bürker counting chamber according to the standard protocol Freshney (2005).

4.2.1.5 Plasmid DNA transfection

Plasmid DNA transfection was done with commercial FuGENE® 6 Transfection Reagent. U2OS cell were plated in 6-well plate at density 150 000 cells per well using 2.5 ml of 10% FBS/D-MEM per well. First, we prepared the "mastermix" solution by mixing the 3 μl of FuGENE® 6 Transfection Reagent per 1 μg of DNA with 97 μl of 1 $\times$ D-MEM without serum and antibiotics. The solution was gently shaken, spinned and incubated at room temperature for 5 minutes.Subsequently, the plasmid DNA was added to the "mastermix" and the solution, gently shaken, spinned and incubated at room temperature for 15 minutes. Finally, DNA - FuGENE® 6 Transfection Reagent solution was added to the cells in 6-well and gently mixed by rocking the plate back and forth.

4.2.1.6 siRNA transfection

siRNA transfection was done with commercial Lipofectamine™ RNAiMAX Transfection Reagent. U2OS cells were plated in 6-well plate at density 150 000 cells per well using 2.5 ml of 10% FBS/D-MEM per well. After 24 hours, cells were transfected with 1 nM of siRNAs. Firstly, 250 μl of Opti-MEM medium without serum was mixed with 4 μl of Lipofectamine™ RNAiMAX Transfection Reagent, gently shaken, spinned and incubated at room temperature for 5 minutes. Secondly, 250 μl of Opti- MEM medium was mixed with 12.5 ul of 200 nM siRNA and incubated at room temperature for 5 minutes. Subsequently, both solutions, were mixed together, and incubated at room temperature for 20 minutes. Finally, RNAi duplex-Lipofectamine RNAiMAX solution was added to the cells and gently mixed by rocking the plate back and forth.

4.2.1.7 Cell synchronization using double thymidine block

Cells were synchronized using thymidine and nocodazol as follows. Cells were plated at 1.3×10^6 per 10 cm plate, next day 2 mM thymidine was added for 12 h, cells were then released into fresh medium. Upon every release from blocking agent, the cells were twice rinsed with pre-warmed 1$\times$PBS. After 10 hours, 2 mM thymidine was added again for 12 h. Subsequently, cells were released

a) into fresh medium; 3 hours after release the samples corresponding to S-phase were harvested; 6 hours after release the samples corresponding to G2-phase were harvested; 12 hours after release the samples corresponding to G1-phase was harvested; b) into medium with nocodazole (100 ng/ml), after 8 hours the mitotic cells were harvested via mitotic shake-off.

4.2.1.8 Cell synchronization using tandem of thymidine block and RO3066 inhibitor

The double-thymidine block did not enable us to synchronize cells that enter mitosis simultaneously. The simultaneous mitotic entry is not necessary in most experiments, since the nocodazole effectively stops the cells in prometaphase and thus enables us to harvest mitotic cells in large numbers. Nevertheless, for experiments, in which we wanted observe protein dynamics during a normal and prolonged mitosis the double-thymidine block synchronization was not sufficient. For this reason we adapted our synchronization protocol and made use of a commercially available CDK1 inhibitor RO3066. The RO3066 effectively inhibits the CDK1 activity and therefore arrests the cells at G2/M transition Vassilev (2006).

Cells were plated at 1.3×10^6 per 10 cm, next day 2 mM thymidine was added for 24 hours and then cells were rinsed twice with pre-warmed 1$\times$PBS and released into fresh medium. Samples corresponding to S-phase were harvested 3 hours after release. After 6 hours 9 μM RO3066 was added. Next day cells were either harvested (G2-phase) or released from RO3066 block into fresh medium with or without nocodazole. Nocodazole treated cells were harvested after 2 hours via mitotic shake-off. Cells released from RO3066 block into medium without nocodazole were harvested after 6 h as a G1-phase sample.

4.2.1.9 γ-irradiation

Cells were irradiated within 6-well plates, overlayed with 3 ml of cultivation media. The irradiation was performed by orthovoltage X-ray instrument T-200 (Wolf-Medizintechnik) at the X-ray radiation facility; Institute of Molecular Genetics of the ASCR, v.v.i. The setting of radiation source used during irradiation is described

in the Table 4.6.

Table 4.6: The setting of orthovoltage X-ray instrument T-200

Dose [Gy]	Time [s]	Voltage[kV]	Current[mA]	Filter	Applicator
9.99	239	200	13	0.3 Al	#1, 20x20/50

4.2.1.10 UV-C irradiation

Cells were irradiated with UV-C light (wavelength 254 nm) using the UltraLum Crosslinker series 800 (CEX-800, 930-0021-01). The cultivation medium was removed from cells prior to UV-C irradiation and returned back immediately after it. This was necessary since the cultivation medium can absorb UV-C. UV-C dose used is described in individual experiments.

4.2.1.11 Cell harvest

To prevent a potential loss of mitotic cells that do not adhere to the plasticware, we collected the medium from cells, washed adherent cells by 1 $\times$ PBS, trypsinized, mixed with the collected medium and spinned at 146 rcf (relative centrifugation force) for 3 minutes.To obtain mitotic cells, floating cells were harvested via a mitotic-shake-off. Subsequently, cell pellet was washed by 1 $\times$ PBS and spinned at 146 rcf for 3 min, twice. Pellet was lysed in appropriate volume of 1 $\times$ Sample buffer (63 mM Tris HCl, 10% Glycerol, 2% SDS, pH 6.8). Samples were sonicated three-times for 15 seconds at 5 microns with 5 seconds pause. Sonicated samples were boiled for 5 minutes.Total protein concentration was quantified by BCA assay and samples were diluted to same concentration. Samples were mixed 3:1 with 4 $\times$ Sample buffer with 0.2% (w/v) Bromophenol blue.

4.2.2 BCA assay

The total amount of protein in cell lysates was quantified using BCA assay to ensure identical loading in western blot Smith *et al.* (1985). The BCA assay was performed according to the manufacturer instructions.

4.2.3 SDS-Polyacrylamide Gel Electrophoresis

SDS-Polyacrylamide Gel Electrophoresis (SDS-PAGE) was performed in the standard two-gel system developed by Laemmli (1970). We used BioRad Mini-PROTEAN Tetra Cell apparatus and corresponding accesories. Mixtures for separating gels were prepared according to the Table 4.7. Subsequently, mixtures were cast into assembled glasses, overlayed by 70% EtOH and let to polymerize. When fully polymerized, EtOH was removed and separating gels were overlayed by stacking gels (Table 4.7), proper combs were inserted and gels let to polymerize. The same total protein amount was loaded into each well. Gels were run at constant current 50 mA per 1 gel. Commercially available 1 $\times$ TGS buffer (25 mM Tris, 192 mM glycine, 0.1% SDS, pH 8.3) was used as running buffer.

Table 4.7: SDS-PAGE gels percentage

		Gel			
Components		**8%**	**10%**	**15%**	**Stacking**
ddH_2O	[mL]	3.6	3.1	1.9	1.8
Buffer A*	[mL]	1.9	1.9	1.9	-
Buffer B**	[mL]	-	-	-	0.75
Acrylamid-Bis 30%	[mL]	2	2.5	3.75	0.75
10% APS	[μl]	50	50	50	24
TEMED	[μl]	12.5	12.5	12.5	6
Total volume***	[mL]	7.6	7.6	7.6	3

* Buffer A - 1.5 mM Tris, 0.4% SDS, pH 8.8, ** Buffer B - 0.5 mM Tris, 0.4% SDS, pH 6.8
*** Coressponding to the one 1.5 mm thick gel in BioRad Mini-PROTEAN system

4.2.4 Western blot

The separated proteins were transferred from gel onto a nitrocellulose membrane through a wet transfer western blot. We used Hoefer western blot apparatus TE22

small transphor unit and corresponding accessories. The western blot was run at constant voltage of 100 V for 1.5 hours. Commercially available 1 $\times$ TG buffer (25 mmol/l Tris, 192 mmol/l glycine, pH 8.3), containing 20% methanol was used as blotting buffer. The quality of protein transfer was verified using Ponceau S staining of the membrane. Subsequently, the nitrocellulose membrane was blocked by 5% [w/v] of nonfat dry milk in 1 $\times$ PBS/0.05% Tween20 for 20 minutes. The blocked membrane was carefully washed by 1 $\times$ PBS/0.05% Tween20 and incubated overnight with a primary antibody, diluted in 3% nonfat dry milk in PBS/0.05% Tween20 with 0.1% of sodium azide. Following day, the membrane was carefully washed by 1 $\times$ PBS/0.05% Tween20 and incubated with secondary antibody for 3 hours. Next, the membrane was washed with 1 $\times$ PBS/0.05% Tween20 and incubated for 3 minutes with mix of equal volume of chemiluminescent ECL reagent 1 and 2 and exposed to the medical X-ray film. The X-ray film was developed by Kodak developing machine.

4.2.5 Immunoprecipitation

All manipulations with cell lysates were performend on ice. Cells were lysed in 300 μl lysis buffer (250 mM NaCl, 0.25% Noniset P40, 1% glycerol, 50 mM HEPES, pH 7.5, 10 mM NEM, 1 $\times$ inhibitors of proteases and phosphatases, diluted in aqua pro injectione), then sonicated at 3 microns three times 15 sec. After sonication, cell lysates were diluted by 200 μl of aqua pro injectione and 0.5 μl of DDT was added to the lysate. Cell lysates were spinned at 16 100 rcf for 20 minutes at 4 °C. Meanwhile, the A/G beads were washed by lysis buffer. The supernatants from cell lysates were collected and precleaned by incubation with 10 μl of A/G beads for 40 minutes at 4 °C with gentle rotation. The relative protein concentration in samples was determined by Bio-Rad protein assay and samples were diluted to the same concentration. Next, the precleared cell lysate was incubated overnight with 10 μl of primary antibody at 4 °C with gentle rotation. Following day, the cell lysate-antibody mixture was incubated with 20 μl of washed A/G beads for 2 hours at 4 °C with gentle rotation. Finally, the mixture was spinned and supernatant discarded. Beads were washed three times with 1 $\times$ PBS and

resuspended in 25 μl of 2 $\times$ Sample buffer.

4.2.6 S-protein tag pulldown

All manipulations with cell lysates were performed on ice. Cells were lysed in 300 μl lysis buffer (2 mM EDTA, 1 mM EGTA, 0.1 Triton-X, 1 $\times$ inhibitors of proteases and phosphatases, diluted in 1 $\times$ PBS), then sonicated at 3 microns three times 15 sec. After sonication, the additional Triton-X was added to final concentration of 1% Triton-X. Cell lysates were spinned at 16 100 rcf for 20 minutes at 4 °C. Meanwhile, the S-protein agarose beads were washed with lysis buffer. After centrifugation, supernatants from cell lysates were collected. Relative protein concentration in samples was measured by Bio-Rad protein assay and samples were diluted to the same concentration. Next, the supernatants from cell lysates were incubated overnight with 20 μl S-protein agarose beads at 4 °C with gentle rotation. Following day, the lysates-beads mixture was spinned and supernatant discarded. Beads were three times washed with 1xPBS and resuspended in 25 μl of 2 $\times$ Sample buffer.

4.2.7 Bio-Rad protein assay

Bio-Rad protein assay, based on the method of Bradford (1976), was performed according to the manufacturer's protocol.

4.2.8 Lambda phosphatase assay

The immunoprecipitated protein on A/G beads was carefully washed with 1 $\times$ PBS, mixed with 1 $\times$ phosphatase buffer supplemented with $MgCl_2$ and 400 units of Lambda phosphatase (Table 4.8) and incubated at 30 °C for 20 minutes.One half of the immunoprecipitated protein was used as mock control. After the Lambda phosphatase treatment, the beads were spinned and supernatatnt was discarded. Finally, 25 μl of 2 $\times$ SB with bromphenol blue was added to the beads and boiled for 5 min.

Table 4.8: Lambda Protein Phosphatase assay

Components		**Lambda Protein Phosphatase**	**Mock control**
Protein on A/G beads	[μl]	20	20
ddH_2O	[μl]	59	60
10 $\times$ Lambda Protein Phosphatase buffer	[μl]	10	10
10 $\times$ $MnCl_2$	[μl]	10	10
Lambda Protein Phosphatase	[μl]	1	0
Total volume	[μl]	100	100

4.2.9 Quantitative reverse transcription PCR (qRT PCR)

4.2.9.1 RNA isolation

Total RNA was isolated using TRI Reagent according to the manufacturer's protocol. The cells were lysed directly on cell culture plate with TRI Reagent (0.5 ml per $1 - 5 \times 10^6$ cells). Next, 100 μl of cold 1-bromo-3-chloropropane was added and incubated at room temperature for 7 minutes. Then the mixture was spinned at 12 000 rcf for 15 minutes at 4 °C. Next, the aqueous phase was transferred into the fresh tube and appropriate amount of isopropanol was added. It was shaken and incubated at room temperature for 7 minutes. Then the mixture was spinned at 12 000 rcf for 10 minutes at 4 °C. The supernatant was removed and pellet was washed with 1ml of 75% ethanol, and spinned at 7 500 rcf for 5 minutes at 4 °C. The pellet was air-dried, resuspended in acceptable volume of RNase-free water and incubated at 58 °C for 5 minutes. The concentration of samples was determined via NanoDrop® ND-1000 Spectrophotometer and samples were diluted to the same concentration.

4.2.9.2 Reverse transcription PCR (RT-PCR)

First strand cDNA was synthesized from 200 ng of total RNA with random hexamer primers using High-Capacity cDNA Reverse Transcription Kit. RT master mix and RNA samples mixture were prepared as described in the Table 4.9. The reverse transcription was run on PTC-200 DNA Engine Cycler using setting described in the Table 4.10. The concentration of samples was determined via NanoDrop® ND-1000 Spectrophotometer and samples were diluted to the same concentration.

Table 4.9: RT-PCR master-mix and RNA samples mixture (per one reaction)

10 × RT Buffer	[μl]	2
ddH_2O	[μl]	11.2
25 × dNTP mix (100 mM)	[μl]	0.8
10 × RT Random Primers	[μl]	2
RNase inhibitor	[μl]	1
Reverse Transcriptase MultiScribe	[μl]	1
RNA 100 μg/μl	[μl]	2
Total volume	[μl]	20

Table 4.10: The setting of RT-PCR program

Step	**Temperature**	**Time**
1	25 °C	10 minutes
2	37 °C	120 minutes
3	85 °C	5 minutes
4	4 °C	forever

4.2.9.3 Quantitative reverse transcription PCR (qRT PCR)

Quantitative reverse transcription PCR was performed on ABI Prism 7300 using SYBR Green I Master Mix. The PCR master mix and cDNA mixtures were prepared as described in the Table 4.11. The setting of ABI Prism 7300 was according to the manufacturer's protocol, see the Table 4.12. The relative cDNA amount was estimated by a standard curve, data normalized to a-tubulin. For quantification of Wip1 were used following primers:
forward: 5'- GGGAGTGATGGACTTTGGAA-3'
reverse: 5'- CAAGATTGTCCATGCTCACC-3'

For quantification of α-tubulin were used following primers:
forward: 5'-GAGTGCATCTCCATCCACGTT-3'
reverse: 5'-TAGAGCTCCCAGCAGGCATT-3'

qRT- PCR was performed in triplicates, the presented results mean the average value.

Table 4.11: PCR master-mix and RNA samples mixture (per one reaction)

cDNA (350 ng/μ)	[μl]	2.5
SYBR Green I Master Mix*	[μl]	6.25
Primers (2.5 uM, forward +rewers)	[μl]	1.5
ddH2O	[μl]	2.25
Total volume	[μl]	12.5

SYBR Green I Master Mix contains SYBR Green I dye, ROX passive reference dye, HotStarTaq DNA Polymerase, and a dNTP mix in an optimized buffer

Table 4.12: The setting of qRT-PCR program including dissociation analysis

Step	**Temperature**	**Time**
1	50 °C	2 minutes
2	95 °C	10 minutes
3	95 °C	15 seconds
4	60 °C	1 minute
5	*40 × repeated the steps 3 and 4*	
6	95 °C	15 seconds
7	60 °C	30 seconds
8	95 °C	15 seconds
9	4 °C	forever

4.2.10 DNA cloning

4.2.10.1 Amplification of DNA insert trough PCR

The DNA insert was amplified from template by the PCR reaction. The PCR reaction mixture and the setting of PCR program are described in Table 4.13 and Table 4.14, respectively.

Table 4.13: PCR mix

Component	Volume	Final concentration
ddH_2O	33.5 μl	-
5 $\times$ Phusion HF Buffer	10 μl	1 $\times$
10 mM dNTPs mixture	1 μl	200 μM for each dNTP
10 μM Primer forward (stock)	2 μl	0.5 μM
10 μM Primer revese (stock)	2 μl	0.5 μM
Template DNA 50 ng/μl	1 μl	1 ng/μl
Phusion DNA polymerase	0.5 μl	0.01 unit
Total reaction volume	50 μl	-

4.2.10.2 DNA electrophoresis

DNA electrophoresis was performed according to the standard protocols using 1% or 2% agarose gels. Gels were run in the TAE buffer (Tris-acetate-EDTA; pH 8.0) at constant voltage 100 V. DNA was visualized by ethidium bromide and UV-transluminator.

4.2.10.3 DNA gel isolation

DNA fragments were isolated from gel via commercially available QIAquick® Gel extraction Kit according to the kit instructions.

Table 4.14: The setting of PCR program

Step	Temperature	Time
1	95 °C	10 minutes
2	95 °C	40 seconds
3	60 °C	50 seconds
4	72 °C	1 minute 15 seconds
5	*33 $\times$ repeated the steps 2 thru 4*	
6	72 °C	2 minutes
7	15 °C	forever

4.2.10.4 DNA digest

The DNA digest was performed with 5 units of restriction enzyme, incubated overnight, using the buffer and temperature as recommended by manufacturer.

4.2.10.5 DNA ligation

The DNA fragments were ligated into DNA backbones with T4 ligase. The amount of fragment used for ligation was approximately 5 $\times$ larger than the amount of backbone. The 5'end of backbone was dephoshorylated by Shrimp alkaline phosphatase (SAP) to prevent ligation of an empty vector. 1 unit of SAP was added to the digested backbone and mixture was incubated at 37 °C for 1 hour. The ligation was performed by 1 unit of T4 ligase in 1 $\times$ T4 DNA ligase buffer at room temperature, overnight.

4.2.10.6 Bacterial transfection

Competent DH5α bacteria were thawed on ice. Consequently, the ligation mixture was added to the bacteria and incubated on ice for 10 minutes. Next, the bacteria were transferred to the heat-block tempered to 42 °C and incubated for 90 seconds, then the bacteria were incubated on ice for 5 minutes. After that 1 ml of LB medium was added and bacteria were incubated at 37 °C for 1 hour. Finally, the transformation mixtures were pipetted onto agar plates with corresponding antibiotics and spread around using a sterilized, bent glass rod spreader. Agar plates were incubated overnight at 37 °C.

4.2.10.7 Plasmid isolation

Selected bacterial colonies were transferred to the 3 ml of LB media, with corresponding antibiotics and incubated overnight at 37 °C, with gentle shaking. Following day, the plasmid DNA was isolated using commercially available JETSTAR 2.0 Plasmid Miniprep Kit. The plasmid DNA isolation was performed according to the kit instructions. Concentration of isolated DNA was measured by NanoDrop® ND-1000 Spectrophotometer.

4.2.10.8 Cloning of pWip1-EGFP

The Wip1-D314A insert was amplified from pcdna4TO-Wip1-D314A template by PCR (Methods) using the following primers:
forward: 5'-AAGCTTGGCCATGGCGGGGCTGTACTCG-3'
reverse: 5'-GGATCCGCAAACACAAACATTTTC-3'

The forward PCR primer includes HindIII restriction site at the 5'-end and a Kozak sequence. The reverse PCR primer includes BamHI restriction site and does not contain any stop codon. After the PCR we added one more amplification step at 68 °C with Taq polymerase that generates T-overhangs and enables subsequent ligation into pGEM-T easy plasmid. DNA fragment corresponding to Wip1-D314A (3.4 kbp) was isolated from agarose gel and ligated into pGEM-T easy. Subsequently, we amplified and isolated pGEM-T-Wip1-D314A from DH5α. Then we cut fragment containing Wip1-D314A using HindIII and BamHI and isolated it from gel. The backbone pEGFPN3 was digested in the same way. Finally we ligated Wip1-D314A into pEGFP-N3 and seeded on kanamycin plates. Plasmid DNA was isolated from individual colonies and screened by digest with SacII. Positive clones were validated by sequencing.

4.2.10.9 Cloning of pLAP-Wip1-S40A-D314A and pLAP-Wip1-S40D-D314A

We cut the 390 bp fragment containing the S40A and S40D point mutations from pcdna4TO-Wip1-D314A-S40A and pcdna4TO-Wip1-D314A-S40D (kindly provided by Libor Macůrek), respectively, using the subsequent digest with KpnI and Cfr9I. The pLAP-Wip1-D314A backbone was digested in the same way. All fragments were isolated from gel and fragments containing the S40A and S40D were ligated into pLAP-Wip1-D314A and seeded on kanamycin plates. Plasmid DNA was isolated from individual colonies and screened by digest with SacII. pLAP-Wip1-S40A-D314A and pLAP-Wip1-S40D-D314A vectors were validated by sequencing.

4.2.11 Western blot densitometry analysis

The western blot densitometry analysis was performed in ImageJ software (Abramoff *et al.*, 2004; Rasband, 1997-2011.). We used MBF_ImageJ build, with collection of plugins organized by Tony Collins, Wright Cell Imaging Facility, Toronto Western Research Institute MacBiophotonics (2010). The densitometry analysis was done according to the software documentation instructions. The X-ray films were scanned at 300 dpi as 16-bit grayscale and saved in lossless TIFF format. No image adjustments were made prior to densitometry analysis. The results were normalized to the loading control (α-tubulin) from the same gel.

5

Results

5.1 Validation and preparation of tools

In the beginning, we aimed to validate our tools for subsequent studies of Wip1, particularly the commercially available Wip1 antibody (Bethyl Laboratories) and anti- Wip1 siRNAs. To validate the specificity of this antibody, we performed knock-down experiments and also compared its reactivity with another available antibody. We also aimed to establish cell lines stably expressing epitope-tagged versions of Wip1.

5.1.1 shRNA knock-down of Wip1

As the first step in validation, we transfected U2OS cell with two independent shRNA plasmids. U2OS cell were transfected with 2 μg of plasmid DNA using FuGENE® 6 Transfection Reagent (Methods). Plasmids pLKO.1 WipH4 and pLKO.1 WipH6 carry different anti-Wip1 shRNAs sequence, and pLKO.1 EMPTY, was used as control (plasmids were described previously in Macůrek *et al.* (2010). Transfected cells were selected with 2 μg/ml purmycin for 6 days, with new medium and puromycin changed every two days. After 6 days cells were passaged onto 6 cm plates and the next day harvested for western-blot analysis (Figure 5.1 A). Densitometry analysis of western blot results revealed that relative of 80 kDa band decreased to 47% in case of WipH4 shRNA knockdown, respectively to 65% in case of WipH6 shRNA knock-down compared to empty vector sample (Figure 5.1 B).

Observed decrease in signal intensity in knockdown samples compared to control speaks in favor of Wip1 Bethyl antibody specificity.

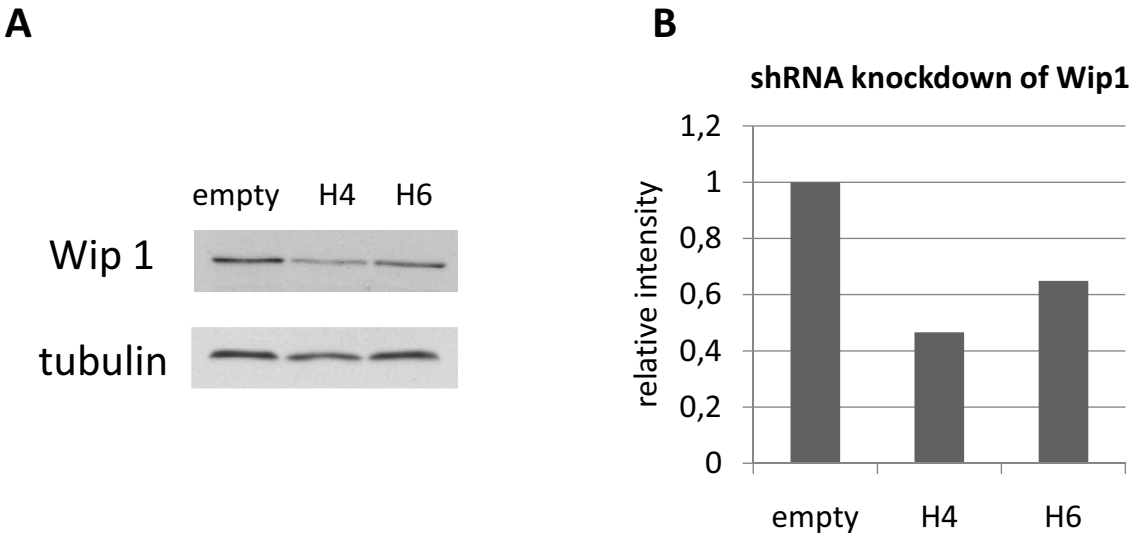

Figure 5.1: shRNA knockdown of Wip1 demonstrates specificity of Wip1 Bethyl antibody - **A:** western-blot analysis of shRNA knock down, first line – control empty vector, second line - WipH4 shRNA, third line - WipH4 shRNA; Total cell lysates were probed with indicated antibodies. **B:** densitometry analysis of western blot, relative signal given by Wip1 Bethyl antibody decreased to 47% in case of WipH4 shRNA knockdown, respectively to 65% in case of WipH6 shRNA knock-down compared to empty vector sample.

5.1.2 siRNA knock-down of Wip1

Four different siRNA were used for siRNA knockdown – siRNA Wip1-1, siRNA Wip1-2, siRNA Wip1-3, siRNA Wip1-4, as well as an equimolar pool of them (Dharmacon). siRNA against GAPDH was used as control. U2OS cell were transfected with 1 nM of siRNAs using RNAi MAX reagent (see Methods). Then, at 48 hours, cells were split 1:2 into two new 6-well plates. At 72 hours cells were harvested for westernblot analysis and qRT-PCR analysis. qRT-PCR results revealed good efficiency of tested siRNAs (Figure 5.2 C). The most effective knock-down was obtained by siRNA Wip1-2, siRNA Wip1-4 and by siRNAs equimolar pool. Western blot analysis and subsequent densitometry showed that decrease in the signal of Wip1 Bethyl antibody was in perfect correlation with qRT-PCR results (Figure 5.2 A and B). According to our results from Wip1 knockdown experiments,

we concluded that Wip1 Bethyl antibody specifically stains a band corresponding to Wip1 full-length protein at about 80 kDa. Notably, the intensity of a 60 kDa band stained by Wip1 Bethyl antibody does not correspond to Wip1 protein, according to the fact that there was no evident decrease in its intensity after siRNAs treatment suggesting that it represents cross-reactivity with an unrelated protein (Figure 5.3). In addition, we compared staining patterns of Wip1 Bethyl antibody and Wip1 Santa Cruz antibody (Figure 5.3). In contrast to the staining pattern of anti-Wip1 antibody from Bethyl, anti-Wip1 St. Cruz antibody specifically recognizes a major band at 60 kDa which probably corresponds to a splice variant of Wip1 (Figure 5.3). In contrast to the staining pattern of anti-Wip1 antibody from Bethyl, anti-Wip1 St. Cruz antibody dominantly recognizes a major band at 60 kDa which probably corresponds to a splice variant of Wip1.

5.1.3 Immunoprecipitation of endogenous Wip1

U2OS cell were plated in 10-cm plates. After 24 hours cell were harvested and lysates were immunoprecipitated with Wip1 St. Cruz antibody. For immunoprecipitation control, one sample was prepared without addition of antibody and one without addition of lysate. Immunoprecipitates together with corresponding lysates were analyzed by western blot, using Wip1 Bethyl antibody (Figure 5.4). We detected a single band at 80 kDa in the sample immunoprecipitated with lysates and Wip1 St. Cruz antibody and no signal was detected in control samples. This result further confirmed the specificity of Wip1 Bethyl antibody.

5.1.4 Preparation of stable monoclonal cell lines expressing Wip1 fusion proteins

For purposes of study of Wip1 dynamics and regulation, we decided to prepare stable monoclonal cell lines expressing Wip1 fusion proteins. We transfected U2OS cells with EGFP-Wip1 and pLap-Wip1-D314A plasmids which we had currently at hand (plasmids were obtained from Libor Macurek). EGFP-Wip1 codes for Wip1 protein N-terminally fused with GFP. pLap-Wip1-D314A codes for phosphatase dead mutant of Wip1 (Wip1-D314-A) fused with N-terminal LAP tag. LAP tag

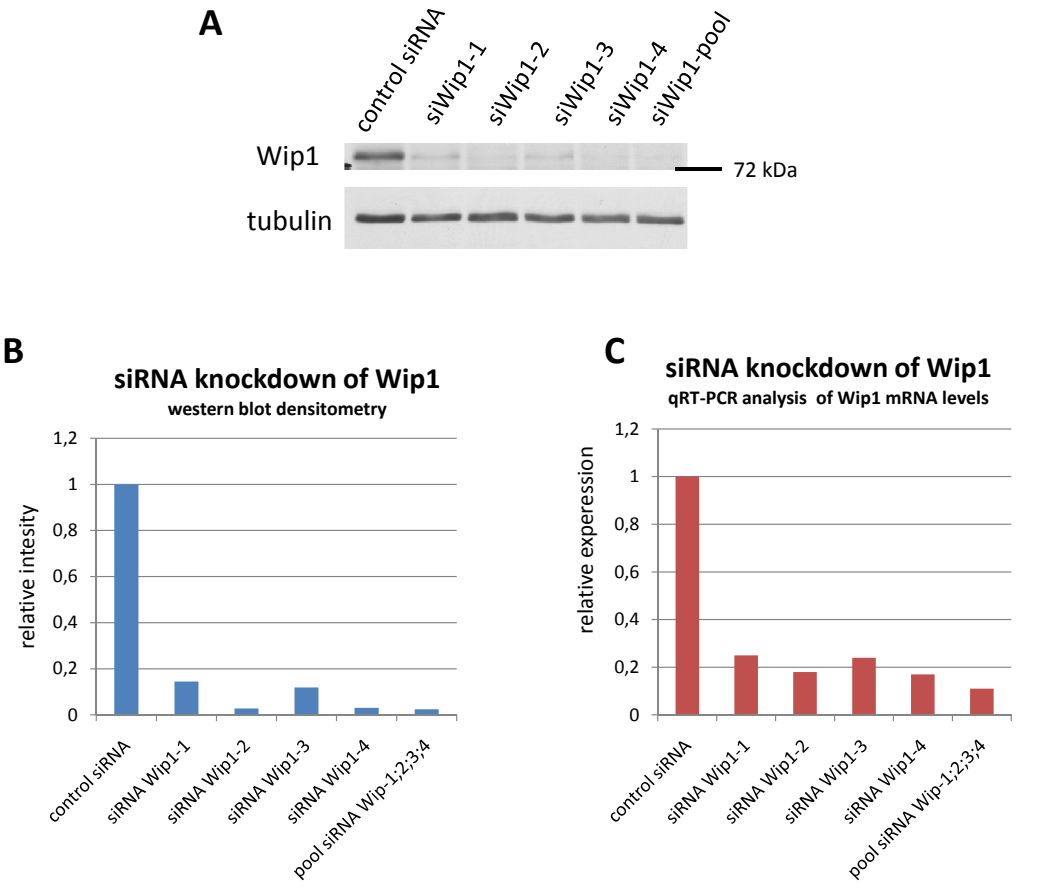

Figure 5.2: siRNA knockdown of Wip1 demonstrates specificity of Wip1 Bethyl antibody - U2OS cells were transfected with four independent siRNAs, siRNAs pool and control siRNA. **A:** Western blot analysis of siRNA knockdown; Total cell lysates were probed with indicated antibodies. **B:** Densitometry analysis of western blot - anti Wip1 siRNAs demonstrate overall good efficiency. **C:** qRT-PCR analysis of siRNA knock-down showed the perfect correlation with western-blot results.

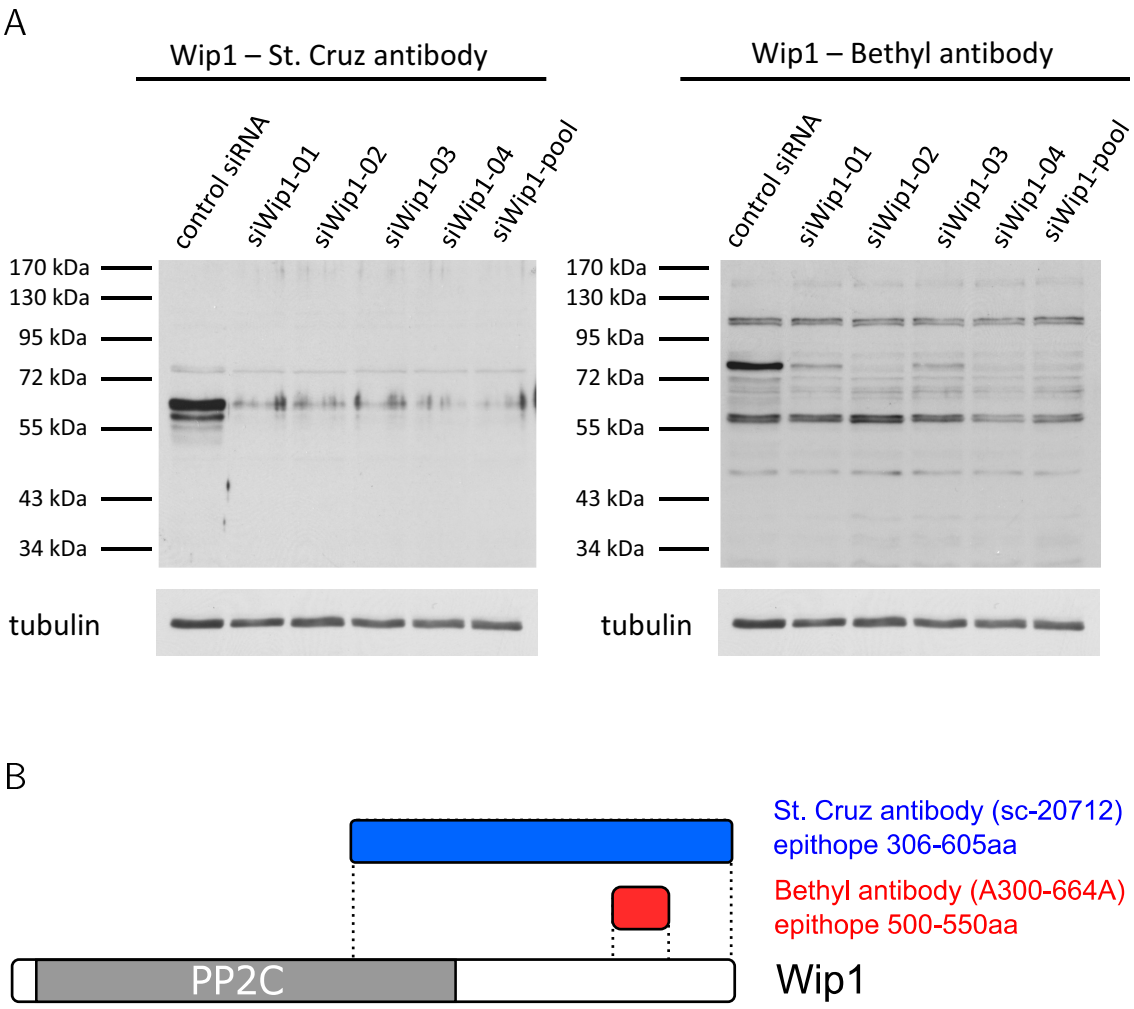

Figure 5.3: siRNA knockdown of Wip1 – comparison of Wip1 St. Cruz antibody and Wip1 Bethyl antibody - **A:** U2OS cells were transfected with four independent siRNAs, total cell lysates were probed with indicated antibodies. **B:** Scheme of epitopes recognized by Wip1 St. Cruz antibody and Wip1 Bethyl antibody (made according to the vendor's information).

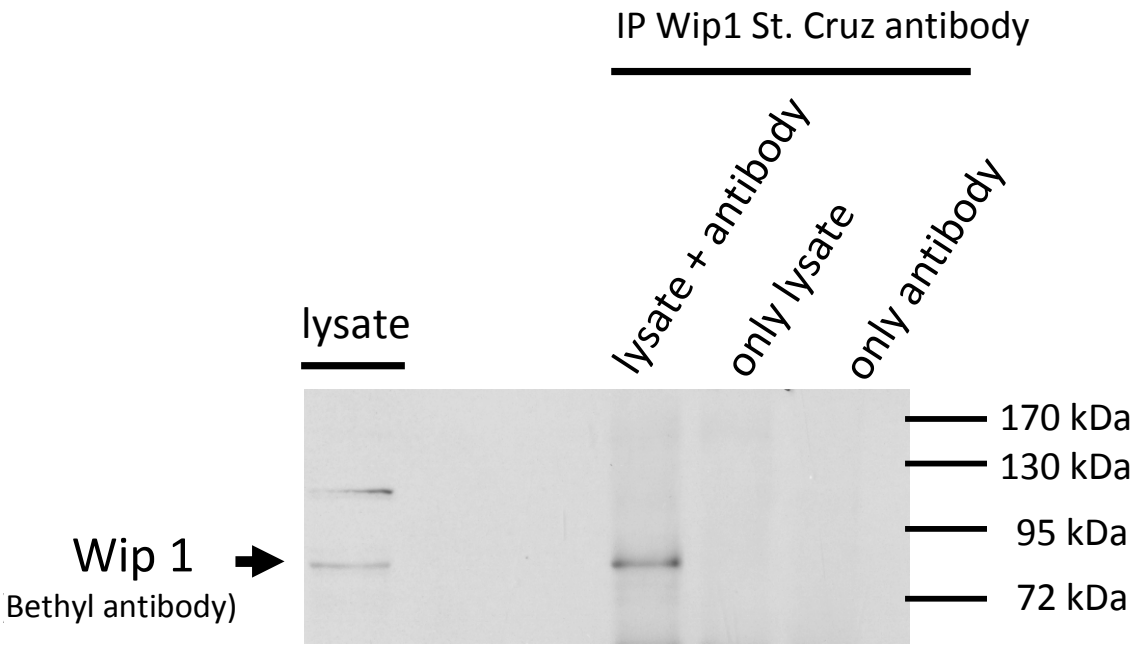

Figure 5.4: Immunoprecipitation of endogenous Wip1 with Wip1 St. Cruz antibody, probed by Wip1 Bethyl antibody - This result further confirmed the specificity of Wip1 Bethyl antibody.

system consists of S-protein, TEV site and GFP. This system can be beneficially used in a modified tandem affinity purification (TAP) to isolate interacting partners of Wip1 in high purity for mass-spec analysis Cheeseman and Desai (2005). So far we did not proceed to TAP and mass-spec analysis by the end of finishing this thesis, yet we plan to perform them in the near future.

U2OS cells were plated in 6-well plate at density 150 000 cells per well. After 24 hours, cells were transfected with 2 μg of plasmids carrying fusion Wip1 cDNA and gentamicin resistance and 0.4 μg pBABE PURO using Fugene transfection reagent. We employed cotransfection with pBABE PURO, carrying puromycin resistance, due to the fact that we repeatedly failed to perform effective selection using G418. Cells were selected by 2 μg/ml puromycin for 6 days, with fresh media and antibitotic exchange once per 2 day. Fluorescent microscopy observations of both transfectants showed nuclear localization of Wip1 fusion proteins, demonstrating that fused-N-terminal tags did not alter Wip1 physiological localization. After puromycin selection, we performed a limiting dilution and plated cells into 96-well plates. For cultivation in these low dilutions we used D-MEM medium with

increased concentration of FBS to 15% v/v and no antibiotics were added. After one week we screened wells for viable and EGFP positive colonies, which were raised presumably from one ancestor cell. Positive colonies were chosen for further propagation. EGFP-Wip1 transfected cells exhibited decreased viability during propagation, in contrast pLap-Wip1-D314A transfectants, and we were not able to obtain viable monoclonal cell line in this cloning. For pLap-Wip1-D314A transfectants, four clones were selected and analyzed by western-blotting (Figure 5.5). Western blot results revealed expected band of LAP-Wip1 below 130 kDa. In addition, the band around 80 kDa corresponding to Wip1 protein increased in intensity. This reactivity might be caused by a preterminal stop in translation of LAP-Wip1 fusion protein. Alternatively, proteolytic cleavage of Wip1 fusion proteins may be responsible for presence of this shortened variant of exogenous Wip1. In aim to determine the level of exogenous Wip1 protein overexpression to endogenous Wip1, we diluted serially the sample lysates of clone 1 and compared them to Wip1 levels in nontransfected U2OS (Figure 5.6 A). Densitometry analysis of western blot results showed that levels of exogenous LAP-Wip1 are approximately 40 fold higher compared to levels of endogenous Wip1 in U2OS cells (Figure 5.6 B). The cell line U2OS LAP-Wip1-D314A Clone 1 was used further for our studies, as described later.

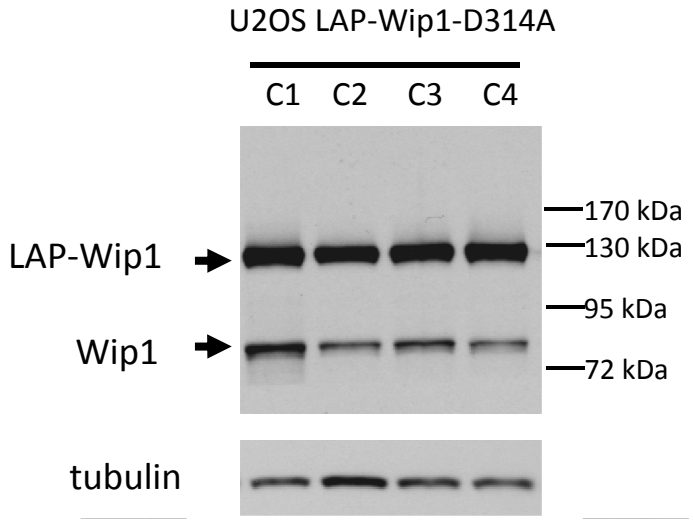

Figure 5.5: Prepared monoclonal U2OS cell lines express LAP-Wip1 - Total cell lysates were probed with indicated antibodies.

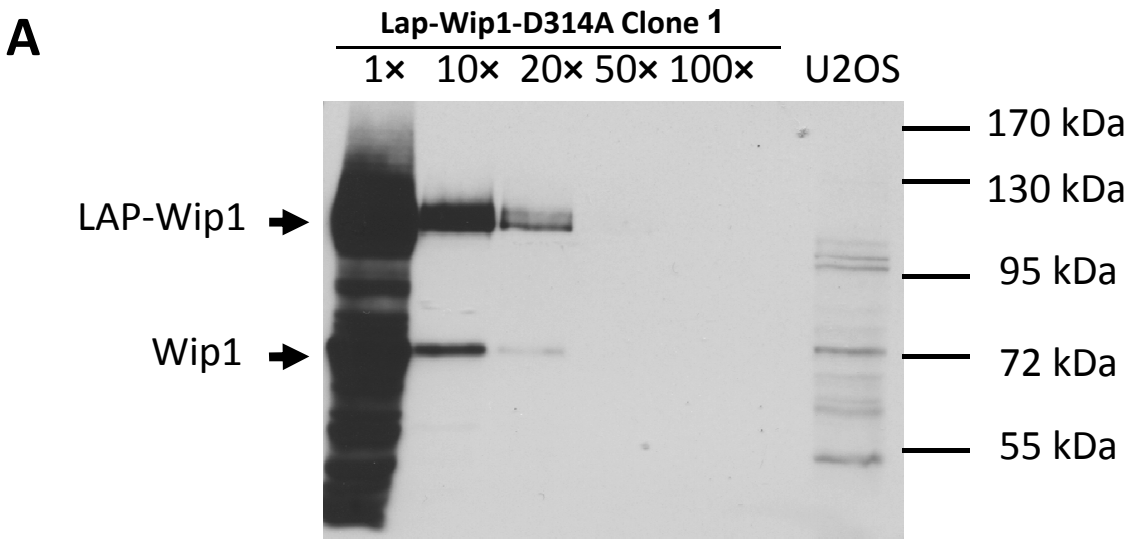

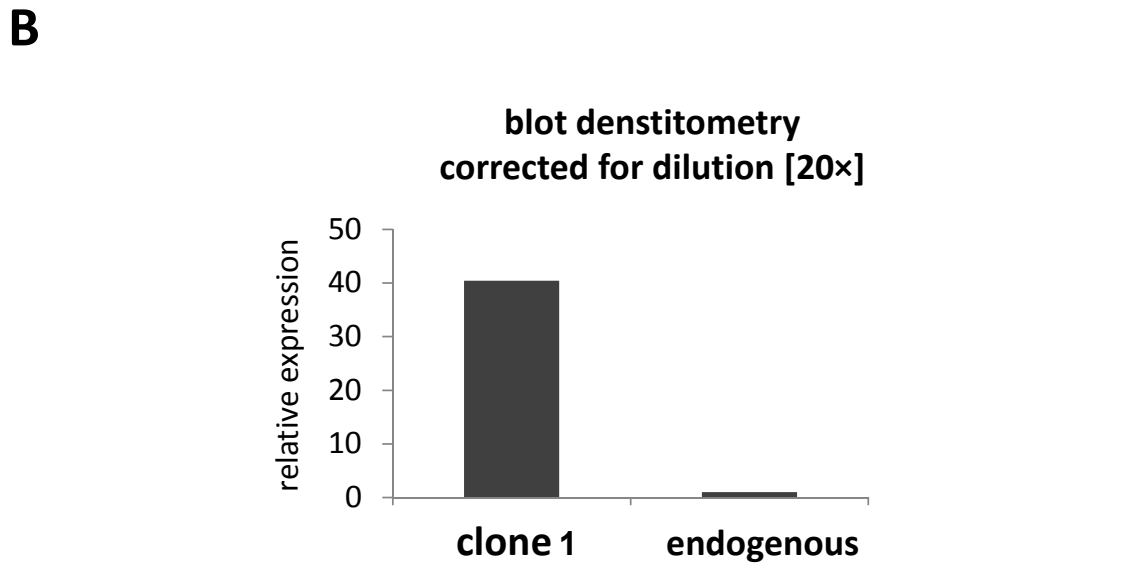

Figure 5.6: Levels of exogenous LAP-Wip1 are approximately 40 fold higher compared to levels of endogenous Wip1 in U2OS cells - **A:** Western blot results, the total lysate from pLap-Wip1-D314A clone 1 was serially diluted as indicated. Total cell lysates were probed with indicated antibodies. **A:** Densitometry quantification of western blot result, corrected for dilution 20 $\times$.

5.1.5 FACS sorting of transfectants according to their GFP signal intensity

As the monoclonal cell line expressing pLAP-Wip1-D314A showed a considerable overexpression of the fusion protein which might interfere with some analysis, we decided to sort transfected cells based on their GFP signal intensity by FACS.

U2OS cell were plated on 6-well plate with density 150 000 cells per well. After 24 hours cells were transfected with lower amount of plasmid DNA than in previous case, particularly with 0.5 μg of plasmid carrying fusion Wip1 and 0.1 μg of pBABE PURO using Fugene transfection reagent. Cells were selected by 2 μg/ml puromycin for 5 days. After selection cells were transferred to serum-free D-MEM and subjected to FASC sorting. Both transfectants were sorted into four different groups based on their GFP signal intensity. These cells were further propagated and analyzed by western blot for levels of exogenous Wip1 (Figure 5.7). Group SW4 (sorted group expressing GFP-Wip1) exhibited highest fluorescence signal from GFP-Wip1 wild-type transfectants, however, this signal was localized to cytosol and presumably attributed to expression of sole GFP. Correspondingly, western-blot analysis showed a relatively low level for SW4. With SW4 exception, all other sorted population demonstrated anticipated GFP-Wip1 expression, increasing from SW1 to SW3 and from DS1 to DS4 (sorted groups expressing LAP-Wip-D314A 1 to 4), respectively. SW1, SW2, SD1 and SD2 populations, exhibiting lower GFP-Wip1 expression, were chosen for subsequent cloning.

5.1.6 Single cell cloning by FACS sorting in 96 well

SW1, SW2, SD1 and SD2 populations were amplified to approximately 10^7 cells, transferred to serum-free D-MEM and subjected to FASC single cell cloning. All four populations were sorted into two 96-well per population, one cell per well. Sorted clones were further propagated and selected clones were subsequently analyzed for GFP-Wip1 expression by western-blot. Single cell cloning by FACS sorting was not very effective for SD1 and SD2 populations, as we obtained very few positive clones. This problem did not occurred during sorting of SW1 and SW2 populations. For cultivation of sorted-cells in low dilutions, we used D-MEM

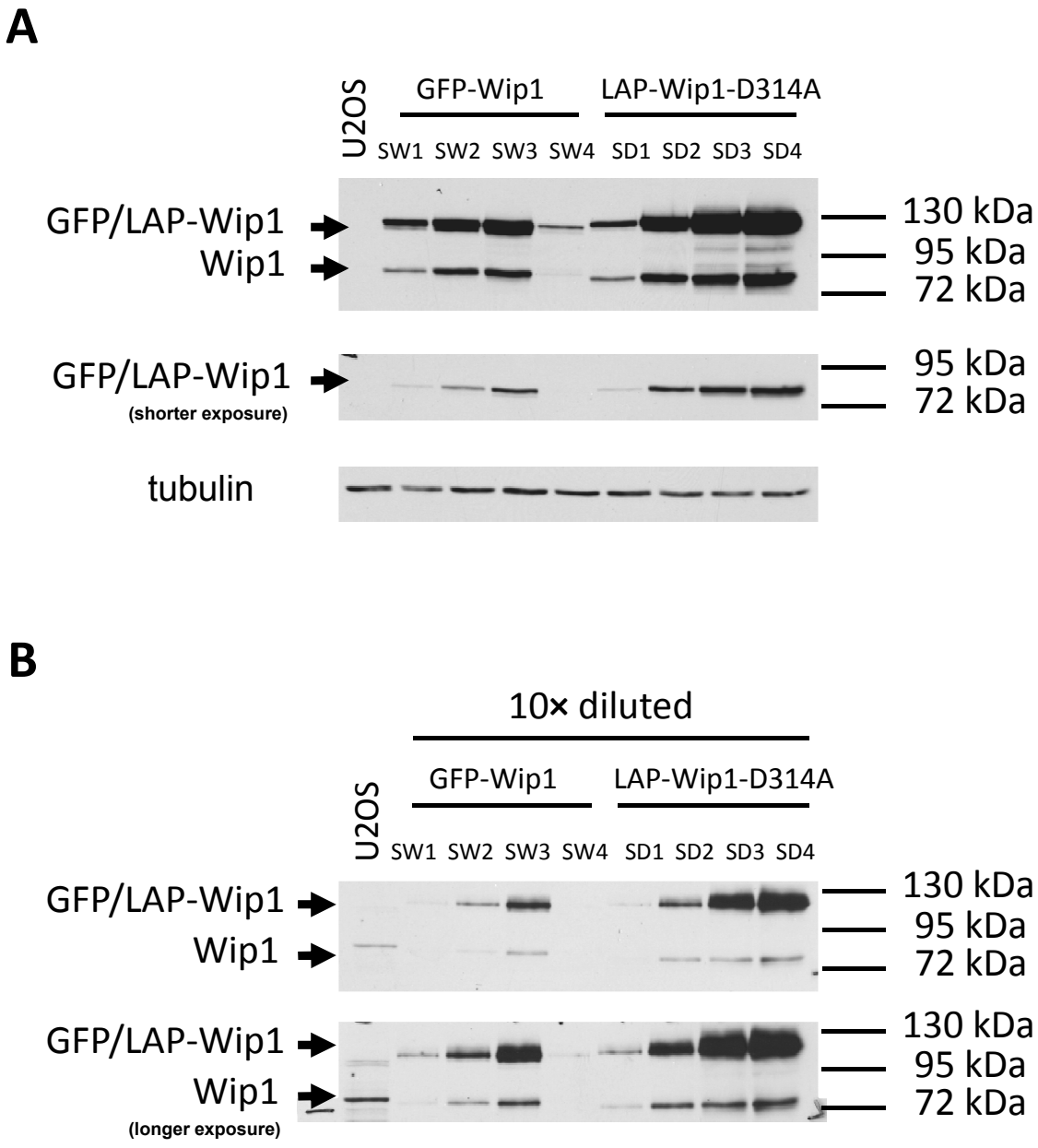

Figure 5.7: pLAP-Wip1-D314A and pEGFP-Wip1 transfectants were sorted by FASC according to their GFP signal intensity - **A:** western blot validated successful sorting in all populations, except the SW4 **B:** Total cell lysates were 10 $\times$ diluted to enable comparison of exogenous and endogenous Wip1. Levels of exogenous LAP-Wip1 in SW1 and SD1 are approximately 4 fold higher compared to levels of endogenous Wip1 in U2OS cells (according to western-blot densitometry). Total cell lysates were probed with indicated antibodies.

medium with increased concentration of FBS to 20% (v/v) and no antibiotics were added. After one week we screened using fluorescent microscopy wells for viable and EGFP positive colonies, which were raised presumably from one ancestor cell. Positive colonies were chosen for further propagation. The expression of fusion Wip1 in selected clones was validated by western blot (Figure 5.8).

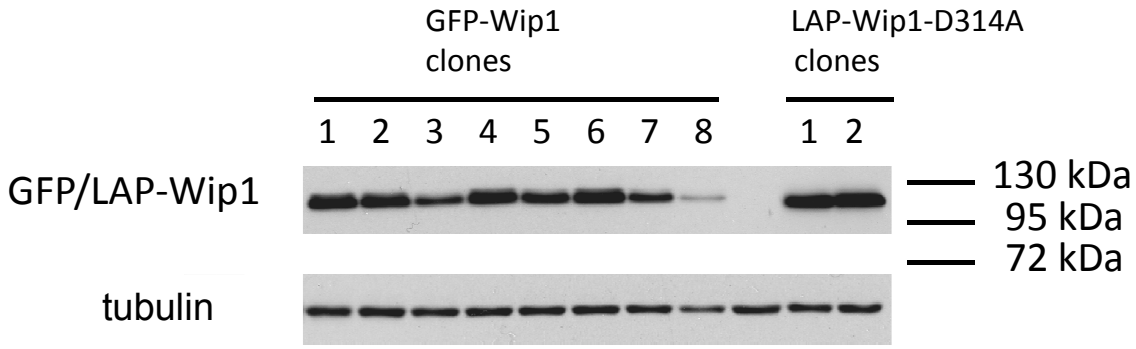

Figure 5.8: Prepared monoclonal U2OS cell lines express GFP-Wip1 and LAP-Wip1 - Total cell lysates were probed with indicated antibodies.

5.1.7 Cloned vectors

5.1.7.1 Cloning of pWip1-EGFP

pWip1-EGFP features the CMV promoter and RNAi nontargetable phosphatase dead Wip1 fused at the C-terminus with EGFP (Figure 5.9). The pWip1-EGFP vector carries the kanamycin resistance. We prepared this vector to test whether the C-terminally tagged Wip1 will behave differently to currently available N-terminally fused Wip1. We did not proceed to this comparison by the time of finishing this thesis. Detailed cloning procedure is described in Methods.

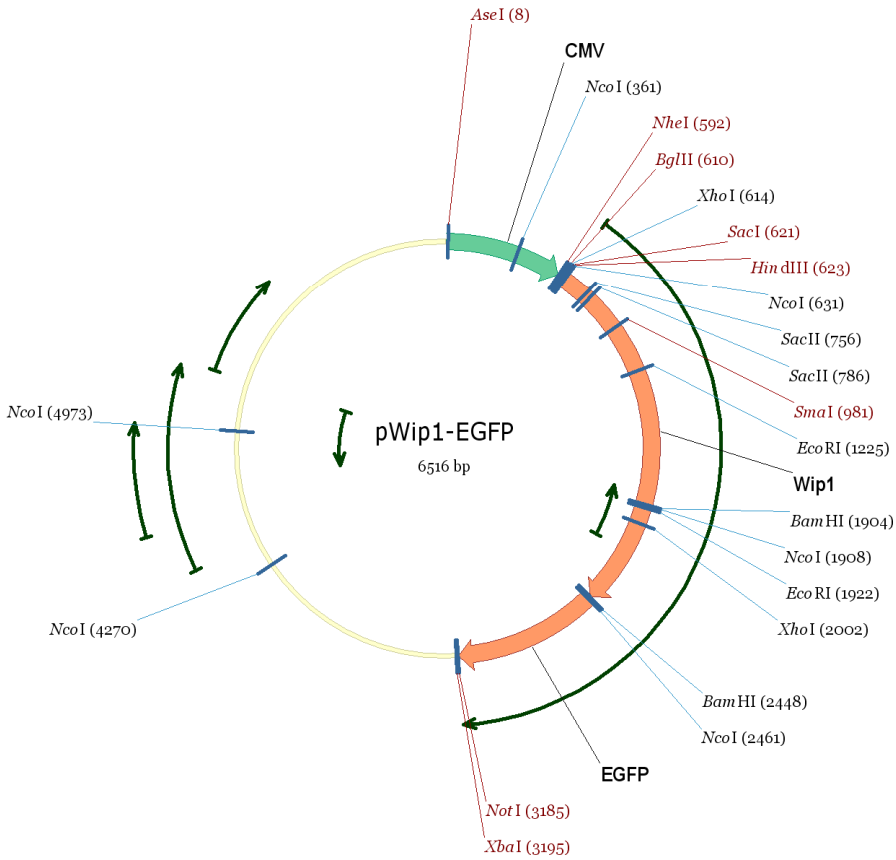

Figure 5.9: Plasmid map of pWip1-D314A-EGFP - the map was generated in Vector NTI® software

5.1.7.2 Cloning of pLAP-Wip1-S40A-D314A and pLAP-Wip1-S40D-D314A

pLAP-Wip1-S40A-D314A and pLAP-Wip1-S40D-D314A feature the mutated serine 40 to alanine and aspartic acid, the non-phosphorylable variant and the phosphate-mimicking variant on background of a phosphatase inactive Wip1-D314A mutant (Figure 5.10). Both vectors carry the kanamycin resistance. These vectors will be used in the future for functional characterization of the phosphorylation of Wip1 during mitosis (Chapter 6.3). Detailed cloning procedure is described in Methods.

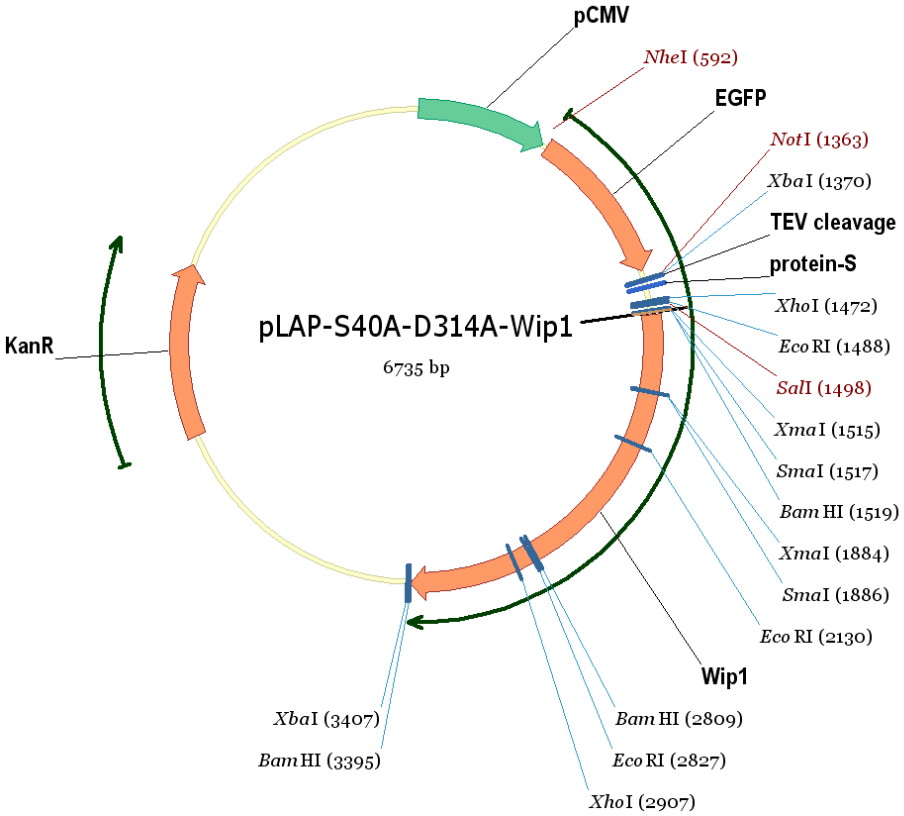

Figure 5.10: Plasmid map of pLAP-Wip1-S40A-D314 (the map of pLAP-Wip1-S40D-D314A is identical aside except of S40 point mutation) - the map was generated in Vector NTI® software

5.2 Dynamics of DNA damage response pathways upon γ-irradiation

Temporal dynamics of p53 upon γ-irradiation has been described to exhibit series of discrete pulses (Chapter 3.6). At the outset of our study, we wanted to reproduce Galit Lahav results and detect the protein dynamics on population level with western blot technique. For this reason we set up our pilot experiment in identical way to the ones published by Galit Lahav lab's Batchelor *et al.* (2008). We irradiated the MCF7 cell line with a dose of 10 Gy and monitored the dynamics of selected DDR proteins up to 12 hours after irradiation. In parallel to examining the total levels of p53, we extensively broadened the scope of observed DDR proteins and assayed also gammaH2AX, p53-pS15, p21, Wip1, Chk2-pT68, total p38MAPK and p38MAPKpT180/pY182, MAPKAPK-2-pS334, and MKK3-pS189/MKK6-pS207. Although the p38MAPK-MAPKAPK-2 pathway is not usually considered as a canonical DNA damage response pathway, we were interested in its dynamics since it is tightly connected to the regulation of p53 circuit (Chapter 3.2). Moreover, recently reported findings of Reinhardt et al., (2010) suggest that the p38MAPK-MAPKAP-K2 pathway is crucial for prolonged maintenance of the checkpoint, further stressing out its importance.

MCF7 cells were plated in 6-well plates at density 200 000 cells per well. Next day, cells were irradiated by a single dose of 10 Gy. Cells were harvested in one hour intervals up to twelve hours. Samples were analyzed by western blot and results were quantified by densitometric analysis (Figures 5.11, 5.12, 5.13). Phosphorylated version of H2AX (γH2AX) was used as a marker of DNA damage. The levels of γH2AX peaked immediately after irradiation and then gradually declined. The levels of Chk2- pT68 showed a similar trend. We observed the expected pulsative dynamics of p53. The first pulse of p53 reached its maximum in the interval of 2 to 4 hours after irradiation, while the second pulse had its maximum at 8 to 10 hours. The amplitude of the second pulse reached only 60% of the first one. The levels of p53-pS15 perfectly correlated with the first pulse of total p53. On the contrary the second pulse was notably lower. We discuss these results further in Discussion. The levels of Wip1 demonstrate single pulse with phase shift

to the p53 pulses (Figure 5.13). This is in good agreement with the described negative feedback loop between p53 and Wip1. The levels of p21 showed a monotone continuous increase, reaching its maximum around 6 hours after irradiation and remained elevated until the 12 hour. The activity of p38MAPK-MAPKAPK-2 pathway dropped immediately after irradiation, but then again increased. The first pulse of p38MAPK-MAPKAPK-2 reached its maximum at approximately 4 to 6 hours. Notably, second pulse of p38MAPK-MAPKAPK-2 activity rose approximately at 9 hours (Figure 5.12).

Since we were able to reproduce the pulsative dynamics of p53 upon gammairradiation in MCF7 cell, we were keen to investigate whether this dynamics is restricted to MCF7 cell line or whether it represents a general phenomenon. For this reason we performed the γ-irradiation in the same experimental setting on U2OS cell line. The γ-irradiation of U2OS cells was performed in two independent experiments (Figures 5.14, 5.15, 5.16, 5.17, 5.18, 5.19). The levels of γH2AX and Chk2-pT68 showed the similar trend as in case of MCF7 (Figures 5.14, 5.17). Interestingly, p53 levels showed a monotone continuous increase, as opposed to the pulses observed in MCF7 cells (Figures 5.14, 5.17). We deliberate this issue in Discussion. The levels of p53-pS15 exhibit a single pulse (Figures 5.14, 5.17). Conversely to the situations in MCF7 cells, Wip1 levels did not demonstrate the discrete pulse with phase shift to the first p53 pulse, but rather slight continuous increase (Figures 5.16, 5.19). The dynamics of p21 was the same as in case of MCF7 cells aside from fact that in the first experiment the levels of p21 were markedly increased in control, not irradiated sample (Figures 5.16, 5.19). We attribute this to possibly stress-full handling with control sample during transfer of cells to the place of irradiation and back to incubator. Again, we observed the two pulses on of p38MAPK-MAPKAPK-2 pathway activation, although the timing and width of pulses varied between experiments (Figures 5.15, 5.18).

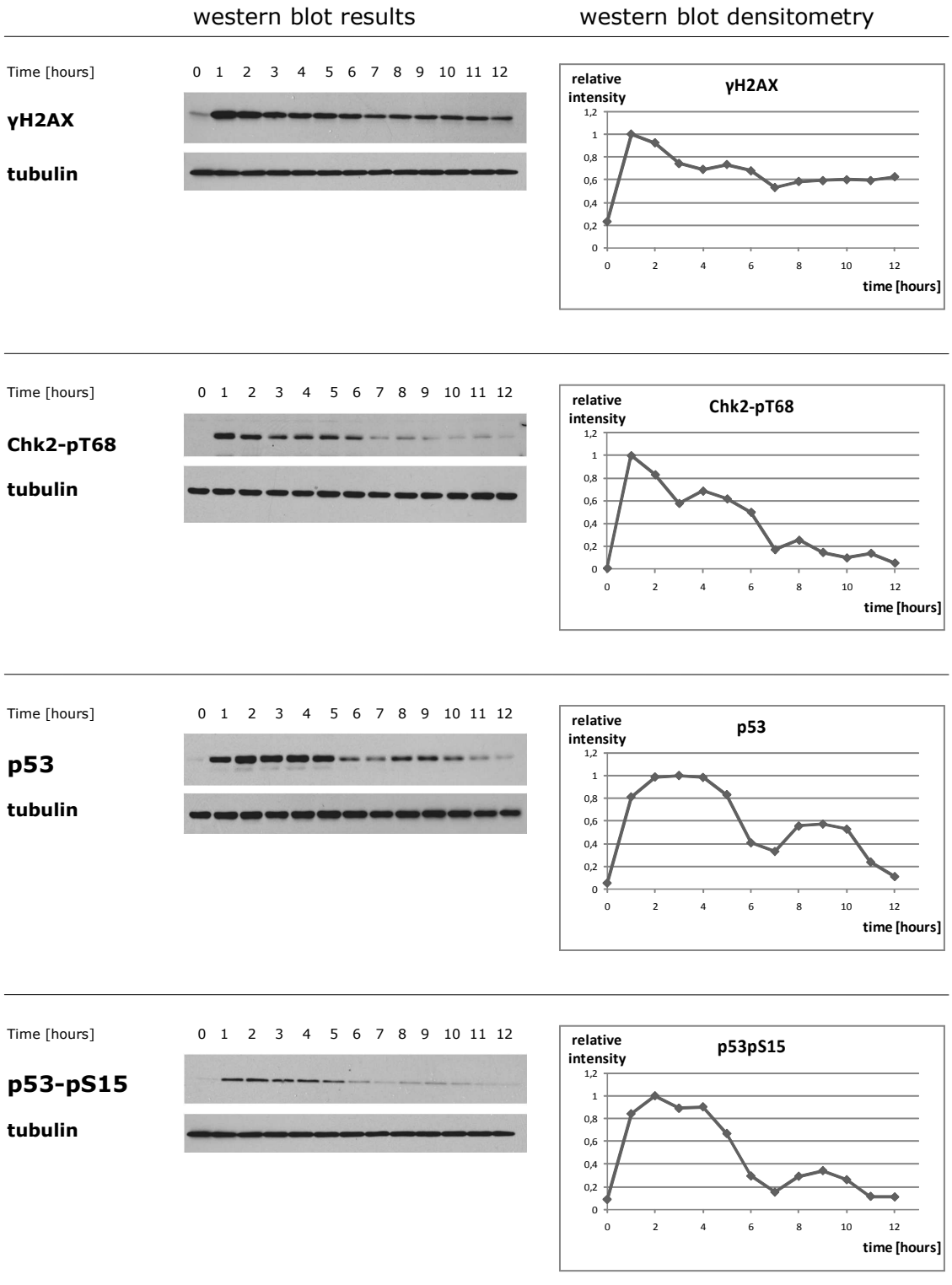

Figure 5.11: MCF7 cells were irradiated with a single dose of 10 Gy and monitored for the dynamics of selected DDR proteins up to 12 hours after irradiation - Exp 1/A. - Total cell lysates were probed with indicated antibodies. The densitometry results were normalized to the loading control (α-tubulin). Details are described in text above.

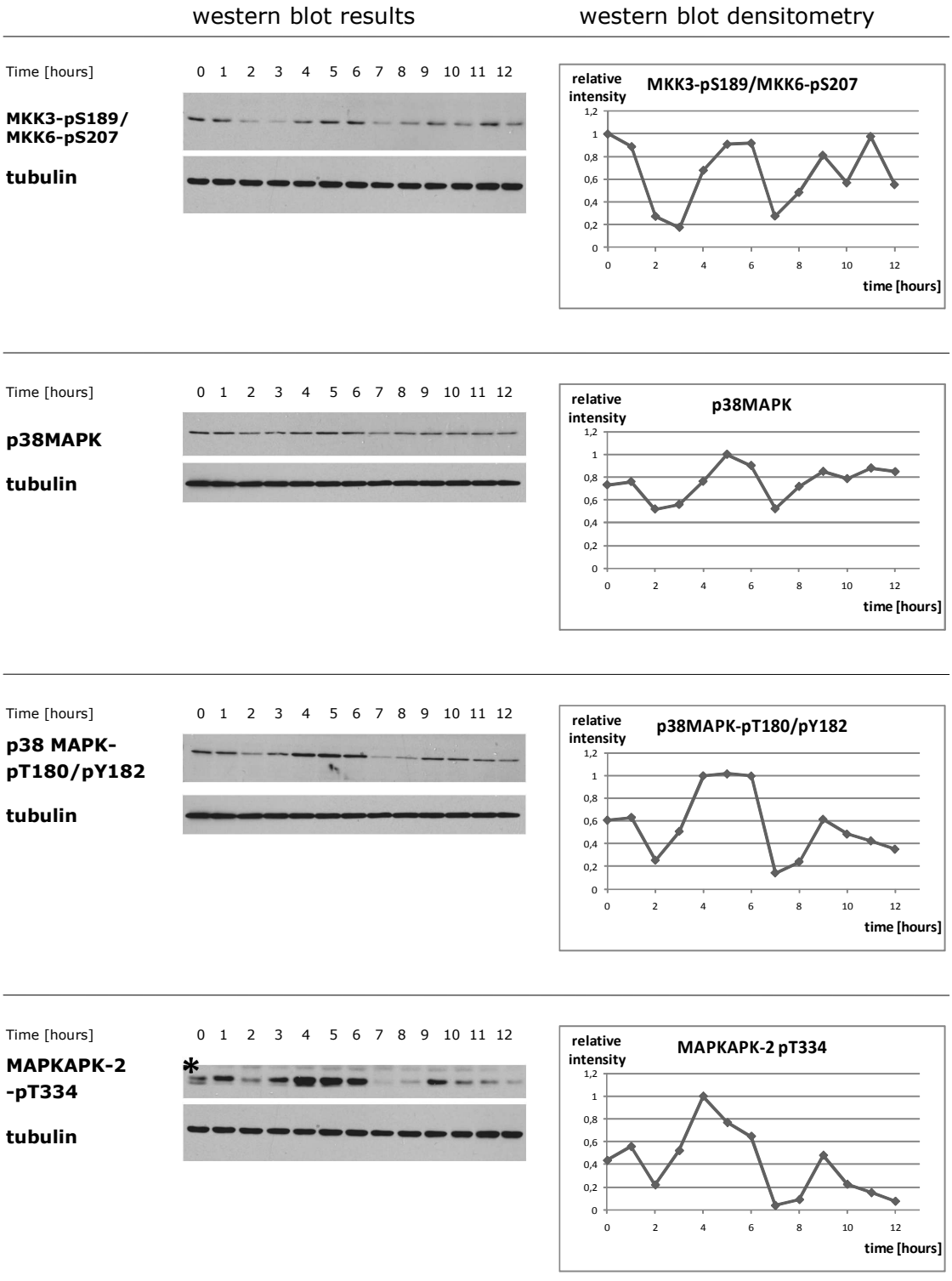

Figure 5.12: MCF7 cells were irradiated with a single dose of 10 Gy and monitored for the dynamics of selected DDR proteins up to 12 hours after irradiation - Exp 1/B - Total cell lysates were probed with indicated antibodies. The densitometry results were normalized to the loading control (α-tubulin). Details are described in text above.

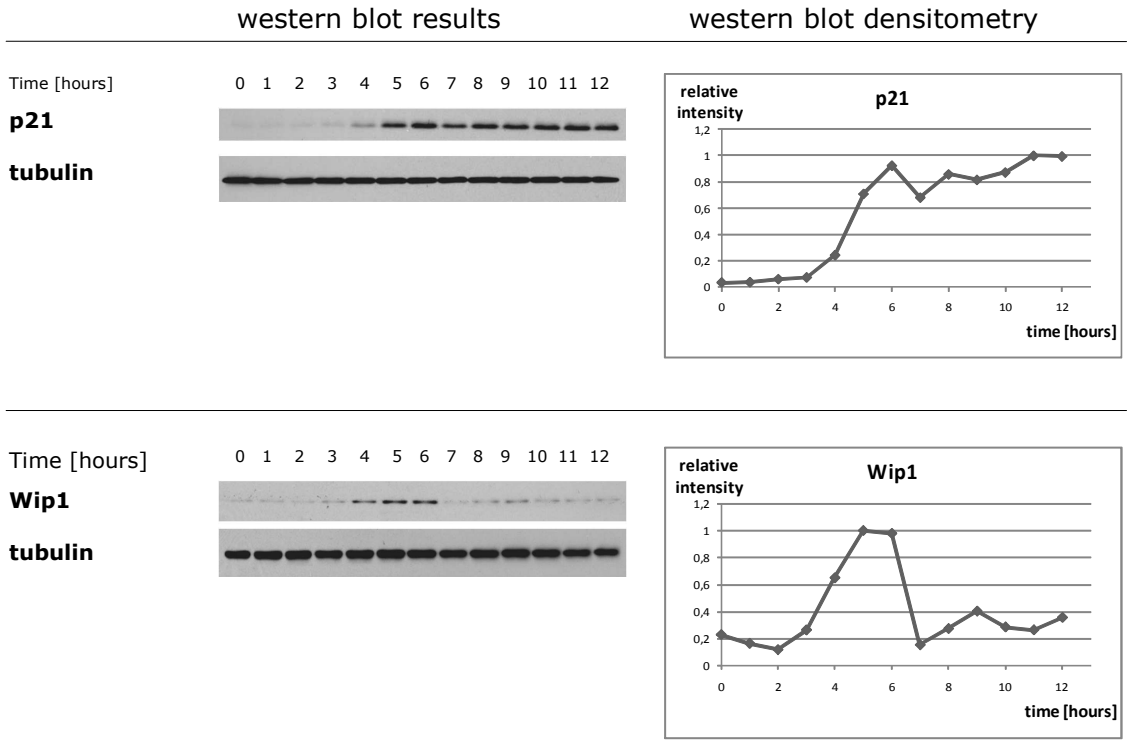

Figure 5.13: MCF7 cells were irradiated with a single dose of 10 Gy and monitored for the dynamics of selected DDR proteins up to 12 hours after irradiation - Exp 1/C - Total cell lysates were probed with indicated antibodies. The densitometry results were normalized to the loading control (α-tubulin). Details are described in text above.

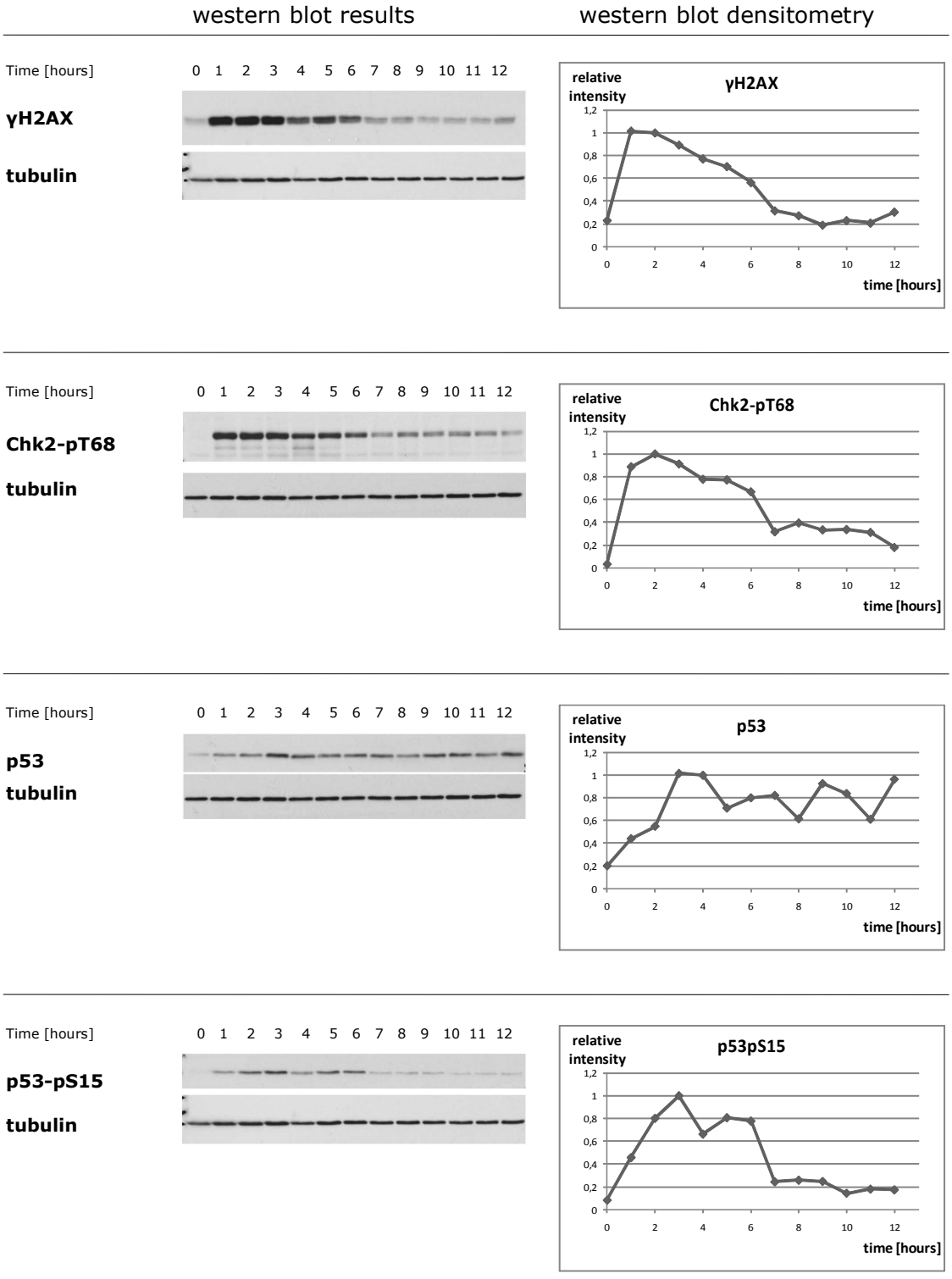

Figure 5.14: U2OS cells were irradiated with a single dose of 10 Gy and monitored for the dynamics of selected DDR proteins up to 12 hours after irradiation - Exp 1/A - Total cell lysates were probed with indicated antibodies. The densitometry results were normalized to the loading control (α-tubulin). Details are described in text above.

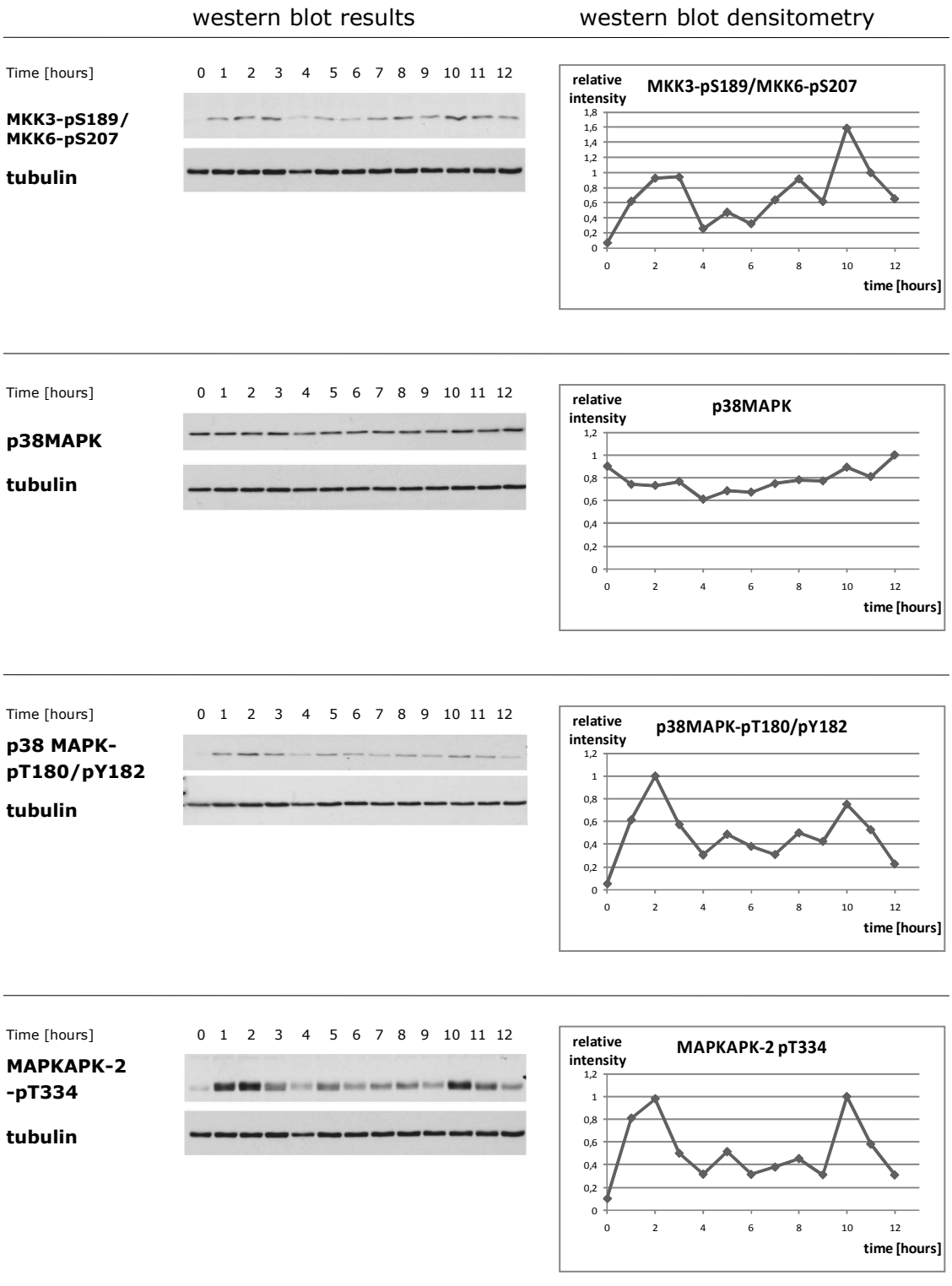

Figure 5.15: U2OS cells were irradiated with a single dose of 10 Gy and monitored for the dynamics of selected DDR proteins up to 12 hours after irradiation - Exp 1/B - Total cell lysates were probed with indicated antibodies. The densitometry results were normalized to the loading control (α-tubulin). Details are described in text above.

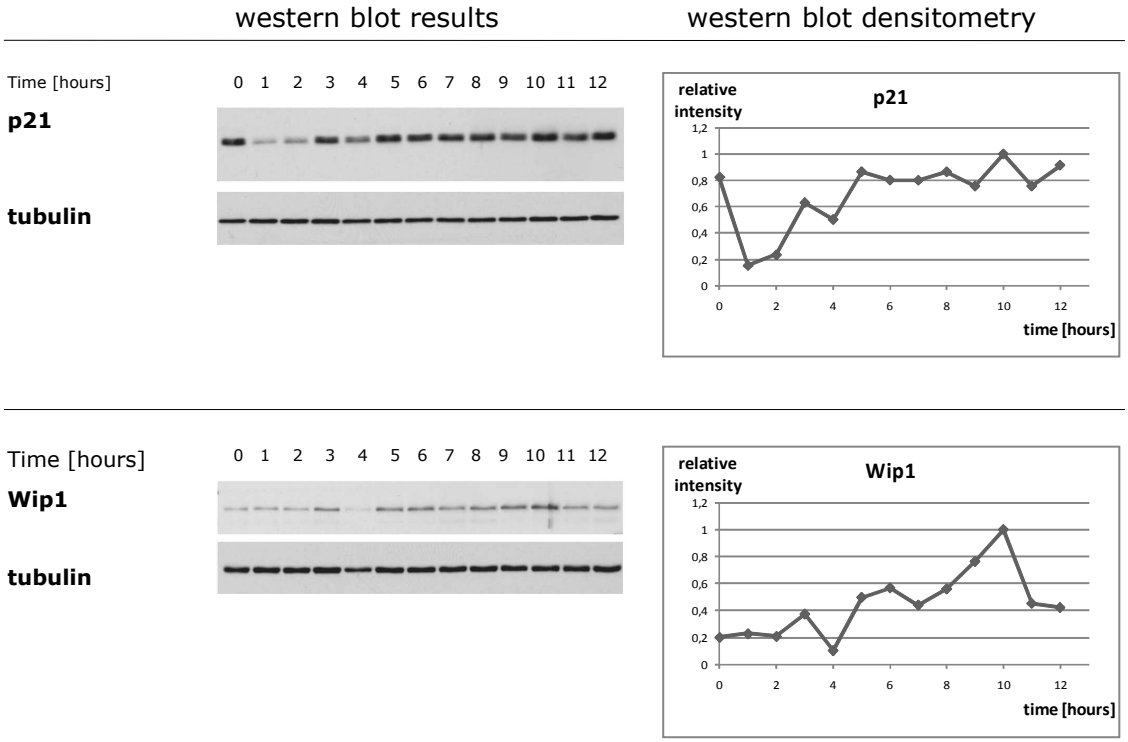

Figure 5.16: U2OS cells were irradiated with a single dose of 10 Gy and monitored for the dynamics of selected DDR proteins up to 12 hours after irradiation - Exp 1/C - Total cell lysates were probed with indicated antibodies. The densitometry results were normalized to the loading control (α-tubulin). Details are described in text above.

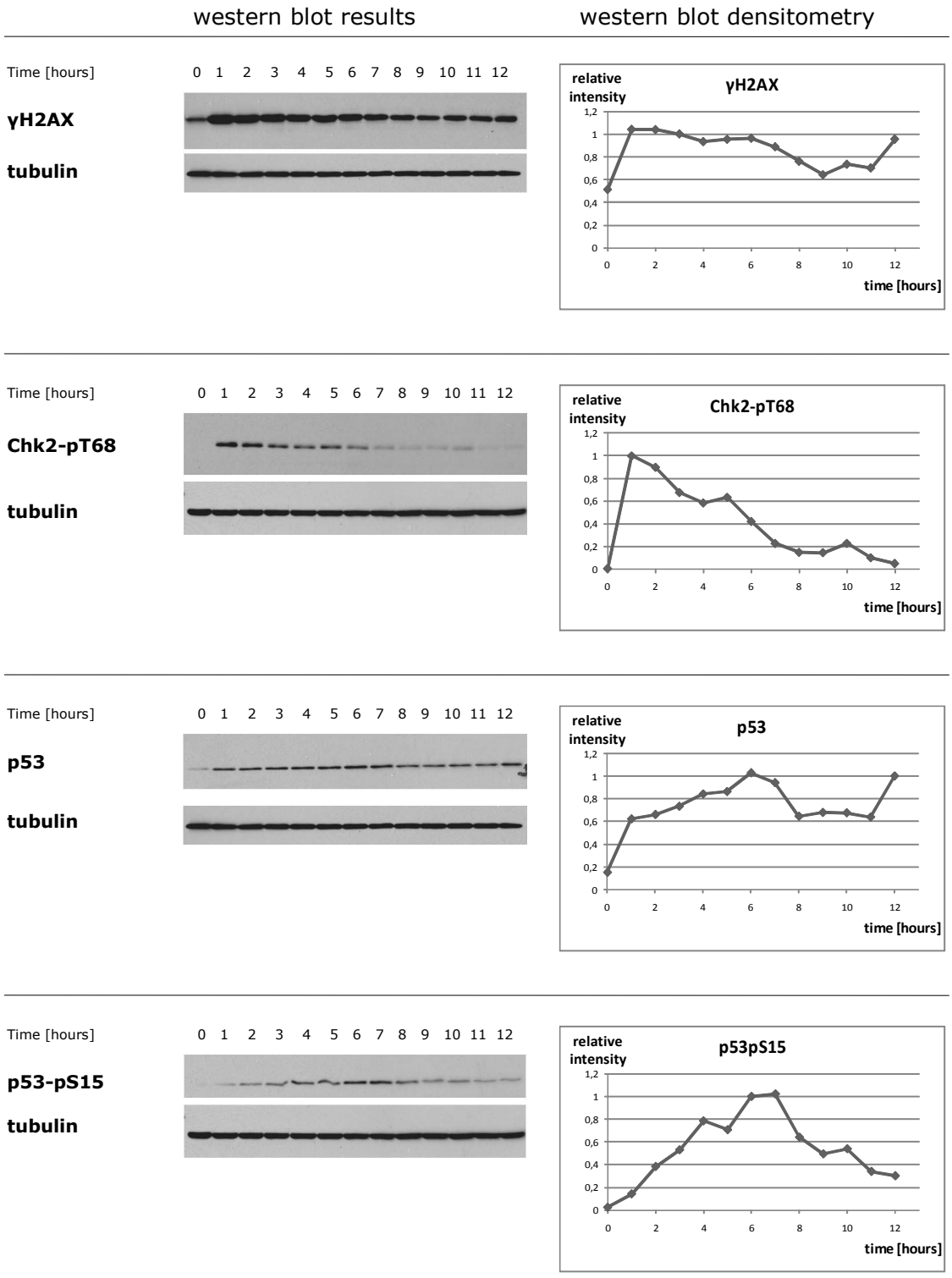

Figure 5.17: U2OS cells were irradiated with a single dose of 10 Gy and monitored for the dynamics of selected DDR proteins up to 12 hours after irradiation - Exp 2/A - Total cell lysates were probed with indicated antibodies. The densitometry results were normalized to the loading control (α-tubulin). Details are described in text above.

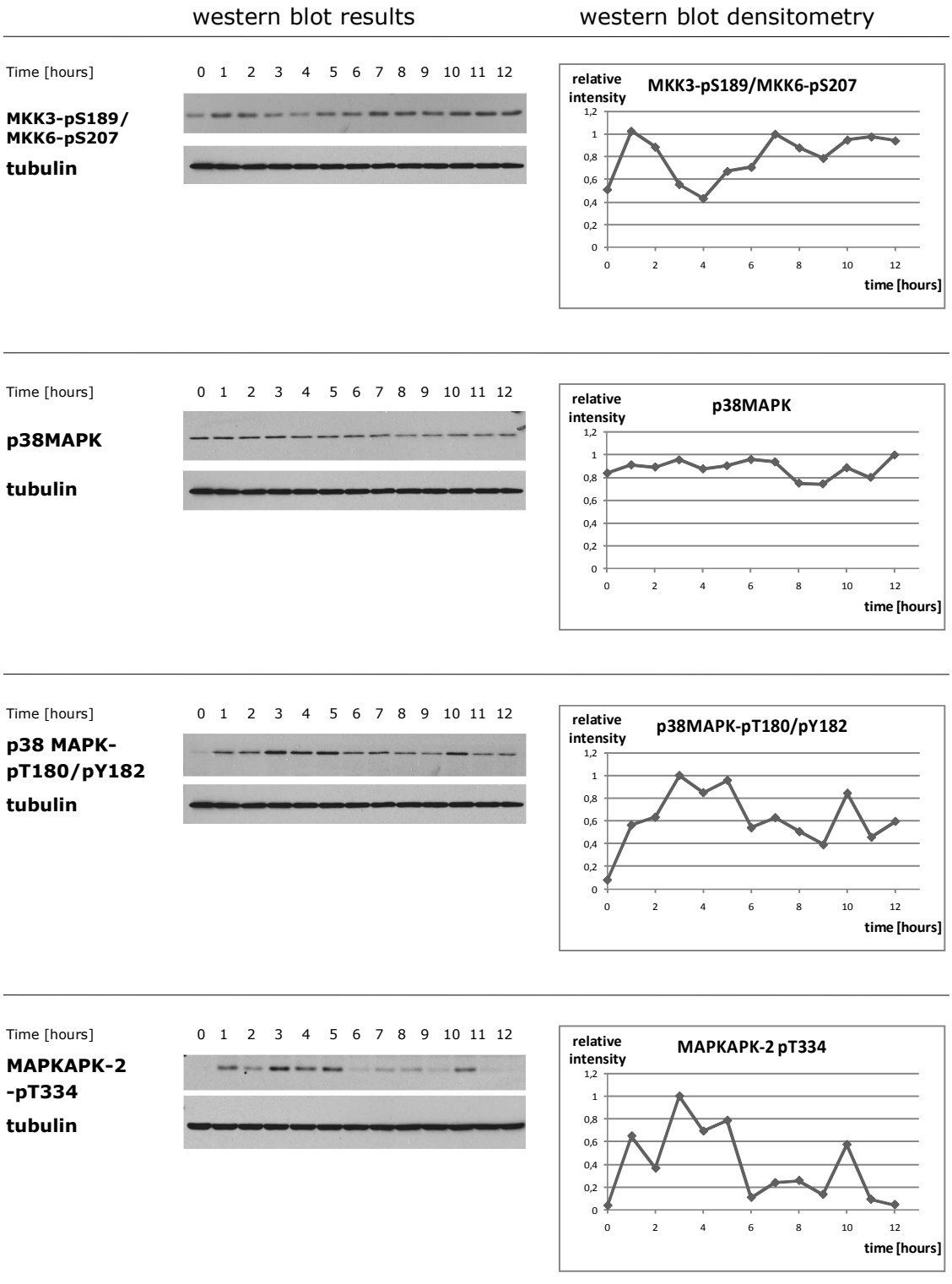

Figure 5.18: U2OS cells were irradiated with a single dose of 10 Gy and monitored for the dynamics of selected DDR proteins up to 12 hours after irradiation - Exp 2/B - Total cell lysates were probed with indicated antibodies. The densitometry results were normalized to the loading control (α-tubulin). Details are described in text above.

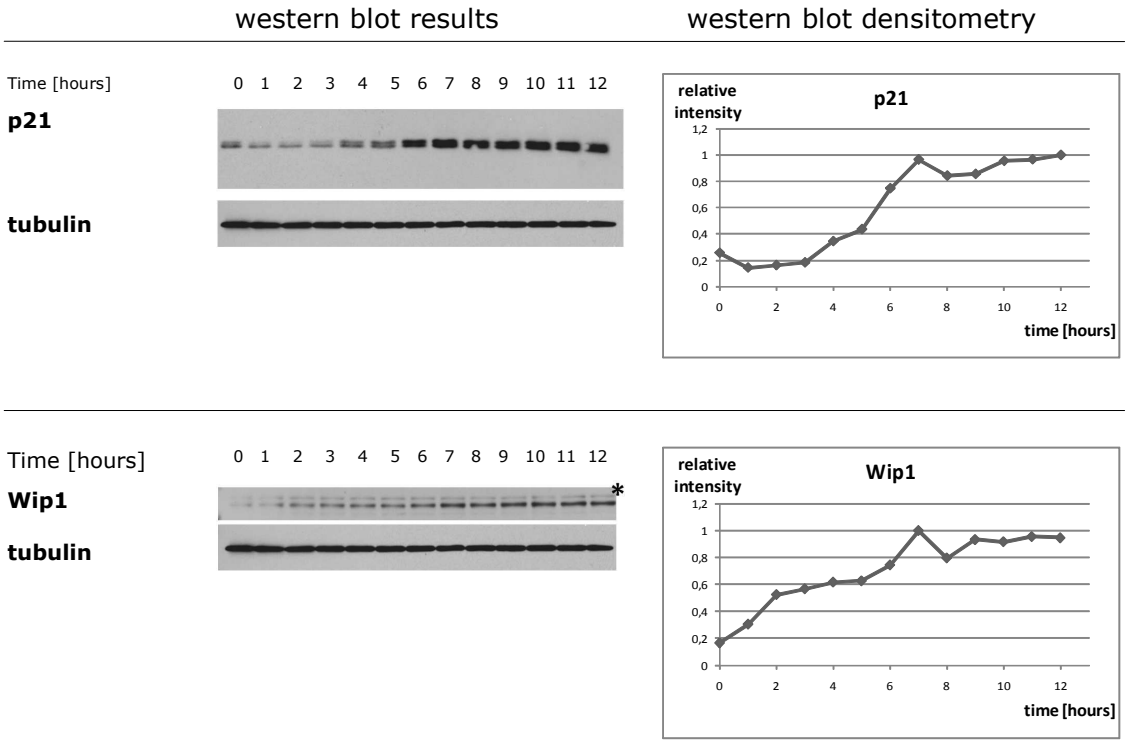

Figure 5.19: U2OS cells were irradiated with a single dose of 10 Gy and monitored for the dynamics of selected DDR proteins up to 12 hours after irradiation - Exp 2/C - Total cell lysates were probed with indicated antibodies. The densitometry results were normalized to the loading control (α-tubulin). Details are described in text above.

5.3 Dynamics of DNA damage response pathways upon UV-C irradion

5.3.1 Determining dose of UV-C irradiation

First we decided to determine an appropriate dose of UV-C irradiation, the one that leads to full activation of DDR, but does not cause apoptotic response. For this aim we irradiated cells by several UV-C doses of increasing intensities (5, 20, 50, 100, 200, 500, 2000 J/m^2) and looked for activation of ATR-Chk1 pathway and cell viability. U2OS cells were plated in 6-cm plates at day prior to irradiation. Two 6-cm plates were used per one irradiation burst. First plate was harvested one hour after irradiation for western-blot analysis (Figure 5.20). Second plate was observed after 24 h for cell viability. At UV-C doses below 20 J/m^2 the majority of cells stayed viable at 24 h after UV-C irradiation. On the contrary at doses above 50 J/m^2 most cells exhibited cell death. Nearly all cells died at dose of 200 J/m^2 and higher. Phosphorylation of Chk1 on serine 317 was used as a marker of activation of ATR-Chk1 pathway. We observed strong increase of this phosphorylation even after relatively low doses (5 J/m^2) of UV-C irradiation and it did not significantly increased further in higher doses. Minor activation of Chk1 detected in the control could be attributed to physiological activation of ATR-Chk1 pathway during S-phase progression. In addition, we checked for activation of ATM-Chk2 pathway, since there have been reported possible cross-talks between ATR-Chk1 and ATM-Chk2. Phosphorylation of Chk2 on threonine 68 was used as the marker of activation of ATM-Chk2 pathway. We were able to detect a substantial increase of this phosporylation in higher UV-C doses, yet to much lower extent than phosphorylation of Chk1. Activation of Chk2 pathway at higher doses of UV-C might be also caused by DNA double strand breaks, which might be caused by excessive DNA damage. We concluded that even relatively low doses of UV-C irradiation lead to full activation of ATR-Chk1 pathway as opposed to activation of ATM-Chk2 pathway. Majority of cells stayed viable at low UV-C doses, below 20 J/m^2, in contrast to higher doses, which led to strong apoptotic response. With respect to these findings we decided to use dose of 10 J/m^2 for our further experiments.

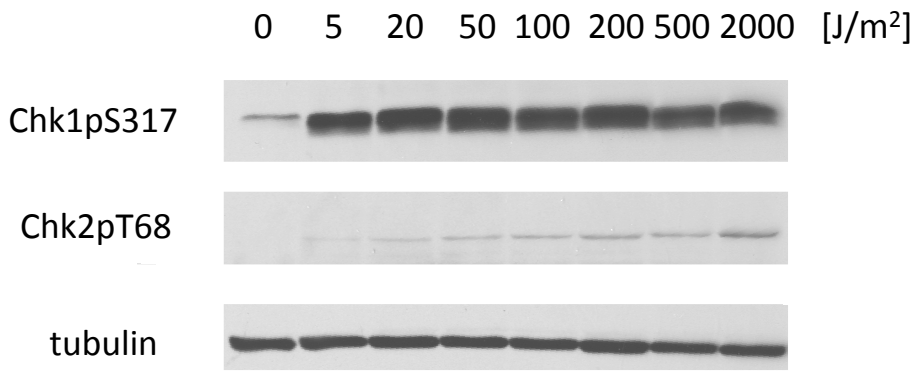

Figure 5.20: UV-C irradiation leads to activation of Chk1 kinase - U2OS cells were irradiated by UV-C doses of 5, 20, 50, 100, 200, 500, 2000 J/m^2; Cells were harvested one hour after irradiation and analyzed through western blot for activation of ATR-Chk1 and ATM-Chk2 pathways – represented by phosphorylation of Chk1, respectively Chk2. Total cell lysates were probed with indicated antibodies. Chk1 reached its full activation even after low doses of UV-C irradiation, on the contrary Chk2 was activated in minor extent and only after high doses of UV-C irradiation. Details are described in text above.

5.3.2 Dynamics of DNA damage response pathways upon UV-C irradion

To compare the dynamics of DDR upon different genotoxic stresses, we irradiated the U2OS cell line with a dose of 10 J/m^2 UV-C and monitored the dynamics of selected DDR proteins up to 12 hours after irradiation, similarly to experimental setting of γ-irradiation.

U2OS cells were plated on 10 cm plates at density 2×10^6. Next day, the cells near confluence were irradiated by a single short burst of UV-C with intensity 10 J/m^2. Cells were harvested in one hour interval up to twelve hours. Samples were analyzed by western blot and results were quantified by densitometry analysis. The UV-C irradiation of U2OS cells was performed in three independent experiments. In the first experiment only the levels of γH2AX, Chk1-pS317, p53-pS15 and Wip1 were measured due to technical reasons (Figure 5.21). In two remaining experiments we assayed for γH2AX, p53-pS15, p21, Wip1, Chk1-pS317, total p38MAPK and p38MAPK-pT180pY182, MAPKAPK-2-pS334, and MKK3-pS189/MKK6-pS207 (Figures 5.22, 5.23, 5.24, 5.25, 5.26, 5.27). In case of second experiment we excluded the sample from the 10 hour from the densitometry analysis, with respect to the fact that the levels of γH2AX, used as marker of DNA damage, were

notably lower in this sample then in the samples from 9 and 11 hours. We speculate that this sample was probably improperly irradiated. Since the similar results made on MCF7 cells were published during the course of this thesis (Batchelor et al., 2011), we did not reproduce our experiments on this cell line. The levels of γH2AX showed monotone continuous increase during the 12 hours time course (Figures 5.21, 5.22, 5.25). The activation of Chk1 demonstrated single pulse from 1 to approximately 6 hours after irradiation and then slowly decrease (Figures 5.21, 5.22, 5.25). Notably, the levels of p53 and p53pS15 showed good correlation with a monotone continuous increase (Figures 5.21, 5.22, 5.25). Interestingly, p21 levels decreased immediately after irradiation and then again rose in series of two pulses. The timing and width of the first p21 pulse, approximately 3 to 6 hours, correlated well between experiments, the timing of second pulse differed between the independent experiments (Figures 5.24, 5.27). Additionally, we repeatedly observed the two pulses of p38 MAPK-MAPKAPK-2 pathway activation, although the width and timing of pulses vary between experiments (Figures 5.23, 5.26). These observations are discussed in detail in Discussion. The dynamics of Wip1 did not exhibit particularly good correlation between independent experiments (Figures 5.21, 5.24, 5.27). We addressed this issue in following experiments.

5.3.3 The independent measurement of UV-C Crosslinker UV-C dose

The UV-C crosslinker used in our study is designed to deliver the proper dose of UV-C, correcting for the inherent intensity fluctuations that can occur during UV lamp operation (Crosslinkers 800 and 1500 series operation manual; UltraLum). However, during our experiments we doubted about the reproducibility of doses generated by the crosslinker, especially when we used low UV-C doses (short times). For this reason, we measured the UV-C intensity given by UltraLum Crosslinker series 800 by independent UV-C light meter (Lutron Electronic Enterprise Co., Ltd.; model UVC-254) (Figure 5.28) and observed that the intensity of UV-C given by UltraLum crosslinker was variable. The UV-C crosslinker is able to

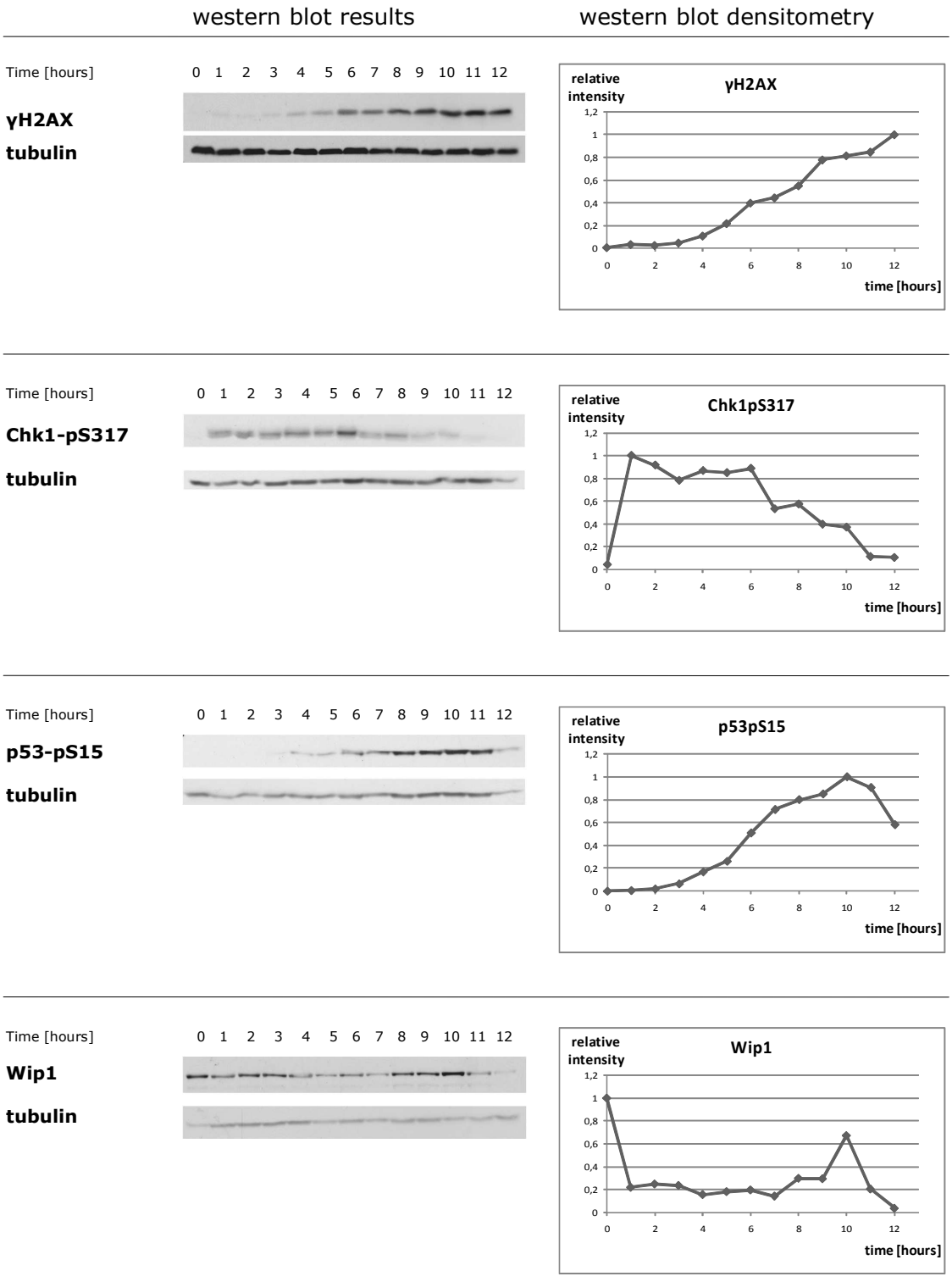

Figure 5.21: U2OS cells were irradiated with a single dose of 10 J/m^2 and monitored for the dynamics of selected DDR proteins up to 12 hours after irradiation - Exp 1/A - Total cell lysates were probed with indicated antibodies. The densitometry results were normalized to the loading control (α-tubulin). Details are described in text above.

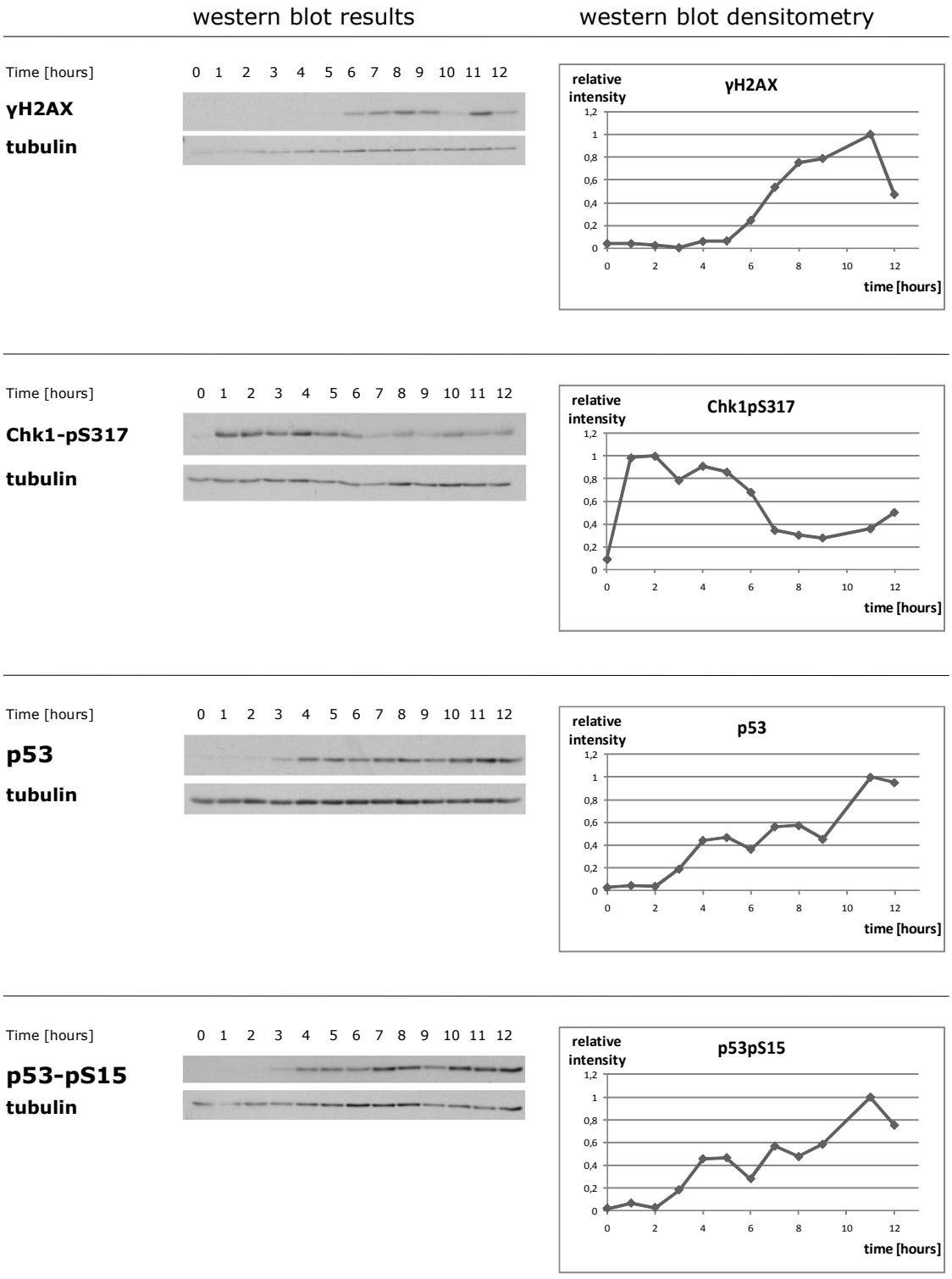

Figure 5.22: U2OS cells were irradiated with a single dose of 10 J/m^2 and monitored for the dynamics of selected DDR proteins up to 12 hours after irradiation - Exp 2/A - Total cell lysates were probed with indicated antibodies. The densitometry results were normalized to the loading control (α-tubulin). The sample from the 10 hour was excluded from the densitometry analysis. Details are described in text above.

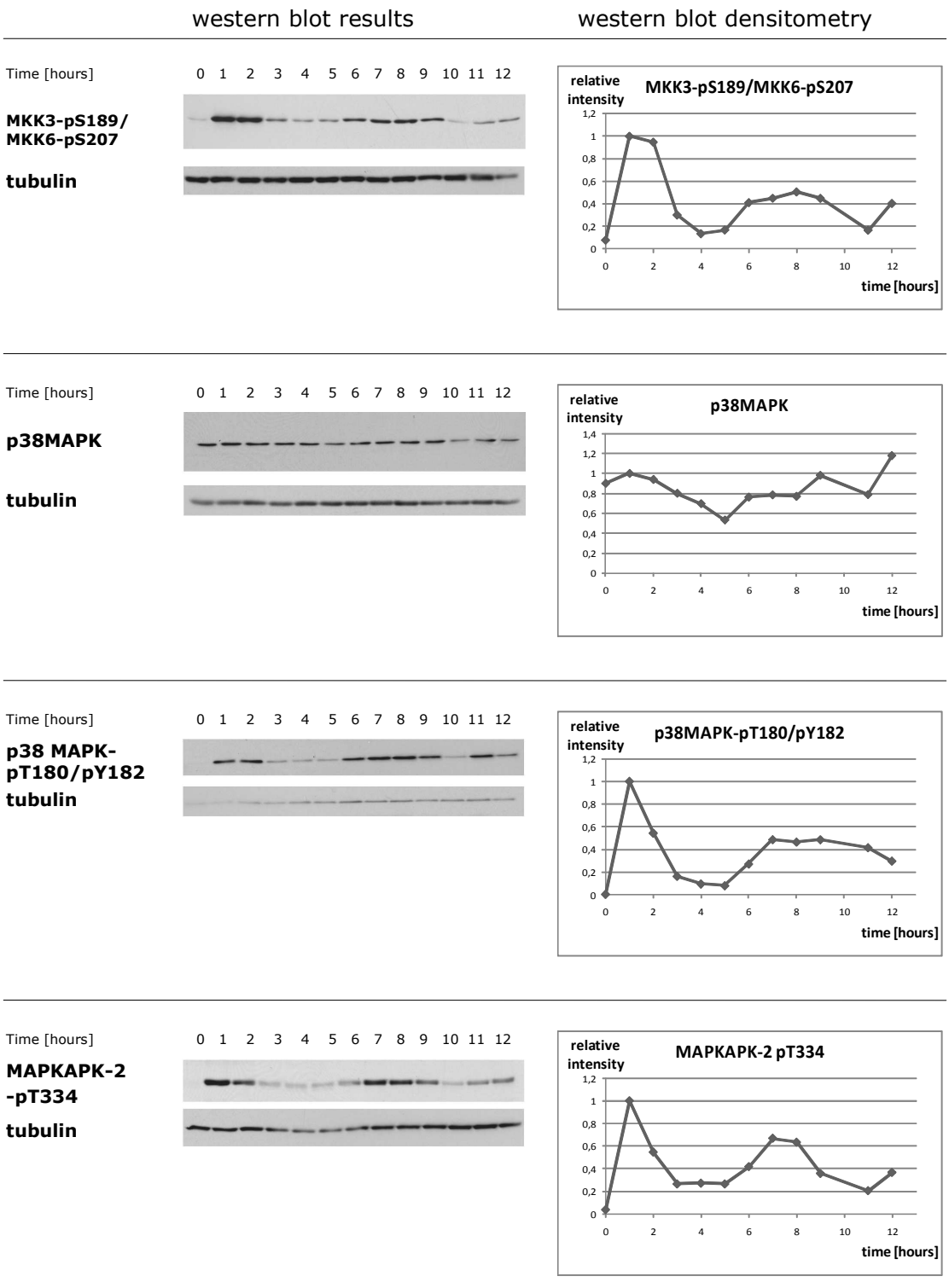

Figure 5.23: U2OS cells were irradiated with a single dose of 10 J/m^2 and monitored for the dynamics of selected DDR proteins up to 12 hours after irradiation - Exp 2/B - Total cell lysates were probed with indicated antibodies. The densitometry results were normalized to the loading control (α-tubulin). The sample from the 10 hour was excluded from the densitometry analysis. Details are described in text above.

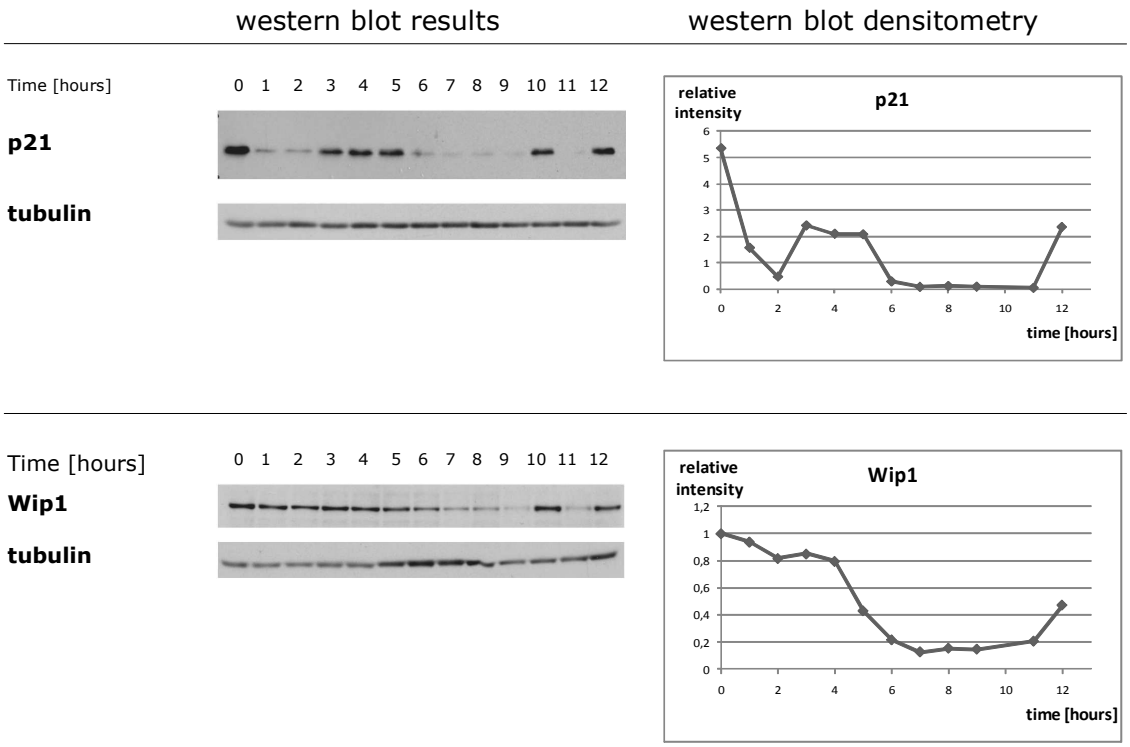

Figure 5.24: U2OS cells were irradiated with a single dose of 10 J/m^2 and monitored for the dynamics of selected DDR proteins up to 12 hours after irradiation - Exp 2/C - Total cell lysates were probed with indicated antibodies. The densitometry results were normalized to the loading control (α-tubulin). The sample from the 10 hour was excluded from the densitometry analysis. Details are described in text above.

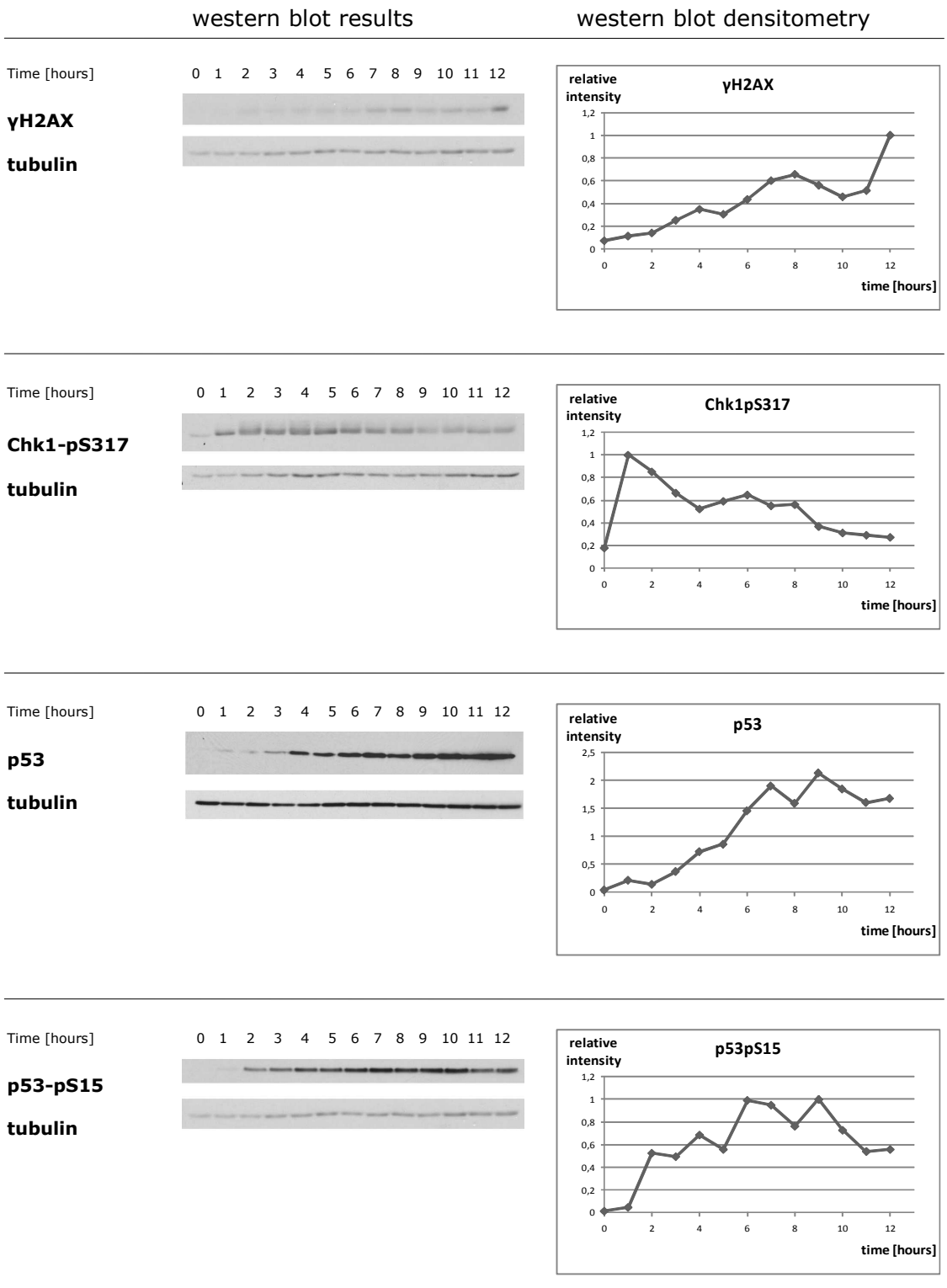

Figure 5.25: U2OS cells were irradiated with a single dose of 10 J/m^2 and monitored for the dynamics of selected DDR proteins up to 12 hours after irradiation - Exp 3/A - Total cell lysates were probed with indicated antibodies. The densitometry results were normalized to the loading control (α-tubulin). Details are described in text above.

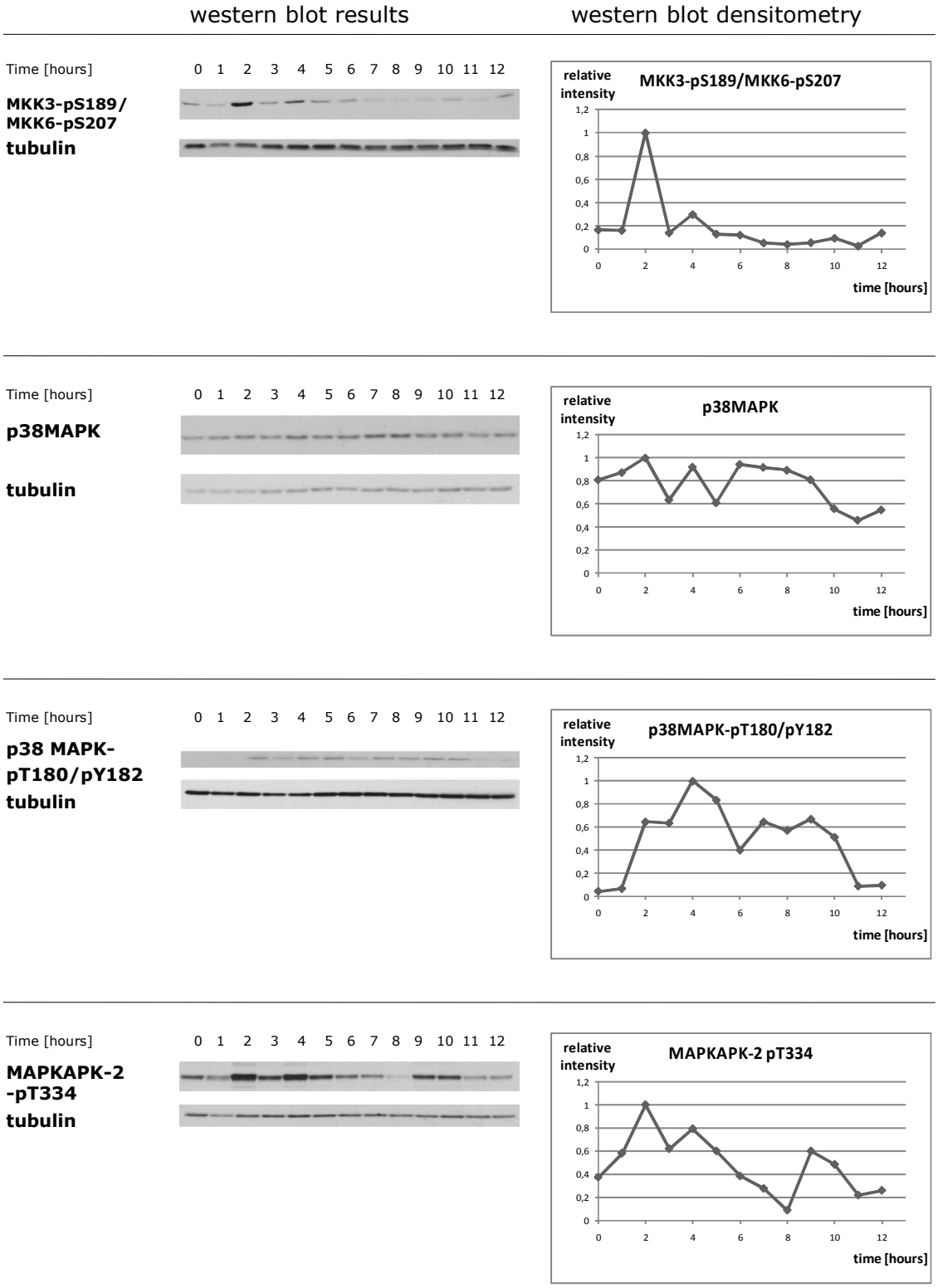

Figure 5.26: U2OS cells were irradiated with a single dose of 10 J/m^2 and monitored for the dynamics of selected DDR proteins up to 12 hours after irradiation - Exp 3/B - Total cell lysates were probed with indicated antibodies. The densitometry results were normalized to the loading control (α-tubulin). Details are described in text above.

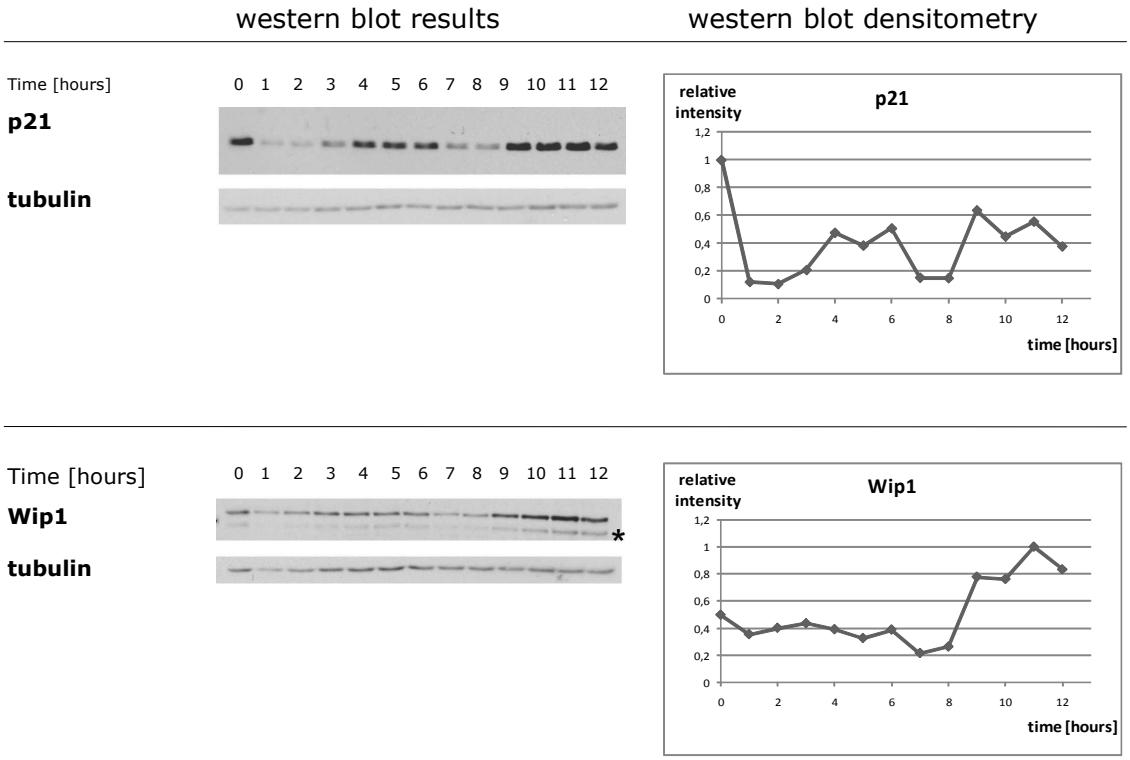

Figure 5.27: U2OS cells were irradiated with a single dose of 10 J/m^2 and monitored for the dynamics of selected DDR proteins up to 12 hours after irradiation - Exp 3/C - Total cell lysates were probed with indicated antibodies. The densitometry results were normalized to the loading control (α-tubulin). Details are described in text above.

sense the actual intensity of UV-C and correct for it for the delivery of final UV-C dose (Figure 5.28). Nevertheless, our measurements show that it is not absolutely precise (Figure 5.28). Moreover, since regulation of total UV-C dose is facilitated mainly by manipulating the irradiation time, there is reason for suspect that the variance of total UV-C doses in low dose of UV-C (below 50 J/m^2) and corresponding short times (few seconds) might be even larger.

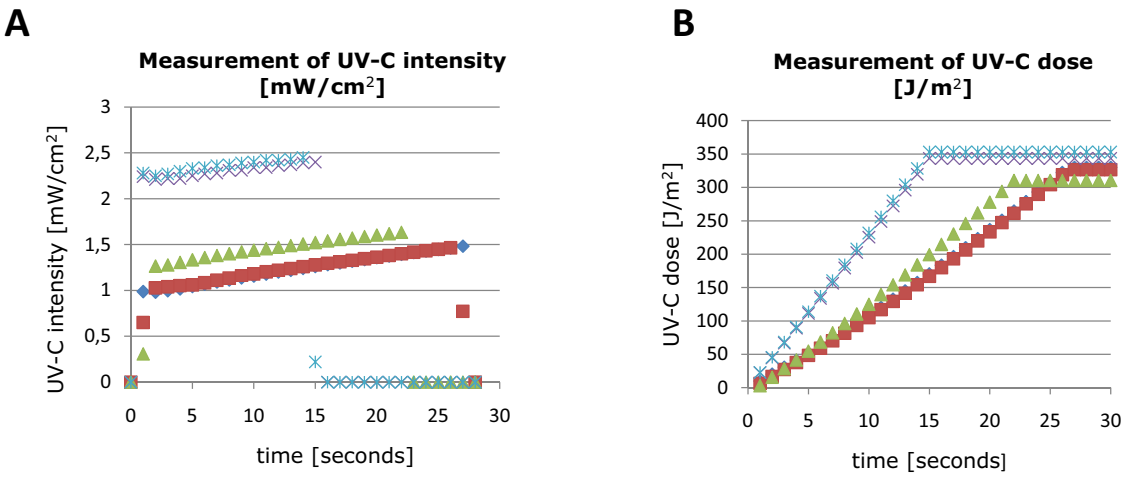

Figure 5.28: Measurement of UV-C Crosslinker UV-C dose demonstrates the variance of total UV-C doses - differentially colored symbols represent the individual measurements. **A:** The actual intensity of UV-C irradiation significantly vary between independent irradiations. **B:** The total dose of UV-C irradiation is corrected by crosslinker, yet not perfectly – the maximum observed variance between independent irradiations was approximately 30 J/m^2.

5.3.4 Wip1 half-life is approximately 2.5 hours

Regulation of the protein stability represents an essential mechanism by which cells control numerous physiological processes. This is well illustrated by the regulation of p53 upon stress stimuli (Chapter 3.3). Since we were interested in a possible regulation of Wip1 via alternations of its turn-over, we firstly determined its physiological half-life. The half life of a protein is defined as the time needed for removal of half of the protein (Eden et al., 2011). For this aim, we employed a treatment with cycloheximide that blocks the translational elongation and thus prevents proteosynthesis. Therefore in the presence of cycloheximide, we are able to observe degradation rate of protein.

U2OS cells were plated in 6-cm plates. Following day, cells were treated with 50 ug/ml cycloheximide. Samples were harvested in 1 to 6 hours time-points after cycloheximide addition and analyzed by western blot (Figure 5.29 A). Densitometry analysis of western blot results from two independent experiments showed that Wip1 half-life is approximately 2.5 hours (Figure 5.29 B). In addition, we examined whether the Wip1 half-live is altered upon UV-C dose of 20 J/m^2. We show that Wip1 half-life is not significantly altered by this dose of UV (Figure 5.29 C, D). The levels of p53 served as control for cycloheximide efficiency and also for DNA damage induction, since its turn-over is very quick in unstressed conditions, whereas it becomes stabilized upon DNA damage. We did not measured Wip1 half-life upon higher doses of UV-C, since higher doses of UV-C lead to apoptotic response, which would interfere with result interpretation.

5.3.5 Wip1 dynamics after UV-C irradiation is dose dependent

Results of Wip1 levels dynamics varied upon UV-C irradiation. With respect to the fact that used UV-C source (UltraLum Crosslinkers 800) exhibited a dose variation between the irradiations, we examined whether Wip1 dynamics changed with a dose intensity. U2OS cells were plated on 6-cm plates at density 7×10^5 per plate. Next day cells were irradiated by 5 J/m^2 and 50 J/m^2, respectively. Since we observed that doses of 50 J/m^2 induce apoptotic response, we subjected one plate per UV-C dose to the treatment with 1 μM Z-VAD-FMK that acts as a pan caspase inhibitor and thus prevents trigerring of apoptosis. By Z-VAD-FMK treatment we ruled out the possibility that changes in Wip1 levels were caused by apoptotic processes. Correspondingly, one plate was treated by a proteasomal inhibitor MG132, to investigate whether possible changes in Wip1 levels can be attributed to protein degradation. Both inhibitors were added to cell media immediately after irradiation. Cells were harvested 6 hours after UV-C irradiation and analyzed by western blot (Figure 5.30). Western blot results revealed that Wip1 levels slightly increased upon the dose of 5 J/m^2. On the contrary, at dose of 50 J/m^2, we observed a notable decrease in Wip1 protein level. This decrease cannot be attributed to apoptotic processes as sample treated with inhibited apoptotic

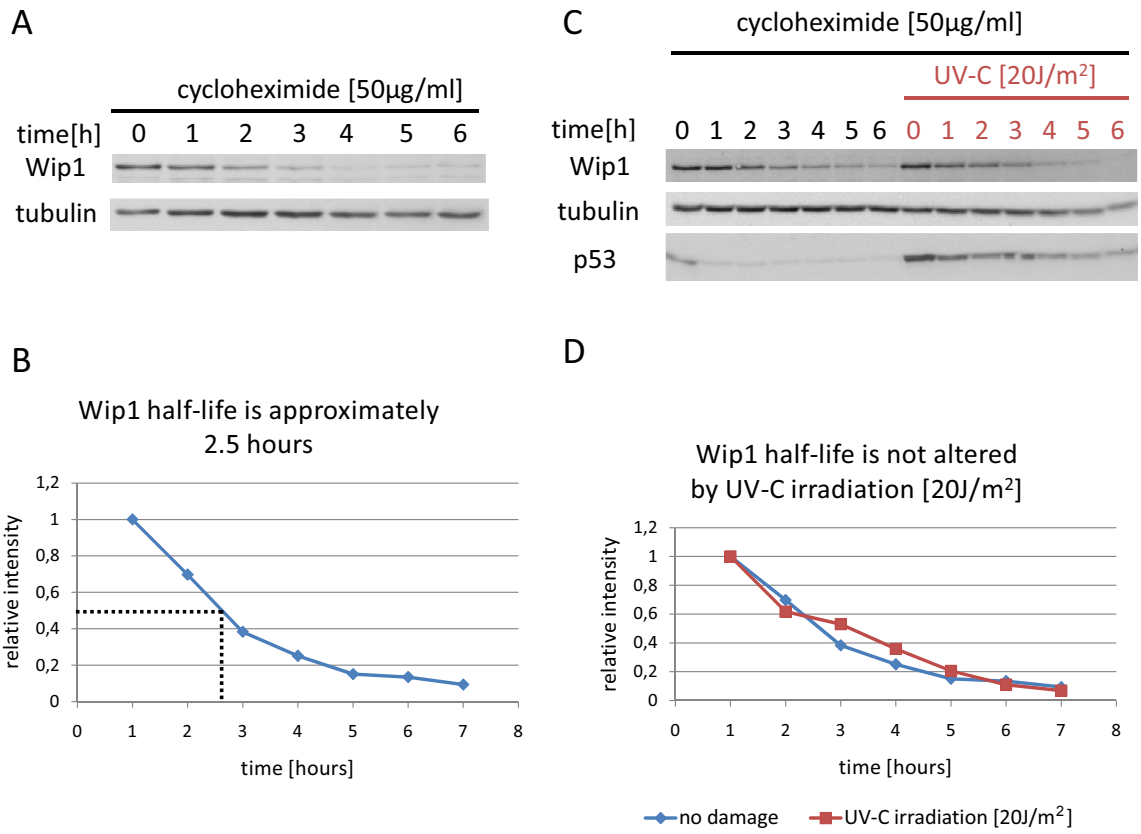

Figure 5.29: Wip1 half-life is approximately 2.5 hours and it is not altered by low dose (20 J/m^2) of UV-C irradiation - **A:** Determining the Wip1 half-life with cycloheximide treatment 50 μg/ml **B:** Quantification of westernblot from two independent experiments. (A; C) **C:** Determining the Wip1 half-life with cycloheximide treatment [50 μg/ml] in unstressed conditions and upon UV-C irradiation [20 J/m^2] **D:** Comparison of western blot densitometries demonstrates that Wip1 half-life is not significantly altered upon low dose of UV-irradiation.

response showed the same decrease. Efficiency of Z-VAD-FMK was confirmed by immunoblotting of PARP. Upon apoptosis, PARP is subjected to caspase-dependent cleavage and fragments of 89 kDa and 24 kDa can be detected. We did not detect any signal at position of cleaved PARP in Z-VAD-FMK treated sample, as opposed to untreated sample. Therefore we can conclude that apoptotic response was efficiently blocked. Visual observation of cells at the time of harvest was in agreement with cleaved PARP results, since we did not observe any cell death in Z-VAD-FMK treated sample. Treatment with MG132 resulted in abrogation of Wip1 levels decrease. Taken together, we suggest that Wip1 is degraded upon high doses of UV-C irradiation (50 J/m^2), but not after low doses of irradiation (5 J/m^2). p53 and p53pSer15 levels were examined as marker of activated DNA damage response.

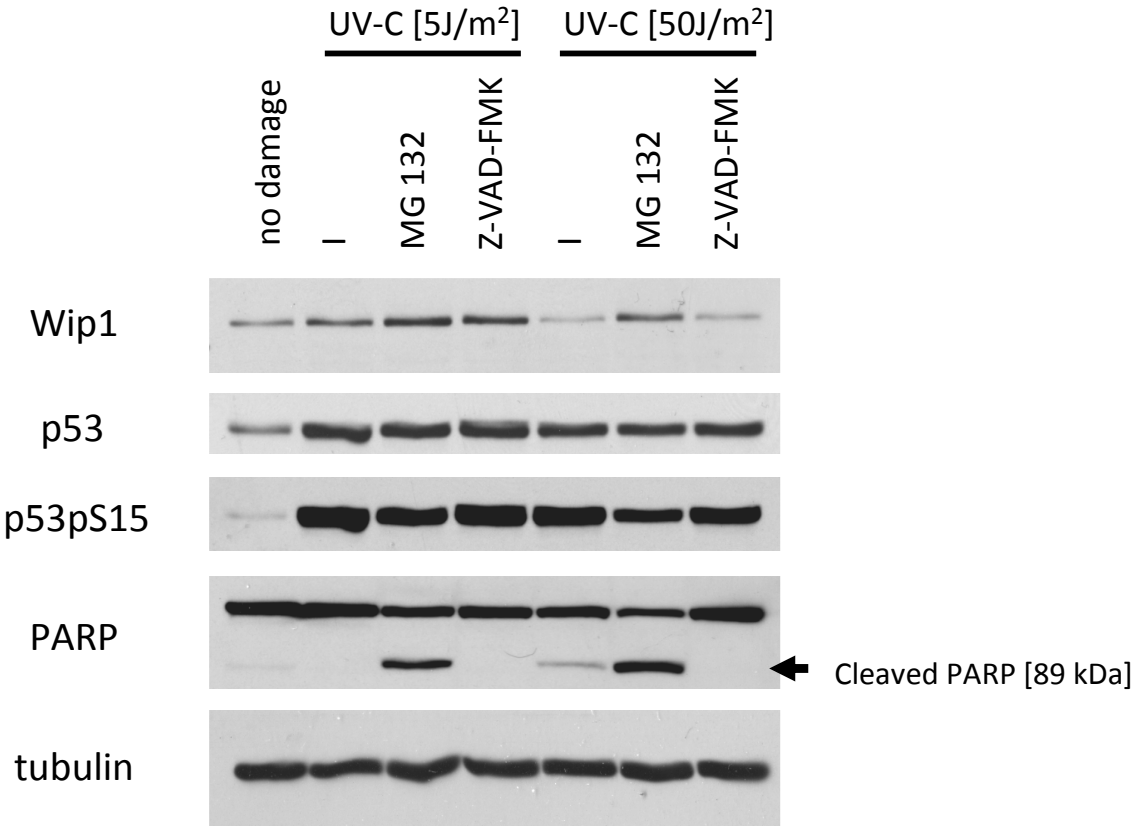

Figure 5.30: Wip1 dynamics after UV-C irradiation is dose dependent - Wip1 is degraded upon high doses of UV-C irradiation (50 J/m^2), but not after low doses of irradiation (5 J/m^2); Total cell lysates were probed with indicated antibodies

5.3.6 Wip1 is phosphorylated on pSQ/pTQ motif upon UV-C irradiation

We aimed to investigate whether the role of Wip1 in DNA damage response can be regulated also at the level of post-translational modifications. To test this we made use of a commercially available antibody recognizing phosphorylated pSQ/pTQ motifs.

LAP-Wip1-D314A-C1 U2OS cells were plated in 10 cm plates at density of 2×10^6 per plate. Next day, one plate was irradiated by dose of 50 J/m^2, second plate was used as control. Cells were harvested one hour after irradiation and lysates were precipitated with S-protein beads (see Methods). Immunoprecipitated samples together with corresponding lysates were analysed by western blot (Figure 5.31 A). Staining with anti-pSQ/pTQ antibody detected a band corresponding to Wip1 in immunoprecipitated samples of irradiated cells. Therefore Wip1 is phoshorylated on pSQ/pTQ motif upon UV-C irradiation. Phosphorylation of Chk1 on serine 317 was used as the marker of activation of DNA damage response.

We further examined the dynamics of Wip1 phosphorylation. LAP-Wip1-D314A-C1 U2OS cells were plated at density 2×10^6 in 10 cm plates. Next day, cells were irradiated by dose of 20 J/m^2 and harvested in intervals of 0.5, 1, 2 and 5 hours after irradiation. Cell lysates were incubated with S-protein beads (see Methods) and then analysed by western blot (Figure 5.31 B). We showed that pSQ/pTQ phosphorylation peaked 30 minutes after UV-C irradiation and then progressively declined.

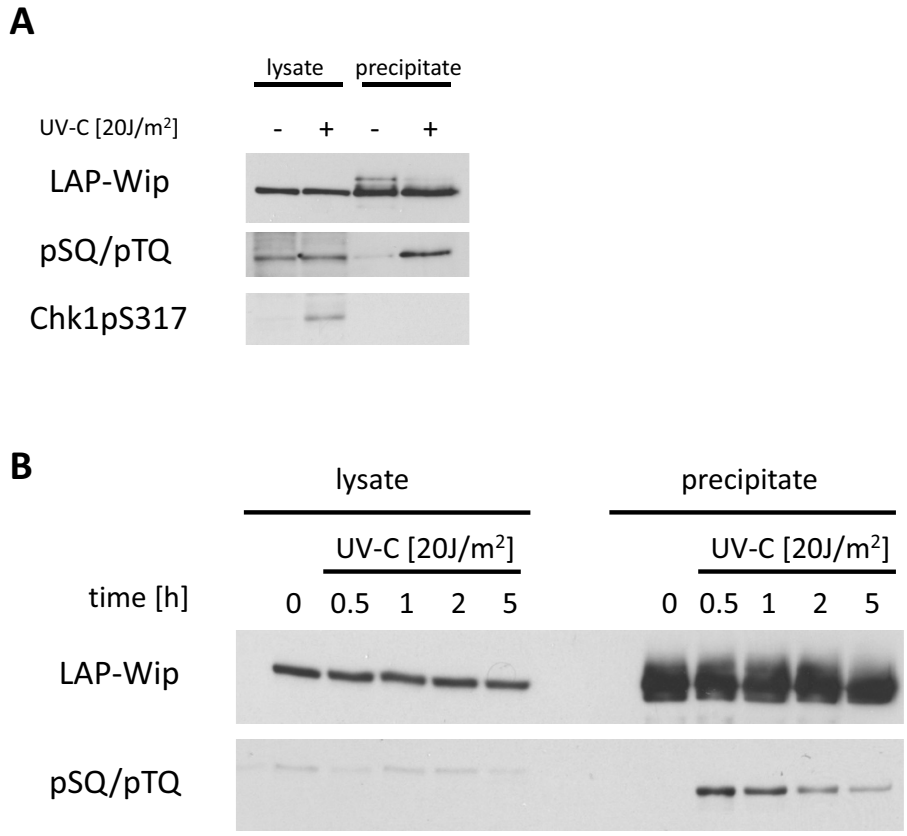

Figure 5.31: Wip1 is phosphorylated on pSQ/pTQ motif upon UV-C irradiation (A) - **B:** pSQ/pTQ phosphorylation peaked 30 minutes after UV-C irradiation and then progressively declined. Precipitates and total cell lysates were probed with indicated antibodies.

5.4 Wip1 dynamics during the cell cycle progression

Since regulation of DDR proteins is tightly connected to the cell cycle progression we decided to investigate Wip1 expression in different stages of cell cycle. U2OS cells were synchronized by a double thymidine block (see Methods). Samples from different stages of cell cycle were collected and analyzed by westernblot and RT-PCR (Figure 5.32). We found that the expression of Wip1 on mRNA level was not significantly altered during the cell cycle progression.

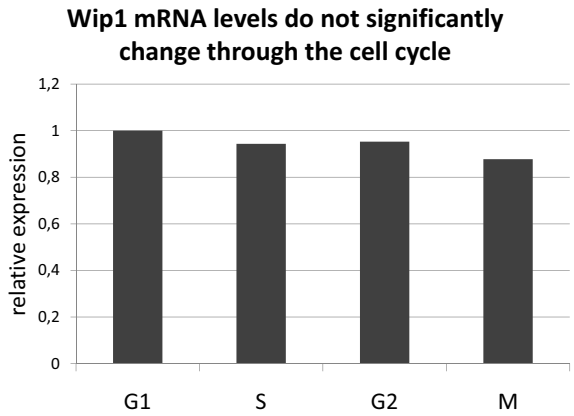

Figure 5.32: Wip1 mRNA level does not significantly change during the cell cycle progression - Cells were synchronized by double thymidine block (see Methods).

Conversely, western blot analysis revealed a decrease in Wip1-corresponding band intensity in mitotic sample, compared to interphase samples (Figure 5.33 A). Notably, a second band with a slower electrophoretical mobility was also detected. The same result was observed in MCF7 cell line (Figure 5.33 B). Cyclin A, cyclin B and H3pS10 were used as markers of cell synchronization.

In addition, we were able to detect this decrease and a band shift also for exogenous fusion GFP-Wip1 protein in our cell line U2OS-LAP-Wip1-D314A-C1 (Figure 5.34 A). Nevertheless, we were unable to detect any drop in GFP signal intensity in mitotic U2OS-LAP-Wip1-D314A-C1 cells. Yet as levels of exogenous LAP-Wip1 are significantly higher in this cell line, there was still a considerable portion of Wip1 left. It is possible that the remaining portion of LAP-Wip1 restrained us from detection of small changes in GFP signal intensity. We tried to overcome this obstacle by preparation of cell line expressing lower levels of LAP/GFP-Wip1

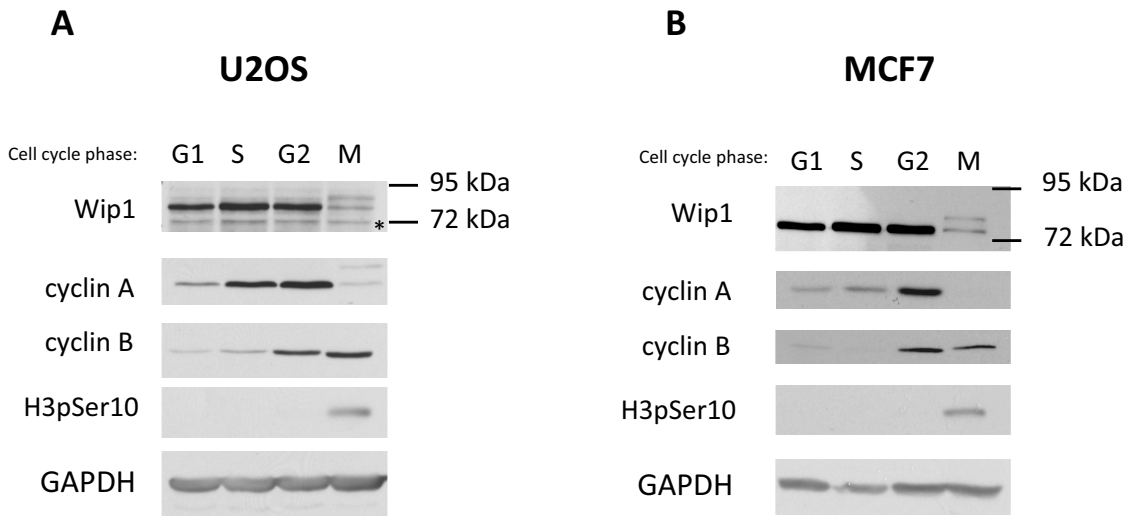

Figure 5.33: Wip1 protein level throughout the cell cycle in U20S (A) and MCF7 (B) cell lines - mitotic samples in both cell lines exhibit decrease in Wip1 signal and band shift - Cells were synchronized by double thymidine block (Methods); total cell lysates were probed with indicated antibodies.

(described above). Interestingly, it seemed that all exogenous Wip1 was shifted-up in mitotic samples, since we were unable to detect any remaining signal in the position of original notshifted band as opposed to results from endogenous Wip1 in U2OS and MCF7 cells. MCF7 and U2OS-LAP-Wip1-D314A-C1 cell lines were plated and synchronized according to the same protocol as described above.

5.4.1 Wip1 is phosphorylated in mitosis

We have reproducibly detected a notable band shift in portion of Wip1 in mitotic samples (Figures 5.33, 5.34). As such shift can correspond to a post-translational modification of protein, we were keen to investigate this possibility further. We focused on phosphorylation first, since this modification can be easily confirmed by treatment of the precipitated protein with lambda-phosphatase. The U2OS-Wip1-FLAG-D7 cells, carrying tet-inducible fusion Wip1-FLAG (described in Lindqvist *et al.* (2009), were synchronized via thymidine block and RO3066 inhibitor to G2 phase and after release from RO3066 block to the mitosis using nocodazole. At the same time as RO3066 was added (12 h before mitotic release), cells were also treated with 1 uM doxycyclin to induce Wip1-FLAG expression. G2 and mitotic cells were harvested and immunoprecipitation with Wip1 St. Cruz antibody was

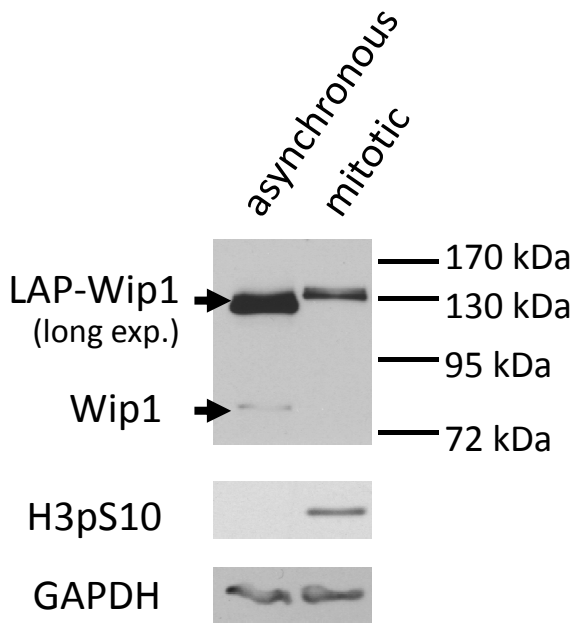

Figure 5.34: LAP-Wip1 exogenous protein levels in asynchronous population and in mitotic cells in U2OS-LAP-Wip1-D314A-C1 exhibit decrease in Wip1 signal and band shift - Cells were synchronized via double thymidine block (see Methods); total cell lysates were probed with indicated antibodies.

performed (see Methods). After immunoprecipitation, mitotic sample was divided into two halves. One was subjected to lambda phosphatase treatment, the other was used as a control. Immuprecipitation samples with corresponding cell lysates were analysed by westernblot and detected via anti-FLAG antibody (Figure 5.35). The mitotic size shift was lost after treatment with lambda phosphatase, giving evidence that it is caused by protein phosphorylation.

5.4.2 Wip1 is degraded in mitosis?

We observed that the intensity of bands corresponding to Wip1 was decreased during mitosis and the sum of both bands, the original and shifted one, still did not seem to constitute interphase intensity of Wip1 signal (Figure 5.33). Therefore we hypothesized that Wip1 could be specifically degraded in mitosis. To test this hypothesis, we treated U2OS cells with a proteasomal inhibitor MG132 immediately before mitotic entry, at time of release from RO3066 block and checked for Wip1 stabilization. In addition, we were interested in temporal changes in Wip1 levels in prolonged mitosis and potential activation of stress response, particularly for

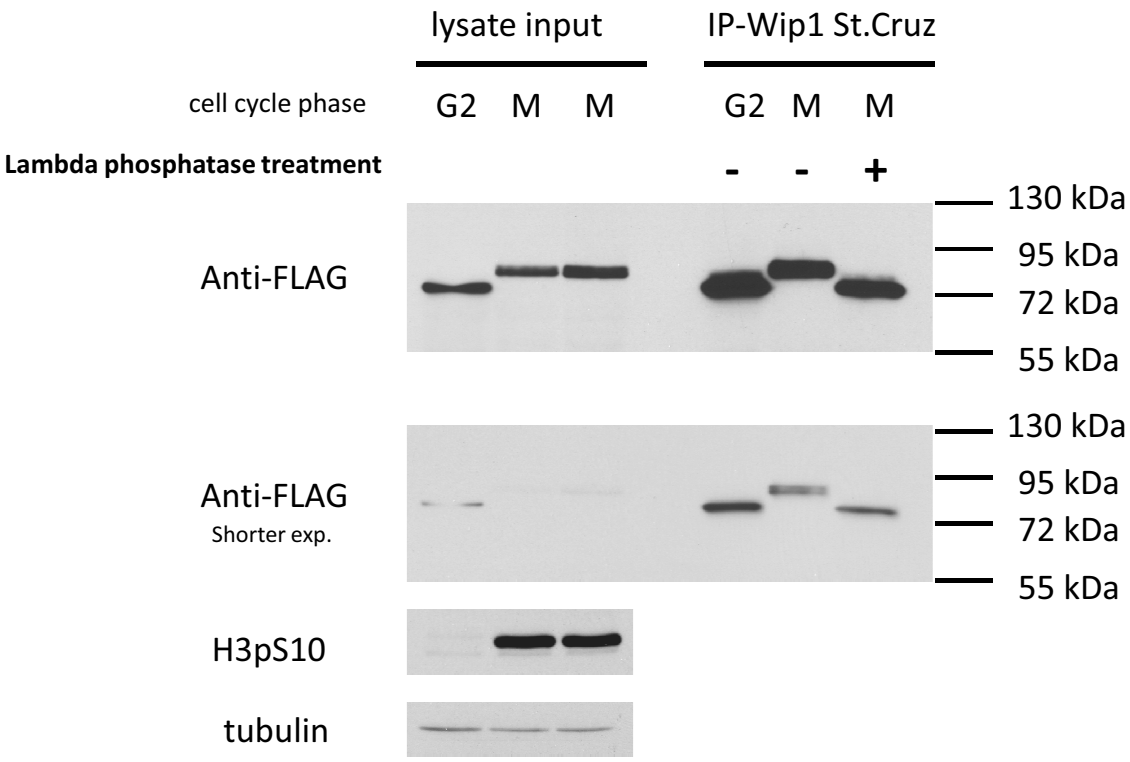

Figure 5.35: Lamda phosphatase treatment of precipitated mitotic Wip1 shows that the mitotic size shift is attributed to the Wip1 phosphorylation - Cells were synchronized via thymidine block and RO3066 (see Methods); total cell lysates and immunoprecipitates were probed with indicated antibodies. Wip1 protein was immunoprecipitated with Wip1 St.Cruz antibody.

activation of p53 and p38.

The U2OS cells were synchronized by a thymidine block and RO3066 (see Methods). At the time of release from RO3066 block, cells were treated by proteasomal inhibitor MG132 and nocodazol. The mitotic cells were harvested in indicated timepoints of 1, 1.5, 2, 3 and 4 hours after release from the RO3066 block and analyzed by western blot (Figure 5.36). Majority of cells entered mitosis until 1 hour after RO3066 release, based on observation of their morphological changes. Nevertheless, the samples collected at 1 h were not fully mitotic, according to lower levels of mitotic marker histone 3 phosphorylated on S10 (Figure 5.36). The intensity of Wip1 signal was not lowered at 1 h. At 1.5 h, the levels of histone 3 phosphorylated on serine 10 reached its full levels. Notably, the intensity of Wip1 signal decreased in sample from 1.5 h without MG132 treatment and conversely did not decrease in sample with MG132. Similar results were obtained for all following timepoints suggesting that treatment with MG132 leads to stabilizations of Wip1 levels in mitosis. Nevertheless, we would be careful to interpret these results as proof that Wip1 is really degraded upon mitotic entry. We further address this issue in Discussion.

We further used the samples collected from this experiment to examine the possible activation of p53 and p38 during prolonged mitosis. We have become interested to this issue due to observations made by Uetake and Sluder (2010). They demonstrated that if the prometaphase is prolonged over approximately 1.5 hour, then cells irreversibly arrest in the following G1 phase. Additionally, the G1 arrest has been suggested to be p38 and p53 dependent. If the p53 or p38 will be activated during mitosis than we might hypothesize that Wip1 actions need to be downregulated to enable their activation. We discuss these assumptions in detail in Discussion. We do not observe increased levels of total p38 during prolonged mitosis. In samples treated with MG132, expectable increase of p53 levels was detected, since otherwise rapid turnover of p53 was prevented by a proteasomal inhibition. We observed a minor increase in levels of p38MAPK-pT180/pY182 in mitosis prolonged over 3 hours.

Additionally, we released cells from prolonged nocodazol block (1, 2 and 4 hours) to G1 phase and checked for p53-pS15 and p38-pT180/pY182 (Figure 5.37).

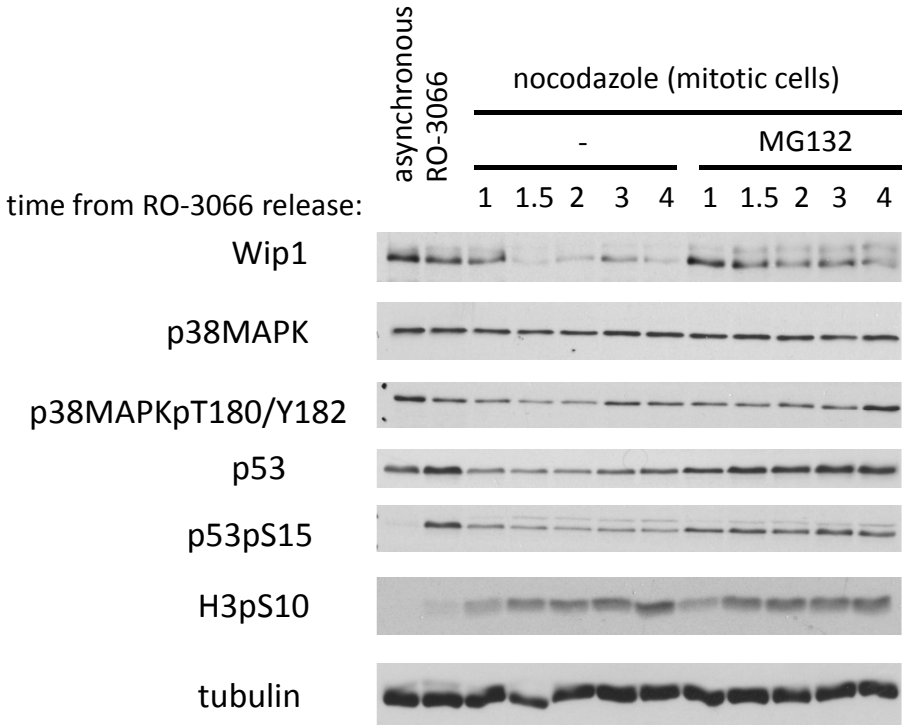

Figure 5.36: Wip1 levels during mitosis are stabilized upon proteasomal inhibition - Cells were synchronized via thymidine block and RO3066 (); Total cell lysates were probed with indicated antibodies.

We observed increased levels of p53-pS15 in all three conditions. This result was not very conclusive, since the p53-pS15 levels were increased also in the sample which was held in mitosis less than 1.5 hours and therefore activation of "prolonged prometaphase checkpoint" should not happen. Again, we cannot rule out that sole handling with cells during experiment, particularly the synchronization with RO-3066, did not cause the p53-pS15 increase. Interestingly, the levels of p38MAPK-pT180/pY182 were increased only in samples which were held in mitosis over 2 hour and they were in correlation with p38MAPK-pT180/pY182 levels observed during prolonged mitosis.

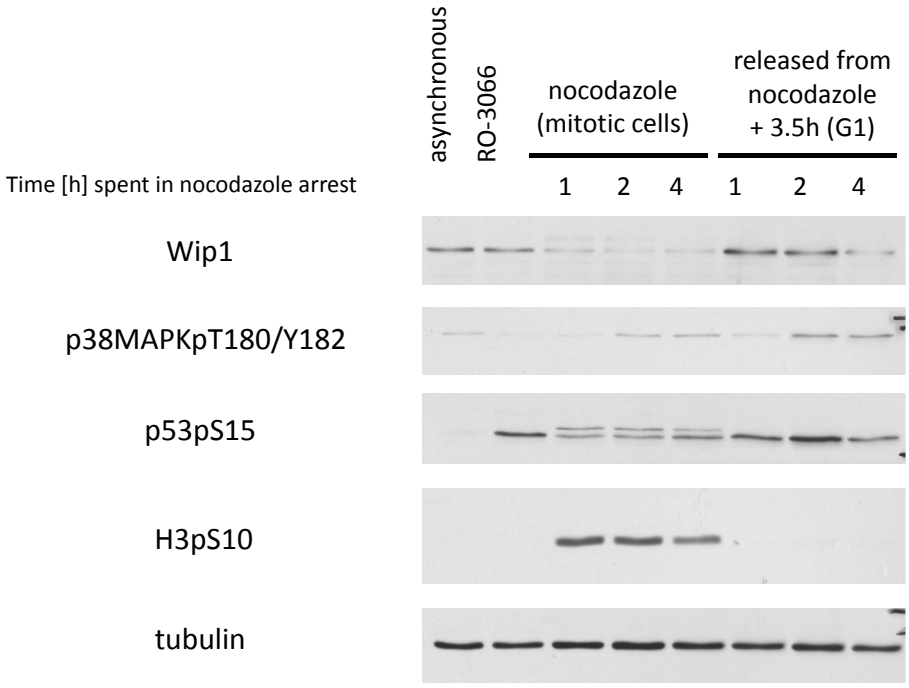

Figure 5.37: Prolonged mitosis leads to activation of p38MAPK - the issue is discussed in detail in text above and in Disscusion; cells were synchronized via thymidine block and RO3066 (see Methods); total cell lysates were probed with indicated antibodies.

6

Discussion

6.1 Dynamics of DNA damage response proteins upon γ-irradiation and UV-C irradiation

We described the temporal dynamics of key DNA damage response proteins under γ-irradiation and UV-C irradiation. The knowledge of which proteins are activated, when and in what dynamics will hopefully contribute to unraveling of the complex regulatory network and identify key signaling events for diverse imputes and outputs of the DNA damage response.

6.1.1 Dynamics of p53

Galit Lahav's group showed that γ-irradiation initiates a series of discreate undamped p53 pulses. The p53 pulses exhibit fixed amplitude and the number of pulses positively correlates with the irradiation dose. This implies that p53 response to γ-irradiation behaves in a digital way rather than analog (Chapter 3.6).

We irradiated MCF7 cell line, the same cell line as used in Galit Lahav's group work, with γ-irradiation dose of 10 Gy to see if we are able to reproduce Lahavs group's results. Indeed, we observed the expected pulsative dynamics of p53 (Figures 5.11). However, the amplitude of the second pulse reached only 60% of the first one. Since the observation was made at the cell population level and not at individual cells, the lower amplitude of second pulse might be attributed to the

averaging the variable number of undamped pulses in single cells (Chapter 3.6, (Lahav *et al.*, 2004). In addition, we checked levels of activated p53-pS15. The levels of p53-pS15 perfectly correlated with the first pulse of total p53. On the contrary the second pulse was notably lower. It suggests that although the cells trigger the second pulse of p53, its posttranslational activation does not necessarily follow. This speaks in favor of hypothesis that repetitive degradation of p53 serves as "master reset" of its posttranslational modifications and thus provides cell a chance to choose the appropriate response for its current state (Chapter 3.6.1, (Lahav *et al.*, 2004).

Unexpectedly, when we reproduced the γ-irradiation with 10 Gy on U2OS cell line, p53 levels showed a monotone continuous increase 5.22, 5.25). To clarify this discrepancy, we looked up the literature whether the genetic background of MCF7 and U2OS cell lines differ in key modulators of p53. We found that while U2OS cells harbor a single copy of *PPM1D* gene, that encodes Wip1, MCF7 have amplified the *PPM1D* gene locus (Bulavin *et al.*, 2002). Correspondingly, MCF7 also exhibits higher levels of Wip1 protein compared to U2OS (Lu *et al.*, 2005). We speculate that the lower levels of Wip1 in U2OS prevented us from observing the p53 pulses. Given that the p53-Mdm2 negative feedback loop should be sufficient to give rise of p53 pulsative dynamic, we do not think that lower levels of Wip1 would lead to abrogation of p53 pulses. On the other hand, Wip1 was described to be indispensable for maintenance of the pulse uniformity. It was shown on MCF7 cells that Wip1 downregulation via siRNA results in deviations from the stereotypical pulse amplitude and width (Batchelor *et al.*, 2008). Therefore, we propose that lower level of Wip1 in U2OS compared to MCF7 might not be sufficient for the maintenance of the pulses uniformity. Since we observed the p53 dynamics at population level, the lack of synchrony and uniformity of p53 pulses between individual cells might prevent us from detection of discrete pulses and thus the p53 response was demonstrated as monotone increase of p53 (Chapter 3.6). Alternatively, Batchelor *et al.* (2011) suggested, based on a mathematical modeling, that removal of Wip1-ATM negative feedback loop should be sufficient for switching the p53 dynamics from repeated pulses in to a single continuous pulse. Hence it is possible that p53 pulses in U2OS are really abrogated. Notably,

in MCF7 the levels of Wip1 showed a discrete pulse, which corresponded to the decline of the first p53 pulse (Figure 5.13). On the contrary, in U2OS the Wip1 levels exhibit a slight continuous increase (Figures 5.16, 5.19). This further supports the view that MCF7 and U2OS significantly differ in the regulation of Wip1. Naturally, we cannot exclude the possibility that other currently unknown factors contribute to the discrepancy in p53 dynamics between MCF7 and U2OS cells. The observed absence of p53 pulsative dynamics in U2OS questions the physiological relevance of p53 pulses. With regard to the amplified *PPM1D* gene locus in MCF7, this cell line might not be the best representative model of p53 physiological regulation. The study of more cell lines, particularly the non-transformed ones might contribute to elucidation of this issue.

When we irradiated U2OS cells with UV-C (10 J/m^2) we observed a monotone continuous increase in levels of p53 (Figures 5.22, 5.25). These results are in consistence with recent findings of Batchelor *et al.* (2011), who performed a similar experiment on MCF7 cells. Moreover, Batchelor *et al.* (2011) examined the p53 dynamics in single cells, using the p53-Venus fusion and time-lapse fluorescence microscopy. It was shown that the p53 dynamics in single cells also shows the single continuous peak of p53 levels. The amplitude and duration of p53 response was increasing proportionally to dose of UV-C (Batchelor *et al.*, 2011). As described, the UV-C irradiation triggers the ATR-Chk1-p53 pathway, while γ-irradiation initiates the ATM-Chk2-p53 pathway. These two pathways share similar network architecture - ATM/ATR and Chk2/Ckh1 activates in feed-forward motif the p53, which is in turn inhibited by negative feedback by Mdm2 and Wip1 (Chapters 3.1.1.2 and 3.1.2.3). However, there is one main difference. ATR is not negatively regulated by Wip1, as opposed to ATM. With respect to our findings and in agreement with Batchelor *et al.* (2011), we propose that the negative feedback between upstream DDR kinase and Wip1 represents key regulatory circuit that determines the p53 dynamics. The presence of this negative feedback loop leads to repeated pulses of p53, while its absence or deficiency results in single continuous pulse of p53 response (Figure 6.1).

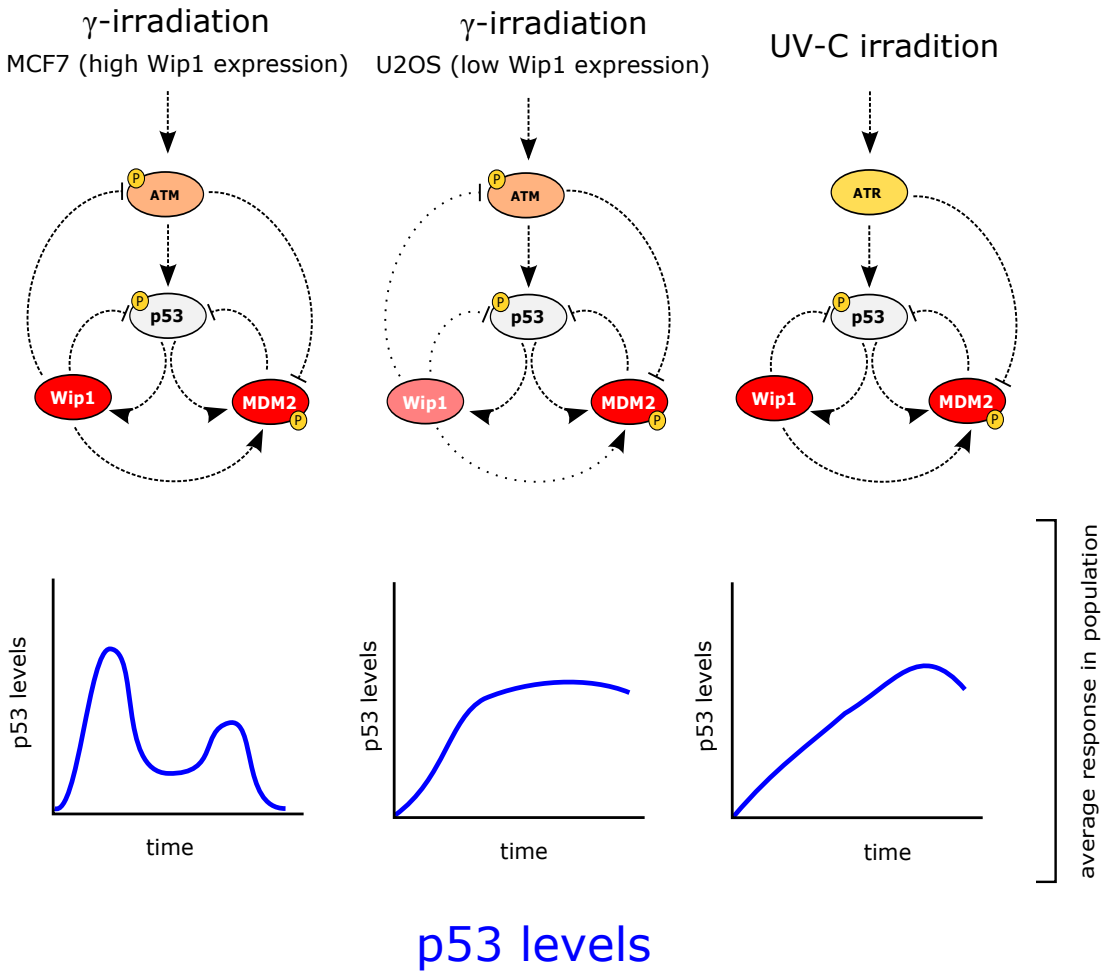

Figure 6.1: The negative feedback loop between upstream DDR kinase and Wip1 determines the p53 dynamics - In MCF7 cells, the high levels of Wip1 efficiently dephosphorylates ATM, this results in negative feedback loop that leads to repeated pulses of p53. On the contrary, lower Wip1 levels in U2OS are not sufficient for establishment of effective negative feedback loop and thus p53 response exhibits single continuous pulse. The UV-C activates the ATR-Chk1-p53 pathway, which lacks the negative feedback loop between the upstream DDR kinase (ATR) and Wip1, therefore p53 response also exhibits single continuous pulse. Similar conclusions for the differential dynamics of p53 upon γ-irradiation and UV-C irradiation were suggested by Batchelor *et al.* (2011).

6.1.2 Dynamics of p21

In response to γ-irradiation with 10 Gy we observed a monotone continuous increase in levels of p21, which reached its maximum around 6 hours after irradiation and remained elevated until the last of examined timepoints (12 hours). Similar dynamics was observed for MCF7 and U2OS cell lines Figures 5.13, 5.16, 5.19). These observations are consistent with the described role of p21 in γ-irradiation induced cell cycle checkpoint (Leonardo *et al.*, 1994; Macleod *et al.*, 1995). The elevated p21 inhibits the CDK-cyclins complexes and thus prevents the cell cycle progression (el Deiry *et al.*, 1993; Harper *et al.*, 1993).

Interestingly, upon UV-C irradiation with 10 J/m^2 we detected initial decrease of p21 levels that was followed by pulse of p21 increase (Figures 5.24, 5.27). The timing and width of the first p21 pulse showed good correlation between experiments. In addition to the first p21 pulse, we observed a second one with similar amplitude, yet its timing differed between the independent experiments (Figures 5.24, 5.27). Literature reports about the dynamics of p21 after UV-C irradiation are inconsistent and contradictory. While some reports suggest that the p21 levels decline upon UV-C, others imply that the p21 is upregulated upon UV-C (summarized in Bendjennat *et al.* (2003). The work of Bendjennat *et al.* (2003) proposed that dynamics of p21 is dose dependent and the low (<30 J/m2) but not high doses of UV-C irradiation results in p21 proteasomal degradation. Yet again, Lee *et al.* (2006) showed the direct opposite, that high (<40 J/m2) but not low doses of UV-C lead to p21 degradation. Notably, both studies examined, among others, U2OS cell line, suggesting that their contradictory results were not caused by differences between cell lines. Our findings of p21 pulses might help to elucidate this issue. We can speculate that since the authors of mentioned studies examined the p21 levels in single or very few timepoints they might have detected the different phase of p21 pulse. Some might be detecting the pulse maximum and thus interpret it as no p21 degradation, whereas others detected the pulse minimum, leading them to conclusion that p21 is degraded. Since we observed the p21 only upon the low dose of UV-C (10 J/m2), we cannot clarify whether the dynamics of p21 is dose dependent and in which manner. According

to discussed literature it seems probable the dynamic of p21, possibly the timing or duration of pulses vary with UV-C dose. The p21 was suggested to be dispensable for UV-C-induced cell cycle arrest (Bendjennat *et al.*, 2003). On the other hand, upon UV-C irradiation the p21 negatively regulates the DNA repair in a PCNA-dependent manner (Bendjennat *et al.*, 2003). Therefore orchestrated control of its levels seems to have considerable relevance for the cell fate.

6.1.3 Dynamics of p38MAPK-MAPKAP-K2 pathway

We observed two pulses of p38MAPK-MAPKAP-K2 pathway activation both upon γ-irradiation and UV-C irradiation (Figures 5.12, 5.15, 5.18, 5.23, 5.26). The two pulses were reproducible for p38MAPKpT180/pY182 and MAPKAPK-2-pT334 between independent experiments, although the width and timing of pulses vary. We did not detect any pulsative dynamics of total levels of p38. For this reason we suggest that pulses were not attributed to repetitive degradation of p38, as it is in the case of p53 pulses. Conversely, p38MAPK-MAPKAP-K2 dynamics is most probably caused by repetitive reversal of activatory postranslational modification. The active p38MAPKpT180/pY182 can be dephosphorylated by Wip1 (Takekawa *et al.*, 2000). Therefore it is tempting to speculate that the pulsative dynamics could be attributed to negative feedback loop of p38MAPK-p53-Wip1 circuit. Nevertheless, using U2OS we did not detect correlating pulses in Wip1 levels (Figures 5.16, 5.19, 5.24, 5.24). Yet, we cannot rule out the possibility that the Wip1 activity might be regulated also by postranslational modification in a pulsative manner.

According to our knowledge, this is the first observation of pulsative dynamics in p38MAPK-MAPKAP-K2 activity upon DNA damage. Interestingly, the similar dynamics of p38MAPK activation was observed *in vivo* in mice and *in vitro* in normal human keratinocytes upon treatment with Pemphigus IgG autoantibodies (Lee *et al.*, 2009). The Pemphigus is a group of related autoimmune syndromes characterized by the loss of adhesion between adjacent epithelial cells and resulting blistering in the skin. The Pemphigus autoantibodies are targeted against desmogleins. Desmogleins are components of desmosomes, sites of attachment between epithelial cells, which function is distrupted by Pemphigus autoantibod-

ies (Amagai, 2009). The exact mechanism that couples the loss of cell adhesion and activation of p38MAPKMAPKAP- K2 pathway is not known. This correlation of activation dynamics upon most different stimuli is noteworthy. Still, the physiological relevance of pulses in p38MAPK-MAPKAP-K2 activity remains to be elucidated.

6.2 Wip1 regulation upon UV-C irradiation

6.2.1 Wip1 dynamics after UV-C irradiation is dose dependent

The results of temporal dynamics of Wip1 protein levels upon UV-C did not exhibit particularly good correlation between independent experiments (Figures 5.21, 5.24, 5.27). Since we noticed that UV-C doses delivered by the crosslinker were not precisely constant (Figure 5.28), we decided to investigate whether the Wip1 dynamics is sensitive to irradiation dose. We found that Wip1 levels decrease upon high dose (50 J/m2) of UV-C, but did not decrease upon low UV-C doses (Figure 5.30). This is in agreement with our observations that low-doses of UV-C did not alter the Wip1 turnover (Figure 5.29 C, D). We ruled out the possibility that the Wip1 degradation upon the high UV-C dose is caused by non-specific apoptotic processes, as the Wip1 levels drop even when the apoptosis was blocked (Figure 5.30). Therefore we suggest that Wip1 dynamics after UV-C irradiation is dose dependent and that it is a regulated process. The low dose of UV-C activated the cell cycle checkpoint but did not trigger the apoptotic response (Figure 5.30). Hence, it seems reasonable that cells do not eliminate Wip1, because it is needed for possible checkpoint recovery (Lindqvist *et al.*, 2009). On the contrary, the high doses of UV-C cause the apoptotic response (Figure 5.30), so Wip1 activity is not needed any longer. Moreover, given that Wip1 negatively regulates p53 activation, we can speculate that the Wip1 activity would even interfere with initiation of the apoptotic program. Our results are consistent with the recently published findings of Xia *et al.* (2011), who observed the same phenomenon. In addition, Xia *et al.* (2011) demonstrated that upon high dose of UV-C, the sustained activation of p53 fails to induce the particular p53 targets, including its negative regulators Wip1 and Mdm2 and also checkpoint-promoting proteins p21 and GADD45α.

Conversely, p53 stimulates the proapoptotic genes, including NOXA, PUMA, and BAX in response to high-dose UV-C (Benchimol, 2001). It suggests that cells are able to determine the amount of DNA damage and decide the appropriate response trough the regulation p53 transcriptional specificity.

6.2.2 Wip1 is phosphorylated on pSQ/pTQ motif upon UV-C irradiation

Aside from studying the dynamics of total Wip1 levels after the DNA damage, we were also very keen on investigating its possible regulation by posttranslational modifications. We speculated that Wip1 might be regulated after DNA damage not only by p53, but also by upstream DDR kinases. To test this assumption, we irradiated cells with UV-C and probed precipitated Wip1 protein with commercially available antibody recognizing phosphorylated pSQ/pTQ motifs. As described above, the pSQ/pTQ motifs are phosphorylated by ATM and ATR kinases. We have demonstrated that Wip1 is phosphorylated on pSQ/pTQ motif upon UV-C irradiation (Figure 5.31 A). In addition, we examined the temporal dynamics of pSQ/pTQ phosphorylation and showed that it peaked 30 minutes after UV-C irradiation and then progressively declined (Figure 5.31 B). With respect to this dynamics, we might hypothesize that upstream DDR kinases might downregulate Wip1 activity through this phosphorylation to enable the full activation of DNA damage response immediately after the DNA damage. Subsequently, Wip1 is again activated, e.g. by p53-dependent transcriptional upregulation (Fiscella *et al.*, 1997) and in turn can inhibit the DDR signaling (Yamaguchi *et al.*, 2007).

As Wip1 primary sequence contains four pSQ/pTQ sites, in particular Y25, S46, Y214, S403, we plan to determine which one of these motifs is responsible for the observed reactivity using variants of Wip1 where individual serine residues will be mutated to alanine residues that cannot be phosphorylated. These experiments are currently under progress and together with a detailed functional analysis of this modification will be followed further.

6.3 Wip1 alternations during mitosis

6.3.1 Wip1 is phosphorylated during mitosis

In view of the fact that regulation of many DDR proteins is connected to the cell cycle progression, we investigated whether Wip1 is distinctively regulated in different stages of cell cycle. We have shown that Wip1 undergoes a specific mitotic mobility shift in U2OS and MCF7 cell lines (Figure 5.33). This mobility shift was further confirmed on cell lines expressing exogenous Wip1-fusion proteins (Figure 5.34). Using lambda proteinphosphatase assay we have demonstrated that mobility shift is caused by phosphorylation of Wip1 during mitosis (Figure 5.35).

As the phosphorylation causing the mobility shift of Wip1 strictly occurs in mitosis, we hypothesized that it may be caused by the activity of CDK1. Therefore we screened the primary sequence of Wip1 for motifs corresponding to the CDK1 phosphorylation consensus sequence - p(S/T)PX(KR) where 'p' denotes the phosphorylated residue and 'X' any aminoacid. The ELM software (http://elm.eu.org/; (Gould *et al.*, 2010) revealed one putative Cdk phosphorylation site at serine 40 (S40). In addition, ELM software predicted two putative substrate recognition sites that are able to interact with cyclin and thus increases phosphorylation by cyclin/CDK complexes. The first putative cyclin interaction site was mapped at 480-484 aa (KALTL), the second at 511-515 aa (KNLKM). Taken together, these findings encouraged us to focus on S40 as promising candidate for mitotic phoshorylation site. To validate our presumptions, we subjected the precipitated mitotic Wip1 to mass spectrometric analysis, which was performed at University Medical Center Utrecht. The mass spectrometric analysis results confirmed that S40 is phosphorylated during mitosis. For that reason, we mutated S40 to alanine and aspartic acid, the non-phosphorylable variant and the phosphate-mimicking variant, respectively, to characterize this Wip1 mitotic phosphorylation. Successful cloning of S40A and S40D mutant was described in detail in Results and these plasmids will be used in functional studies of Wip1.

6.3.2 Is Wip1 degraded upon mitotic entry?

Apart from the detected mobility shift, we also observed that the intensity of bands corresponding to Wip1 was decreased during mitosis (Figure 5.33). Even the sum of both bands, the original and shifted one, did not seem to constitute the intensity of Wip1 signal in interphase cells. Conversely, the Wip1 mRNA levels did not change during the cell cycle, including mitosis (Figure 5.32). We suggest two possible explanations. Firstly, it is possible that another mitotic modification gives rise to additional Wip1 subpopulations, which are not detected with anti-Wip1 antibody, perhaps due to a masked epitope. Secondly and more interestingly, it could be that Wip1 undergoes degradation specifically during mitosis.

Microscopic analysis of prepared cell lines expressing GFP tagged-Wip1 did not reveal any significant decrease in the GFP-signal intensity in mitotic cells. Nevertheless, these cell lines expressed considerably higher levels of fusion-Wip1 compared to physiological levels of endogenous Wip1, which may possibly interfere with detection of any decrease. In addition, the morphological changes occurring during mitosis also made the comparison of GFP signal changes between mitotic and interphase cells difficult.

To test our assumption of Wip1 mitotic degradation, we subjected cells to the treatment with proteasomal inhibitor MG132 right before mitotic entry, then released cells into mitosis, and checked for Wip1 stabilization. Indeed, we observed an increase in Wip1 levels compared to untreated mitotic control (Figure 5.36). This increase did not reach the levels of interphase Wip1 in all samples, yet this could be explained by only partial efficiency of the proteasomal inhibition. Nevertheless the interpretation of these results is still ambiguous. We can rule out the possibility that the increase in Wip1 levels was due to the preventing its physiological turnover, as the MG132-dependent increase of Wip1 levels was detectable even at 1 hour after release from the G2/M block and we know from our previous experiments that Wip1 half-life is approximately about 2.5 hours (Figure 5.29 A, B). However, we cannot exclude the possibility that MG132 treatment affects the Wip1 levels by other means than just prohibiting its degradation. Inhibition of proteasome represents a particularly stressful event for the cell, which

is well demonstrated by the fact that prolonged treatment with MG132 leads to a strong apoptotic response (Figure 5.30). As Wip1 is tightly connected to cellular stress response, it is possible that this MG132-induced stress would affect its regulation. Moreover, proteasomal inhibition leads to stabilization and increase of p53 levels since p53 turnover is generally very fast (Chapter 3.3.1).

To convincingly prove that Wip1 is really degraded in mitosis, we aimed to isolate ubiquitinated Wip1 using immunoprecipitation of Wip1 from mitotic samples treated with MG132 inhibitor. We performed this experiment using cells expressing FLAG-tagged ubiquitin, yet until finishing of the thesis we were unable to detect any ubiquitinated Wip1. Thus until now it remains unclear whether Wip1 is degraded during mitosis.

It also remains to be elucidated whether the mitotic phosphorylation of Wip1 might have any link to possible degradation of Wip1. Phosphorylation of Wip1 might serve as a recognition motif and mediate specific protein-protein interactions. Good example for such phosphorylation-dependent interaction is binding of F-box proteins to phosphorylated substrates, which leads to proteasomal degradation (reviewed by Kipreos and Pagano (2000). Alternatively, the S40 site resides within the catalytic domain of Wip1 and thus its phosphorylation might affect its catalytic function. We hope to resolve these issues in the future exploiting the prepared S40 mutants and cell lines.

6.3.3 Wip1 downregulation could outweight mitotic deficiency in DNA damage response

Importantly, the DNA damage response to double strand breaks seems to be at least partially attenuated during mitosis. The cells are able to delay mitotic progression in presence of DSBs only to mid prophase (Pines and Rieder, 2001). Once they pass this point, they cannot fully activate the DNA damage checkpoint and do not retard mitotic progression (Rieder and Salmon, 1998). However, presence of γH2AX in γ-irradiated mitotic cells was reported Nakamura *et al.* (2006). Giunta *et al.* (2010) demonstrated that early activations event of DDR happens during mitosis, as they observed accumulation of MRN comlex, MDC1 and γH2AX

at sites of DSBs. On the contrary, no recruitment of RNF8 and RNF168 ubiquitin ligases and 53BP1 was detected in mitotic cells, as opposed to interphase ones. Also, the activation of Chk2 was decreased in mitotic cells. Giunta *et al.* (2010) proposed that cells prioritize the prompt mitotic progress, even in the presence of DNA damage and only marks its site, while the proper response does not happen until the following G1. Nevertheless, the sole mitotic marking of DSBs plays important physiological role, since it prepares cells for a rapid and effective DDR in G1. The mechanism, by which the mitotic cells downregulate the full activation of DDR, is not known.

According to Giunta *et al.* (2010) proposition, we might hypothesize that even basally active Wip1 would interfere with marking of DSBs since DDR is downregulated during mitosis. Hence Wip1 downregulation would outweight mitotic deficiency in DDR. This issue remains to be investigated

6.3.4 Potential role of Wip1 downregulation for "prolonged prometaphase checkpoint"

The proper chromosome segregation is crucial for maintenance of constant number of chromosomes in each daughter cell after the cell division. The defects in chromosome segregation can results in aneuploidy, which may possibly lead to cell death or malignant transformation. Therefore the chromosome segregation is a tightly regulated process. The spindle-assembly checkpoint blocks the metaphase-anaphase transition until kinetochores of all chromosomes are attached to spindle microtubules (in detail described in Musacchio and Salmon, 2007). However, under certain conditions, e.g. when cells are continuously exposed to microtubule inhibitors, cells ultimately exit from mitosis after 12–48 hours even with inappropriatly assembled spindle (Uetake and Sluder, 2010).

Uetake and Sluder (2010) described the existence of a novel mechanism that senses duration of the prometaphase. Normal mitosis is accomplished in about 1 hour. If the prometaphase lasts longer than 1.5 hour, cells are still able to procede through mitosis, but irreversibly arrest in the following G1 phase. This arrest has been suggested to be p38MAPK and p53 dependent. The necessity of

p53 and p38MAPK activation for this arrest has been described to be restricted solely to G1 phase and not to prolonged mitosis. Nevertheless, the suggestion that p53 and p38MAPK are not activated in mitosis was based only on the observation of total p53 levels and on the treatment with p38MAPK inhibitor SB203580 during mitosis that did not lead to abrogation of G1 arrest. Since prolonged prometaphase may indicate troubles in the correct kinetochore attachment, this "prolonged prometaphase checkpoint" can be viewed as a back-up mechanism for the case of the spindle-assembly checkpoint failure.

If p53 and p38MAPK are activated already in mitosis we could hypothesize that Wip1 downregulation might be favorable for the sensitivity and successful execution of the described "prolonged prometaphase checkpoint". As Wip1 was described to negatively regulate p53, we examined total levels of p53 and p38MAPK and also levels of their activated variants p53-pS15, p38-pT180/pY182 during prolonged mitosis induced by a nocodazol treatment (Figure 5.36). We did not observe any notable changes in total level of p53, or p38MAPK during prolonged mitosis. The p53-pS15 levels also do not exhibit increase compared to RO3066 arrested sample. However, interpretation of p53 activation is problematic, since the treatment with RO3066 leads to p53 activation per se. RO3066 treatment was essential for efficient synchronization of cells and allowed us to collect a population of cells that entered mitosis at the same time. Without the RO3066 synchronization, cells entered mitosis in a much longer interval and that made collection of the sample for biochemical analysis impossible.

Intriguingly, we noticed that a portion of p53-pS15 demonstrated a mobility shift specifically in mitosis (Figure 5.36). We speculate that it could correspond to additional posttranslation modification of p53-pS15 subpopulation. According to our knowledge, no p53 modification exclusively specific for mitosis was described, therefore it might be very interesting to investigate this possibility further. We observed an increase in levels of p38MAPK-pT180/pY182 in mitosis prolonged over approximately 3 hours (Figures 5.36, 5.37). This might suggest that p38MAPK is activated during prolonged mitosis.

Additionally, we released cells from prolonged nocodazole block (1, 2 and 4 hours) to G1 phase and checked for p53-pS15 and p38MAPK-pT180/pY182 (Fig-

ure 5.37). Interestingly, the levels of p38MAPK-pT180/pY182 were increased only in samples which were held in mitosis over 2 hours and it was in correlation with p38MAPK-pT180/pY182 levels observed during the prolonged mitosis. Our preliminary results are consistent with the proposed role of p38MAPK in "prolonged prometaphase checkpoint" (Uetake and Sluder; 2010). Nevertheless, further work will be needed to confirm this assumption. Hypothetically, Wip1 downregulation during mitosis might be favorable for proper initiation of "prolonged prometaphase checkpoint".

6.3.5 Wip1-CDK1 may form a double-negative feedback loop

Interesting piece of the puzzle came recently from Park *et al.* (2011) who had demonstrated that Wip1 overexpression leads to increased phoshorylation of CDK1 on tyrosine 15 and thus to its inhibition. It is not clear, how Wip1 can increase CDK1 phosphorylation on tyrosine 15. In fact, it seems very conflicting to the described roles of Wip1 in checkpoint recovery. Wip1 is known to counteract actions of DDR kinases, in case of CDK1 activation most importantly the inhibition of CDC25 phosphatases, activation of Wee1 and p53-dependent activation of p21. Therefore Wip1 should promote CDK1 activation (in greater detail described in... and on fig). Moreover, several works brought evidence that Wip1 promotes checkpoint recovery and mitotic entry (Lindqvist *et al.*, 2009; Takekawa *et al.*, 2000; Yamaguchi *et al.*, 2007) rather than retard cells in G2 as stated by Park *et al.* (2011).

Nevertheless, we considered the possibility that Park *et al.* (2011) suggestions are plausible. Taken them together with our assumption that Wip1 is phosphorylated by CDK1 upon mitotic entry, we might hypothesize that CDK1 and Wip1 are regulated in double-negative feedback loop. In G2, active Wip1 can contribute to CDK1 inhibition and thus to delay of the mitotic progression. Whereas, when activity of CDK1 finally reaches certain level due to actions of CDC25 phosphatases, it could in turn downregulate Wip1 activity or even its levels. This would consequently lead to further increase of CDK1 activity. Hence Wip1 downregulation might be crucial for full activation of CDK1 and proper mitotic entry and progres-

sion. As cell decision to activate CDK1 and to progress to mitosis can be considered as “all-or-none” decision, the regulation via double-negative feedback is particularly convenient. The doublenegative feedback loop can give rise to bistable system, which exhibits two stable steady states, separated by an unstable state, in other words it will provide desired “all-or- none” response (Ferrell, 2008). Importatnly, the dynamics of CDK1 activation corresponds to bistable system. Two different loops have been described to promote this behavior. Firstly, CDK1 can directly phosphorylate and activate CDC25 phosphatases and hence sets a positive feedback loop. Secondly, CDK1 directly inhibits Wee1 kinase and thus sets a double-negative feedback loop (Ferrell, 2008). The double negative feedback between CDK1 and Wip1 might provide the third contribution to this regulatory circuit. Therefore Wip1 could retard cells in G2 providing them with time to fully prepare to mitotic progression. By the time cells are finally ready to enter the mitosis, CDK1 activity would reach a certain level and in a negative feedback it will inhibit Wip1 function, which in turn would result in a full activation of CDK1 and prompt mitotic entry. Considerable problem of this model represent the Wip1 actions that lead to activation of CDC25 phosphatases and inactivation of Wee1 kinase. However, these Wip1 actions are strictly dependent on activation of cell cycle checkpoint. Therefore we speculate that Wip1 might play different regulatory role in normal cell cycle progression and in mitotic entry from checkpoint recovery. During normal cell cycle Wip1 would act as proposed by Park *et al.* (2011). On the other hand during checkpoint recovery, Wip1 activity would lead to activation of CDC25 phosphatases and inactivation of Wee1 kinase and thus would promote mitotic entry. According to this view, the role of Wip1 in regulation of G2/M transition would be much more complex that is currently thought. Yet again we would strongly suggest to further validate Park *et al.* (2011) results. We did not observe any noticeable delay in cell cycle in prepared cell lines overexpressing wild-type GFP-Wip1 during regular cell cultivation. Nevertheless, we did not focus on the measurement of duration of cell cycle phases, especially the G2.

7

Conclusions

1. We validated Wip1 antibody (Bethyl Laboratories; A300-664A) and anti-Wip1 siRNAs (Dharmacon).

2. We prepared stable monoclonal U2OS cell lines expressing wild-type Wip1 N-terminally fused with GFP protein and phosphatase dead Wip1 mutant N-terminally fused with LAP-tag. These will be used for further studies of Wip1 dynamics and regulation and for identifying the new Wip1 interacting partners via tandem affinity purification.

3. We prepared following expression vectors: Wip1-GFP, pLAP-Wip1-S40A-D314A, pLAP-Wip1-S40D-D314A

4. We described the dynamics of selected representative DNA damage response proteins upon γ-irradiation and UV-C irradiation. These included gammaH2AX, Chk2-pT68, Chk1pS317, p53, p53-pS15, p21 and Wip1. Additionally, we described the dynamics of the p38MAPK-MAPKAP-K2 pathway, particularly the proteins MKK3-pS189/MKK6-pS207, p38MAPK, p38MAPK-pT180/pY182 and MAPKAPK-2-p334 upon γ-irradiation and UV-C irradiation

5. We observed that p53 expression pattern in MCF7 cells after γ-irradiation correspond to series of pulses. This is in agreement with the literature data. On the contrary, in U2OS cells, the p53 levels demonstrated a monotone continuous increase. The similar dynamics was shown after UV-C irradiation. The same dynamics of p53 in MCF7 cells after UV-C irradiation was

simultaneously described by Batchelor *et al.* (2008). We suggest that p53 dynamics depends on the presence or absence of effective negative feedback loops between the upstream p53-activating kinases and Wip1 phosphatase.

6. We showed that p21 levels exhibit a pulsative dynamics after UV-C irradiation, conversely to monotone increase after γ-irradiation.

7. We detected pulsative dynamics in activation of the p38MAPK-MAPKAP-K2 pathway upon γ-irradiation and UV-C irradiation.

8. We showed, in consistence with recent findings of Xia et al. (2011) that Wip1 dynamics after UV-C irradiation is dose dependent. Wip1 levels decrease upon high doses of UV-C, but do not drop off upon low UV-C doses.

9. We demonstrated that Wip1 is phosphorylated on pSQ/pTQ motif upon UV-C irradiation. This phosphorylation peaked within 30 minutes after irradiation and then gradually declined.

10. We showed that Wip1 undergoes phosphorylation on serine 40 specifically during mitosis. This implies that Wip1 is distinctly regulated during the cell cycle progression.

Bibliography

Abramoff, M., Magalhaes, P., Ram, S. (2004): Image Processing with ImageJ. Biophotonics International 11: 36–42.

Ackland, S.P., Schilsky, R.L., Beckett, M.A., Weichselbaum, R.R. (1988): Synergistic cytotoxicity and DNA strand break formation by bromodeoxyuridine and bleomycin in human tumor cells. Cancer Res. 48: 4244–4249.

Ahn, J.Y., Schwarz, J.K., Piwnica-Worms, H., Canman, C.E. (2000): Threonine 68 phosphorylation by ataxia telangiectasia mutated is required for efficient activation of Chk2 in response to ionizing radiation. Cancer Res. 60: 5934–5936.

Ali, A., Zhang, J., Bao, S., Liu, I., Otterness, D., Dean, N.M., Abraham, R.T., Wang, X.F. (2004): Requirement of protein phosphatase 5 in DNA-damage-induced ATM activation. Genes Dev. 18: 249–254.

Alvarez-Fernández, M., Halim, V.A., Krenning, L., Aprelia, M., Mohammed, S., Heck, A.J., Medema, R.H. (2010): Recovery from a DNA-damage-induced G2 arrest requires Cdk-dependent activation of FoxM1. EMBO Rep. 11: 452–458.

Amagai, M. (2009): The molecular logic of pemphigus and impetigo: the desmoglein story. Vet. Dermatol. 20: 308–312.

Askari, N., Beenstock, J., Livnah, O., Engelberg, D. (2009): p38alpha is active in vitro and in vivo when monophosphorylated at threonine 180. Biochemistry (Mosc.) 48: 2497–2504.

Bakkenist, C.J., Kastan, M.B. (2003): DNA damage activates ATM through intermolecular autophosphorylation and dimer dissociation. Nature 421: 499–506.

Ball, H.L., Myers, J.S., Cortez, D. (2005): ATRIP binding to replication protein A-single-stranded DNA promotes ATR-ATRIP localization but is dispensable for Chk1 phosphorylation. Mol. Biol. Cell 16: 2372–2381.

Ball, L.G., Xiao, W. (2005): Molecular basis of ataxia telangiectasia and related diseases. Acta Pharmacol. Sin. 26: 897–907.

Bar-Or, R.L., Maya, R., Segel, L.A., Alon, U., Levine, A.J., Oren, M. (2000): Generation of oscillations by the p53-Mdm2 feedback loop: a theoretical and experimental study. Proc. Natl. Acad. Sci. U. S. A. 97: 11250–11255.

Barak, Y., Juven, T., Haffner, R., Oren, M. (1993): mdm2 expression is induced by wild type p53 activity. EMBO J. 12: 461–468.

Bartek, J., Lukas, J. (2003): Chk1 and Chk2 kinases in checkpoint control and cancer. Cancer Cell 3: 421–429.

Bartek, J., Lukas, J. (2007): DNA damage checkpoints: from initiation to recovery or adaptation. Curr. Opin. Cell Biol. 19: 238–245.

Bartkova, J., Horejsí, Z., Koed, K., Krämer, A., Tort, F., Zieger, K., Guldberg, P., Sehested, M., Nesland, J.M., Lukas, C., Ørntoft, T., Lukas, J., Bartek, J. (2005): DNA damage response as a candidate anti-cancer barrier in early human tumorigenesis. Nature 434: 864–870.

Batchelor, E., Loewer, A., Lahav, G. (2009): The ups and downs of p53: understanding protein dynamics in single cells. Nat. Rev. Cancer 9: 371–377.

Batchelor, E., Loewer, A., Mock, C., Lahav, G. (2011): Stimulus-dependent dynamics of p53 in single cells. Mol. Syst. Biol. 7: 488.

Batchelor, E., Mock, C.S., Bhan, I., Loewer, A., Lahav, G. (2008): Recurrent initiation: a mechanism for triggering p53 pulses in response to DNA damage. Mol. Cell 30: 277–289.

Batista, L.F.Z., Chigançcas, V., Brumatti, G., Amarante-Mendes, G.P., Menck, C.F.M. (2006): Involvement of DNA replication in ultraviolet-induced apoptosis of mammalian cells. Apoptosis 11: 1139–1148.

Bekker-Jensen, S., Mailand, N. (2011): The ubiquitin- and SUMO-dependent signaling response to DNA double-strand breaks. FEBS Lett. .

Bell, D.W., Varley, J.M., Szydlo, T.E., Kang, D.H., Wahrer, D.C., Shannon, K.E., Lubratovich, M., Verselis, S.J., Isselbacher, K.J., Fraumeni, J.F., Birch, J.M., Li, F.P., Garber, J.E., Haber, D.A. (1999): Heterozygous germ line hCHK2 mutations in Li-Fraumeni syndrome. Science 286: 2528–2531.

Ben-Levy, R., Leighton, I.A., Doza, Y.N., Attwood, P., Morrice, N., Marshall, C.J., Cohen, P. (1995): Identification of novel phosphorylation sites required for activation of MAPKAP kinase-2. EMBO J. 14: 5920–5930.

Benchimol, S. (2001): p53-dependent pathways of apoptosis. Cell Death Differ. 8: 1049–1051.

Bendjennat, M., Boulaire, J., Jascur, T., Brickner, H., Barbier, V., Sarasin, A., Fotedar, A., Fotedar, R. (2003): UV irradiation triggers ubiquitin-dependent degradation of p21(WAF1) to promote DNA repair. Cell 114: 599–610.

Blazkova, H., Krejcikova, K., Moudry, P., Frisan, T., Hodny, Z., Bartek, J. (2010): Bacterial intoxication evokes cellular senescence with persistent DNA damage and cytokine signalling. J. Cell. Mol. Med. 14: 357–367.

Botuyan, M.V., Lee, J., Ward, I.M., Kim, J.E., Thompson, J.R., Chen, J., Mer, G. (2006): Structural basis for the methylation state-specific recognition of histone H4-K20 by 53BP1 and Crb2 in DNA repair. Cell 127: 1361–1373.

Bradford, M.M. (1976): A rapid and sensitive method for the quantitation of microgram quantities of protein utilizing the principle of protein-dye binding. Anal. Biochem. 72: 248–254.

Brancho, D., Tanaka, N., Jaeschke, A., Ventura, J.J., Kelkar, N., Tanaka, Y., Kyuuma, M., Takeshita, T., Flavell, R.A., Davis, R.J. (2003): Mechanism of p38 MAP kinase activation in vivo. Genes Dev. 17: 1969–1978.

Bulavin, D.V., Higashimoto, Y., Popoff, I.J., Gaarde, W.A., Basrur, V., Potapova, O., Appella, E., Fornace, A.J. (2001): Initiation of a G2/M checkpoint after ultraviolet radiation requires p38 kinase. Nature 411: 102–107.

Bulavin, D.V., Saito, S., Hollander, M.C., Sakaguchi, K., Anderson, C.W., Appella, E., Fornace, A.J. (1999): Phosphorylation of human p53 by p38 kinase coordinates n-terminal phosphorylation and apoptosis in response to UV radiation. EMBO J. 18: 6845–6854.

Bulavin, D.V., Demidov, O.N., Saito, S., Kauraniemi, P., Phillips, C., Amundson, S.A., Ambrosino, C., Sauter, G., Nebreda, A.R., Anderson, C.W., Kallioniemi, A., Fornace, A.J., Appella, E. (2002): Amplification of PPM1D in human tumors abrogates p53 tumor-suppressor activity. Nat. Genet. 31: 210–215.

Bulavin, D.V., Phillips, C., Nannenga, B., Timofeev, O., Donehower, L.A., Anderson, C.W., Appella, E., Fornace, A.J. (2004): Inactivation of the Wip1 phosphatase inhibits mammary tumorigenesis through p38 MAPK-mediated activation of the p16(Ink4a)-p19(arf) pathway. Nat. Genet. 36: 343–350.

Bunz, F., Dutriaux, A., Lengauer, C., Waldman, T., Zhou, S., Brown, J.P., Sedivy, J.M., Kinzler, K.W., Vogelstein, B. (1998): Requirement for p53 and p21 to sustain G2 arrest after Dna damage. Science 282: 1497–1501.

Burma, S., Chen, B.P., Murphy, M., Kurimasa, A., Chen, D.J. (2001): ATM phosphorylates histone H2AX in response to DNA double-strand breaks. J. Biol. Chem. 276: 42462–42467.

Burma, S., Chen, B.P.C., Chen, D.J. (2006): Role of non-homologous end joining (NHEJ) in maintaining genomic integrity. DNA Repair (Amst) 5: 1042–1048.

Busino, L., Donzelli, M., Chiesa, M., Guardavaccaro, D., Ganoth, D., Dorrello, N.V., Hershko, A., Pagano, M., Draetta, G.F. (2003): Degradation of Cdc25A by beta-TrCP during S phase and in response to DNA damage. Nature 426: 87–91.

Cam, L.L., Linares, L.K., Paul, C., Julien, E., Lacroix, M., Hatchi, E., Triboulet, R., Bossis, G., Shmueli, A., Rodriguez, M.S., Coux, O., Sardet, C. (2006): E4F1 is an atypical ubiquitin ligase that modulates p53 effector functions independently of degradation. Cell 127: 775–788.

Campisi, J., d'Adda di Fagagna, F. (2007): Cellular senescence: when bad things happen to good cells. Nat. Rev. Mol. Cell Biol. 8: 729–740.

Canman, C.E., Lim, D.S., Cimprich, K.A., Taya, Y., Tamai, K., Sakaguchi, K., Appella, E., Kastan, M.B., Siliciano, J.D. (1998): Activation of the ATM kinase by ionizing radiation and phosphorylation of p53. Science 281: 1677–1679.

Cheeseman, I.M., Desai, A. (2005): A combined approach for the localization and tandem affinity purification of protein complexes from metazoans. Sci. STKE 2005: pl1.

Chew, J., Biswas, S., Shreeram, S., Humaidi, M., Wong, E.T., Dhillion, M.K., Teo, H., Hazra, A., Fang, C.C., López-Collazo, E., Bulavin, D.V., Tergaonkar, V. (2009): WIP1 phosphatase is a negative regulator of NF-kappaB signalling. Nat. Cell Biol. 11: 659–666.

Chikamori, K., Grozav, A.G., Kozuki, T., Grabowski, D., Ganapathi, R., Ganapathi, M.K. (2010): DNA topoisomerase ii enzymes as molecular targets for cancer chemotherapy. Curr. Cancer Drug Targets 10: 758–771.

Choi, J., Appella, E., Donehower, L.A. (2000): The structure and expression of the murine wildtype p53-induced phosphatase 1 (Wip1) gene. Genomics 64: 298–306.

Choi, J., Nannenga, B., Demidov, O.N., Bulavin, D.V., Cooney, A., Brayton, C., Zhang, Y., Mbawuike, I.N., Bradley, A., Appella, E., Donehower, L.A. (2002): Mice deficient for the wild-type p53-induced phosphatase gene (Wip1) exhibit defects in reproductive organs, immune function, and cell cycle control. Mol. Cell. Biol. 22: 1094–1105.

Chuman, Y., Kurihashi, W., Mizukami, Y., Nashimoto, T., Yagi, H., Sakaguchi, K. (2009): PPM1D430, a novel alternative splicing variant of the human PPM1D, can dephosphorylate p53 and exhibits specific tissue expression. J. Biochem. 145: 1–12.

Cook, P.J., Ju, B.G., Telese, F., Wang, X., Glass, C.K., Rosenfeld, M.G. (2009): Tyrosine dephosphorylation of H2AX modulates apoptosis and survival decisions. Nature 458: 591–596.

Cortez, D., Guntuku, S., Qin, J., Elledge, S.J. (2001): ATR and ATRIP: partners in checkpoint signaling. Science 294: 1713–1716.

Cotta-Ramusino, C., McDonald, E.R., Hurov, K., Sowa, M.E., Harper, J.W., Elledge, S.J. (2011): A DNA damage response screen identifies RHINO, a 9-1-1 and TopBP1 interacting protein required for ATR signaling. Science 332: 1313–1317.

Cuenda, A., Rousseau, S. (2007): p38 MAP-kinases pathway regulation, function and role in human diseases. Biochim. Biophys. Acta 1773: 1358–1375.

d'Adda di Fagagna, F. (2008): Living on a break: cellular senescence as a DNA-damage response. Nat. Rev. Cancer 8: 512–522.

Dalhus, B., Laerdahl, J.K., Backe, P.H., Bjørås, M. (2009): DNA base repair–recognition and initiation of catalysis. FEMS Microbiol. Rev. 33: 1044–1078.

de Graaf, P., Little, N.A., Ramos, Y.F.M., Meulmeester, E., Letteboer, S.J.F., Jochemsen, A.G. (2003): Hdmx protein stability is regulated by the ubiquitin ligase activity of Mdm2. J. Biol. Chem. 278: 38315–38324.

Delacroix, S., Wagner, J.M., Kobayashi, M., ichi Yamamoto, K., Karnitz, L.M. (2007): The Rad9-hus1-Rad1 (9-1-1) clamp activates checkpoint signaling via TopBP1. Genes Dev. 21: 1472–1477.

Doil, C., Mailand, N., Bekker-Jensen, S., Menard, P., Larsen, D.H., Pepperkok, R., Ellenberg, J., Panier, S., Durocher, D., Bartek, J., Lukas, J., Lukas, C. (2009): RNF168 binds and amplifies ubiquitin conjugates on damaged chromosomes to allow accumulation of repair proteins. Cell 136: 435–446.

Donahue, B.A., Yin, S., Taylor, J.S., Reines, D., Hanawalt, P.C. (1994): Transcript cleavage by RNA polymerase ii arrested by a cyclobutane pyrimidine dimer in the Dna template. Proc. Natl. Acad. Sci. U. S. A. 91: 8502–8506.

Durkin, S.G., Glover, T.W. (2007): Chromosome fragile sites. Annu. Rev. Genet. 41: 169–192.

Durkin, S.G., Ragland, R.L., Arlt, M.F., Mulle, J.G., Warren, S.T., Glover, T.W. (2008): Replication stress induces tumor-like microdeletions in FHIT/FRA3B. Proc. Natl. Acad. Sci. U. S. A. 105: 246–251.

Duthie, S.J., Hawdon, A. (1998): DNA instability (strand breakage, uracil misincorporation, and defective repair) is increased by folic acid depletion in human lymphocytes in vitro. FASEB J. 12: 1491–1497.

el Deiry, W.S., Tokino, T., Velculescu, V.E., Levy, D.B., Parsons, R., Trent, J.M., Lin, D., Mercer, W.E., Kinzler, K.W., Vogelstein, B. (1993): WAF1, a potential mediator of p53 tumor suppression. Cell 75: 817–825.

Enslen, H., Raingeaud, J., Davis, R.J. (1998): Selective activation of p38 mitogen-activated protein (MAP) kinase isoforms by the MAP kinase kinases MKK3 and MKK6. J. Biol. Chem. 273: 1741–1748.

Fang, S., Jensen, J.P., Ludwig, R.L., Vousden, K.H., Weissman, A.M. (2000): Mdm2 is a RING finger-dependent ubiquitin protein ligase for itself and p53. J. Biol. Chem. 275: 8945–8951.

Ferrell, J.E. (2008): Feedback regulation of opposing enzymes generates robust, all-or-none bistable responses. Curr. Biol. 18: R244–R245.

Fiscella, M., Zhang, H., Fan, S., Sakaguchi, K., Shen, S., Mercer, W.E., Woude, G.F.V., O'Connor, P.M., Appella, E. (1997): Wip1, a novel human protein phosphatase that is induced in response to ionizing radiation in a p53-dependent manner. Proc. Natl. Acad. Sci. U. S. A. 94: 6048–6053.

Forrest, A., Gabrielli, B. (2001): Cdc25B activity is regulated by 14-3-3. Oncogene 20: 4393–4401.

Freshney, I.R. (2005): Culture of Animal Cells: A Manual of Basic Technique. John Wiley & Sons, Inc., New York.

Fujimoto, H., Onishi, N., Kato, N., Takekawa, M., Xu, X.Z., Kosugi, A., Kondo, T., Imamura, M., Oishi, I., Yoda, A., Minami, Y. (2006): Regulation of the antioncogenic Chk2 kinase by the oncogenic Wip1 phosphatase. Cell Death Differ. 13: 1170–1180.

Gacy, A.M., Goellner, G., Juranić, N., Macura, S., McMurray, C.T. (1995): Trinucleotide repeats that expand in human disease form hairpin structures in vitro. Cell 81: 533–540.

Geva-Zatorsky, N., Rosenfeld, N., Itzkovitz, S., Milo, R., Sigal, A., Dekel, E., Yarnitzky, T., Liron, Y., Polak, P., Lahav, G., Alon, U. (2006): Oscillations and variability in the p53 system. Mol. Syst. Biol. 2: 2006.0033.

Giunta, S., Belotserkovskaya, R., Jackson, S.P. (2010): DNA damage signaling in response to double-strand breaks during mitosis. J. Cell Biol. 190: 197–207.

Goh, A.M., Coffill, C.R., Lane, D.P. (2011): The role of mutant p53 in human cancer. J. Pathol. 223: 116–126.

Gorbunova, V., Seluanov, A., Pereira-Smith, O.M. (2002): Expression of human telomerase (hTERT) does not prevent stress-induced senescence in normal human fibroblasts but protects the cells from stress-induced apoptosis and necrosis. J. Biol. Chem. 277: 38540–38549.

Gorgoulis, V.G., Vassiliou, L.V.F., Karakaidos, P., Zacharatos, P., Kotsinas, A., Liloglou, T., Venere, M., Ditullio, R.A., Kastrinakis, N.G., Levy, B., Kletsas, D., Yoneta, A., Herlyn, M., Kittas, C., Halazonetis, T.D. (2005): Activation of the DNA damage checkpoint and genomic instability in human precancerous lesions. Nature 434: 907–913.

Gould, C.M., Diella, F., Via, A., Puntervoll, P., Gemünd, C., Chabanis-Davidson, S., Michael, S., Sayadi, A., Bryne, J.C., Chica, C., Seiler, M., Davey, N.E., Haslam, N., Weatheritt, R.J., Budd, A., Hughes, T., Pas, J., Rychlewski, L., Travé, G., Aasland, R., Helmer-Citterich, M., Linding, R., Gibson, T.J. (2010): ELM: the status of the 2010 eukaryotic linear motif resource. Nucleic Acids Res. 38: D167–D180.

Graves, P.R., Lovly, C.M., Uy, G.L., Piwnica-Worms, H. (2001): Localization of human Cdc25C is regulated both by nuclear export and 14-3-3 protein binding. Oncogene 20: 1839–1851.

Grenon, M., Gilbert, C., Lowndes, N.F. (2001): Checkpoint activation in response to double-strand breaks requires the Mre11/Rad50/Xrs2 complex. Nat. Cell Biol. 3: 844–847.

Gu, W., Roeder, R.G. (1997): Activation of p53 sequence-specific DNA binding by acetylation of the p53 C-terminal domain. Cell 90: 595–606.

Hande, K.R. (1998): Etoposide: four decades of development of a topoisomerase ii inhibitor. Eur. J. Cancer 34: 1514–1521.

Harper, J.W., Adami, G.R., Wei, N., Keyomarsi, K., Elledge, S.J. (1993): The p21 Cdk-interacting protein Cip1 is a potent inhibitor of G1 cyclin-dependent kinases. Cell 75: 805–816.

Hershko, A., Heller, H., Elias, S., Ciechanover, A. (1983): Components of ubiquitin-protein ligase system. Resolution, affinity purification, and role in protein breakdown. J. Biol. Chem. 258: 8206–8214.

Hirao, A., Cheung, A., Duncan, G., Girard, P.M., Elia, A.J., Wakeham, A., Okada, H., Sarkissian, T., Wong, J.A., Sakai, T., Stanchina, E.D., Bristow, R.G., Suda, T., Lowe, S.W., Jeggo, P.A., Elledge, S.J., Mak, T.W. (2002): Chk2 is a tumor suppressor that regulates apoptosis in both an ataxia telangiectasia mutated (ATM)-dependent and an ATM-independent manner. Mol. Cell. Biol. 22: 6521–6532.

Hirasawa, A., Saito-Ohara, F., Inoue, J., Aoki, D., Susumu, N., Yokoyama, T., Nozawa, S., Inazawa, J., Imoto, I. (2003): Association of 17q21-q24 gain in ovarian clear cell adenocarcinomas with poor prognosis and identification of PPM1D and APPBP2 as likely amplification targets. Clin. Cancer Res. 9: 1995–2004.

Honda, R., Tanaka, H., Yasuda, H. (1997): Oncoprotein MDM2 is a ubiquitin ligase E3 for tumor suppressor p53. FEBS Lett. 420: 25–27.

Hou, M.H., Robinson, H., Gao, Y.G., Wang, A.H.J. (2002): Crystal structure of actinomycin D bound to the CTG triplet repeat sequences linked to neurological diseases. Nucleic Acids Res. 30: 4910–4917.

Huen, M.S.Y., Grant, R., Manke, I., Minn, K., Yu, X., Yaffe, M.B., Chen, J. (2007): RNF8 transduces the DNA-damage signal via histone ubiquitylation and checkpoint protein assembly. Cell 131: 901–914.

Ikura, T., Ogryzko, V.V., Grigoriev, M., Groisman, R., Wang, J., Horikoshi, M., Scully, R., Qin, J., Nakatani, Y. (2000): Involvement of the TIP60 histone acetylase complex in DNA repair and apoptosis. Cell 102: 463–473.

Imbriano, C., Gurtner, A., Cocchiarella, F., Agostino, S.D., Basile, V., Gostissa, M., Dobbelstein, M., Sal, G.D., Piaggio, G., Mantovani, R. (2005): Direct p53 transcriptional repression: in vivo analysis of CCAAT-containing G2/M promoters. Mol. Cell. Biol. 25: 3737–3751.

Jack, M.T., Woo, R.A., Hirao, A., Cheung, A., Mak, T.W., Lee, P.W.K. (2002): Chk2 is dispensable for p53-mediated G1 arrest but is required for a latent p53-mediated apoptotic response. Proc. Natl. Acad. Sci. U. S. A. 99: 9825–9829.

Jackson, S.P., Bartek, J. (2009): The DNA-damage response in human biology and disease. Nature 461: 1071–1078.

Jazayeri, A., Falck, J., Lukas, C., Bartek, J., Smith, G.C.M., Lukas, J., Jackson, S.P. (2006): ATM- and cell cycle-dependent regulation of ATR in response to DNA double-strand breaks. Nat. Cell Biol. 8: 37–45.

Jeong, S.Y., Kumagai, A., Lee, J., Dunphy, W.G. (2003): Phosphorylated claspin interacts with a phosphate-binding site in the kinase domain of Chk1 during ATR-mediated activation. J. Biol. Chem. 278: 46782–46788.

Jiang, X., Sun, Y., Chen, S., Roy, K., Price, B.D. (2006): The FATC domains of PIKK proteins are functionally equivalent and participate in the Tip60-dependent activation of DNA-PKcs and ATM. J. Biol. Chem. 281: 15741–15746.

Jin, J., Shirogane, T., Xu, L., Nalepa, G., Qin, J., Elledge, S.J., Harper, J.W. (2003): SCFbeta-TRCP links Chk1 signaling to degradation of the Cdc25A protein phosphatase. Genes Dev. 17: 3062–3074.

Kasahara, K., Goto, H., Enomoto, M., Tomono, Y., Kiyono, T., Inagaki, M. (2010): 14-3-3gamma mediates Cdc25A proteolysis to block premature mitotic entry after DNA damage. EMBO J. 29: 2802–2812.

Kass, E.M., Jasin, M. (2010): Collaboration and competition between DNA double-strand break repair pathways. FEBS Lett. 584: 3703–3708.

Khanna, K.K., Keating, K.E., Kozlov, S., Scott, S., Gatei, M., Hobson, K., Taya, Y., Gabrielli, B., Chan, D., Lees-Miller, S.P., Lavin, M.F. (1998): ATM associates with and phosphorylates p53: mapping the region of interaction. Nat. Genet. 20: 398–400.

Khosravi, R., Maya, R., Gottlieb, T., Oren, M., Shiloh, Y., Shkedy, D. (1999): Rapid ATM-dependent phosphorylation of MDM2 precedes p53 accumulation in response to DNA damage. Proc. Natl. Acad. Sci. U. S. A. 96: 14973–14977.

Kim, S.J., Hwang, S.G., Shin, D.Y., Kang, S.S., Chun, J.S. (2002): p38 kinase regulates nitric oxide-induced apoptosis of articular chondrocytes by accumulating p53 via NFkappa B-dependent transcription and stabilization by serine 15 phosphorylation. J. Biol. Chem. 277: 33501–33508.

Kipreos, E.T., Pagano, M. (2000): The F-box protein family. Genome Biol. 1: REVIEWS3002.

Konat, G.W. (2003): H2O2-induced higher order chromatin degradation: a novel mechanism of oxidative genotoxicity. J. Biosci. 28: 57–60.

Krakoff, I.H., Brown, N.C., Reichard, P. (1968): Inhibition of ribonucleoside diphosphate reductase by hydroxyurea. Cancer Res. 28: 1559–1565.

Kremer, E.J., Pritchard, M., Lynch, M., Yu, S., Holman, K., Baker, E., Warren, S.T., Schlessinger, D., Sutherland, G.R., Richards, R.I. (1991): Mapping of DNA instability at the fragile X to a trinucleotide repeat sequence p(CCG)n. Science 252: 1711–1714.

Kumagai, A., Dunphy, W.G. (2003): Repeated phosphopeptide motifs in Claspin mediate the regulated binding of Chk1. Nat. Cell Biol. 5: 161–165.

Kumagai, A., Lee, J., Yoo, H.Y., Dunphy, W.G. (2006): TopBP1 activates the ATR-ATRIP complex. Cell 124: 943–955.

Laemmli, U.K. (1970): Cleavage of structural proteins during the assembly of the head of bacteriophage T4. Nature 227: 680–685.

Lahav, G., Rosenfeld, N., Sigal, A., Geva-Zatorsky, N., Levine, A.J., Elowitz, M.B., Alon, U. (2004): Dynamics of the p53-Mdm2 feedback loop in individual cells. Nat. Genet. 36: 147–150.

Lakin, N.D., Hann, B.C., Jackson, S.P. (1999): The ataxia-telangiectasia related protein ATR mediates DNA-dependent phosphorylation of p53. Oncogene 18: 3989–3995.

Lavin, M.F., Kozlov, S. (2007): ATM activation and DNA damage response. Cell Cycle 6: 931–942.

Lee, H.E., Berkowitz, P., Jolly, P.S., Diaz, L.A., Chua, M.P., Rubenstein, D.S. (2009): Biphasic activation of p38MAPK suggests that apoptosis is a downstream event in pemphigus acantholysis. J. Biol. Chem. 284: 12524–12532.

Lee, H., Zeng, S.X., Lu, H. (2006): UV induces p21 rapid turnover independently of ubiquitin and Skp2. J. Biol. Chem. 281: 26876–26883.

Lee, J.H., Goodarzi, A.A., Jeggo, P.A., Paull, T.T. (2010): 53BP1 promotes ATM activity through direct interactions with the MRN complex. EMBO J. 29: 574–585.

Lee, J.H., Paull, T.T. (2004): Direct activation of the ATM protein kinase by the Mre11/Rad50/Nbs1 complex. Science 304: 93–96.

Lee, J., Kumagai, A., Dunphy, W.G. (2007): The Rad9-Hus1-Rad1 checkpoint clamp regulates interaction of TopBP1 with ATR. J. Biol. Chem. 282: 28036–28044.

Lees-Miller, S.P., Sakaguchi, K., Ullrich, S.J., Appella, E., Anderson, C.W. (1992): Human DNA-activated protein kinase phosphorylates serines 15 and 37 in the amino-terminal transactivation domain of human p53. Mol. Cell. Biol. 12: 5041–5049.

Lemaire, M., Froment, C., Boutros, R., Mondesert, O., Nebreda, A.R., Monsarrat, B., Ducommun, B. (2006): CDC25B phosphorylation by p38 and MK-2. Cell Cycle 5: 1649–1653.

Leonardo, A.D., Linke, S.P., Clarkin, K., Wahl, G.M. (1994): DNA damage triggers a prolonged p53-dependent G1 arrest and long-term induction of Cip1 in normal human fibroblasts. Genes Dev. 8: 2540–2551.

Li, J., Yang, Y., Peng, Y., Austin, R.J., van Eyndhoven, W.G., Nguyen, K.C.Q., Gabriele, T., McCurrach, M.E., Marks, J.R., Hoey, T., Lowe, S.W., Powers, S. (2002): Oncogenic properties of PPM1D located within a breast cancer amplification epicenter at 17q23. Nat. Genet. 31: 133–134.

Li, Q., Wang, X., Wu, X., Rui, Y., Liu, W., Wang, J., Wang, X., Liou, Y.C., Ye, Z., Lin, S.C. (2007): Daxx cooperates with the Axin/HIPK2/p53 complex to induce cell death. Cancer Res. 67: 66–74.

Lieber, M.R., Karanjawala, Z.E. (2004): Ageing, repetitive genomes and DNA damage. Nat. Rev. Mol. Cell Biol. 5: 69–75.

Lindqvist, A., de Bruijn, M., Macurek, L., Brás, A., Mensinga, A., Bruinsma, W., Voets, O., Kranenburg, O., Medema, R.H. (2009): Wip1 confers G2 checkpoint recovery competence by counteracting p53-dependent transcriptional repression. EMBO J. 28: 3196–3206.

Little, M.P. (2003): Risks associated with ionizing radiation. Br. Med. Bull. 68: 259–275.

Liu, Q., Guntuku, S., Cui, X.S., Matsuoka, S., Cortez, D., Tamai, K., Luo, G., Carattini-Rivera, S., DeMayo, F., Bradley, A., Donehower, L.A., Elledge, S.J. (2000): Chk1 is an essential kinase that is regulated by Atr and required for the G(2)/M DNA damage checkpoint. Genes Dev. 14: 1448–1459.

Lodish, H., Baltimore, D., Berk, A., Zipursky, S.L., Matsudaira, P., Darnell, J. (1995): Molecular Cell Biology. W. H. Freeman and Company, New York.

Loewer, A., Batchelor, E., Gaglia, G., Lahav, G. (2010): Basal dynamics of p53 reveal transcriptionally attenuated pulses in cycling cells. Cell 142: 89–100.

Longhese, M.P., Bonetti, D., Guerini, I., Manfrini, N., Clerici, M. (2009): DNA double-strand breaks in meiosis: checking their formation, processing and repair. DNA Repair (Amst) 8: 1127–1138.

Lowe, J.M., Cha, H., Yang, Q., Fornace, A.J. (2010): Nuclear factor-kappaB (NF-kappaB) is a novel positive transcriptional regulator of the oncogenic Wip1 phosphatase. J. Biol. Chem. 285: 5249–5257.

Lu, X., Bocangel, D., Nannenga, B., Yamaguchi, H., Appella, E., Donehower, L.A. (2004): The p53-induced oncogenic phosphatase PPM1D interacts with uracil DNA glycosylase and suppresses base excision repair. Mol. Cell 15: 621–634.

Lu, X., Ma, O., Nguyen, T.A., Jones, S.N., Oren, M., Donehower, L.A. (2007): The wip1 Phosphatase acts as a gatekeeper in the p53-Mdm2 autoregulatory loop. Cancer Cell 12: 342–354.

Lu, X., Nannenga, B., Donehower, L.A. (2005): PPM1D dephosphorylates Chk1 and p53 and abrogates cell cycle checkpoints. Genes Dev. 19: 1162–1174.

Lu, X., Nguyen, T.A., Moon, S.H., Darlington, Y., Sommer, M., Donehower, L.A. (2008a): The type 2C phosphatase Wip1: an oncogenic regulator of tumor suppressor and DNA damage response pathways. Cancer Metastasis Rev. 27: 123–135.

Lu, X., Nguyen, T.A., Zhang, X., Donehower, L.A. (2008b): The Wip1 phosphatase and Mdm2: cracking the "Wip" on p53 stability. Cell Cycle 7: 164–168.

Luck, G., Zimmer, C., Reinert, K.E., Arcamone, F. (1977): Specific interactions of distamycin A and its analogs with (A-T) rich and (G-C) rich duplex regions of DNA and deoxypolynucleotides. Nucleic Acids Res. 4: 2655–2670.

Lukusa, T., Fryns, J.P. (2008): Human chromosome fragility. Biochim. Biophys. Acta 1779: 3–16.

MacBiophotonics (2010): Online Manual for the 'ImageJ for Microscopy' bundle. http://www.macbiophotonics.ca/imagej/.

Macleod, K.F., Sherry, N., Hannon, G., Beach, D., Tokino, T., Kinzler, K., Vogelstein, B., Jacks, T. (1995): p53-dependent and independent expression of p21 during cell growth, differentiation, and DNA damage. Genes Dev. 9: 935–944.

Macůrek, L., Lindqvist, A., Voets, O., Kool, J., Vos, H.R., Medema, R.H. (2010): Wip1 phosphatase is associated with chromatin and dephosphorylates gammaH2AX to promote checkpoint inhibition. Oncogene 29: 2281–2291.

Macůrek, L., Lindqvist, A., Lim, D., Lampson, M.A., Klompmaker, R., Freire, R., Clouin, C., Taylor, S.S., Yaffe, M.B., Medema, R.H. (2008): Polo-like kinase-1 is activated by aurora A to promote checkpoint recovery. Nature 455: 119–123.

Magenis, R.E., Hecht, F., Lovrien, E.W. (1970): Heritable fragile site on chromosome 16: probable localization of haptoglobin locus in man. Science 170: 85–87.

Mah, L.J., El-Osta, A., Karagiannis, T.C. (2010): gammaH2AX: a sensitive molecular marker of DNA damage and repair. Leukemia 24: 679–686.

Mailand, N., Bekker-Jensen, S., Faustrup, H., Melander, F., Bartek, J., Lukas, C., Lukas, J. (2007): RNF8 ubiquitylates histones at DNA double-strand breaks and promotes assembly of repair proteins. Cell 131: 887–900.

Malkin, D. (2011): Li-fraumeni syndrome. Genes Cancer 2: 475–484.

Maltzman, W., Czyzyk, L. (1984): UV irradiation stimulates levels of p53 cellular tumor antigen in nontransformed mouse cells. Mol. Cell. Biol. 4: 1689–1694.

Mamely, I., van Vugt, M.A., Smits, V.A.J., Semple, J.I., Lemmens, B., Perrakis, A., Medema, R.H., Freire, R. (2006): Polo-like kinase-1 controls proteasome-dependent degradation of Claspin during checkpoint recovery. Curr. Biol. 16: 1950–1955.

Manke, I.A., Nguyen, A., Lim, D., Stewart, M.Q., Elia, A.E.H., Yaffe, M.B. (2005): MAPKAP kinase-2 is a cell cycle checkpoint kinase that regulates the G2/M transition and S phase progression in response to UV irradiation. Mol. Cell 17: 37–48.

Maya, R., Balass, M., Kim, S.T., Shkedy, D., Leal, J.F., Shifman, O., Moas, M., Buschmann, T., Ronai, Z., Shiloh, Y., Kastan, M.B., Katzir, E., Oren, M. (2001): ATM-dependent phosphorylation of Mdm2 on serine 395: role in p53 activation by DNA damage. Genes Dev. 15: 1067–1077.

McKenzie, L., King, S., Marcar, L., Nicol, S., Dias, S.S., Schumm, K., Robertson, P., Bourdon, J.C., Perkins, N., Fuller-Pace, F., Meek, D.W. (2010): p53-dependent repression of polo-like kinase-1 (PLK1). Cell Cycle 9: 4200–4212.

Medema, R.H., Macurek, L. (2011): Checkpoint recovery in cells: how a molecular understanding can help in the fight against cancer. F1000 Biol. Rep. 3: 10.

Meek, D.W. (2009): Tumour suppression by p53: a role for the DNA damage response? Nat. Rev. Cancer 9: 714–723.

Melander, F., Bekker-Jensen, S., Falck, J., Bartek, J., Mailand, N., Lukas, J. (2008): Phosphorylation of SDT repeats in the MDC1 N terminus triggers retention of NBS1 at the DNA damage-modified chromatin. J. Cell Biol. 181: 213–226.

Melixetian, M., Klein, D.K., Sørensen, C.S., Helin, K. (2009): NEK11 regulates CDC25A degradation and the IR-induced G2/M checkpoint. Nat. Cell Biol. 11: 1247–1253.

Meulmeester, E., Maurice, M.M., Boutell, C., Teunisse, A.F.A.S., Ovaa, H., Abraham, T.E., Dirks, R.W., Jochemsen, A.G. (2005): Loss of HAUSP-mediated deubiquitination contributes to DNA damage-induced destabilization of Hdmx and Hdm2. Mol. Cell 18: 565–576.

Molinari, M., Mercurio, C., Dominguez, J., Goubin, F., Draetta, G.F. (2000): Human Cdc25 A inactivation in response to S phase inhibition and its role in preventing premature mitosis. EMBO Rep. 1: 71–79.

Momand, J., Zambetti, G.P., Olson, D.C., George, D., Levine, A.J. (1992): The mdm-2 oncogene product forms a complex with the p53 protein and inhibits p53-mediated transactivation. Cell 69: 1237–1245.

Nakamura, A., Sedelnikova, O.A., Redon, C., Pilch, D.R., Sinogeeva, N.I., Shroff, R., Lichten, M., Bonner, W.M. (2006): Techniques for gamma-H2AX detection. Methods Enzymol. 409: 236–250.

NCBI (2011): The National Center for Biotechnology Information advances science and health by providing access to biomedical and genomic information. http://www.ncbi.nlm.nih.gov.

Nelms, B.E., Maser, R.S., MacKay, J.F., Lagally, M.G., Petrini, J.H. (1998): In situ visualization of DNA double-strand break repair in human fibroblasts. Science 280: 590–592.

O'Connell, M.J., Raleigh, J.M., Verkade, H.M., Nurse, P. (1997): Chk1 is a wee1 kinase in the G2 DNA damage checkpoint inhibiting cdc2 by y15 phosphorylation. EMBO J. 16: 545–554.

O'Driscoll, M., Ruiz-Perez, V.L., Woods, C.G., Jeggo, P.A., Goodship, J.A. (2003): A splicing mutation affecting expression of ataxia-telangiectasia and Rad3-related protein (ATR) results in Seckel syndrome. Nat. Genet. 33: 497–501.

Pan, Y., Chen, J. (2003): MDM2 promotes ubiquitination and degradation of MDMX. Mol. Cell. Biol. 23: 5113–5121.

Park, H.K., Panneerselvam, J., Dudimah, F.D., Dong, G., Sebastian, S., Zhang, J., Fei, P. (2011): Wip1 contributes to cell homeostasis maintained by the steady-state level of Wtp53. Cell Cycle 10.

Pei, H., Zhang, L., Luo, K., Qin, Y., Chesi, M., Fei, F., Bergsagel, P.L., Wang, L., You, Z., Lou, Z. (2011): MMSET regulates histone H4K20 methylation and 53BP1 accumulation at DNA damage sites. Nature 470: 124–128.

Pellegrini, M., Celeste, A., Difilippantonio, S., Guo, R., Wang, W., Feigenbaum, L., Nussenzweig, A. (2006): Autophosphorylation at serine 1987 is dispensable for murine Atm activation in vivo. Nature 443: 222–225.

Peng, C.Y., Graves, P.R., Thoma, R.S., Wu, Z., Shaw, A.S., Piwnica-Worms, H. (1997): Mitotic and G2 checkpoint control: regulation of 14-3-3 protein binding by phosphorylation of Cdc25C on serine-216. Science 277: 1501–1505.

Perry, J.A., Kornbluth, S. (2007): Cdc25 and Wee1: analogous opposites? Cell Div 2: 12.

Peschiaroli, A., Dorrello, N.V., Guardavaccaro, D., Venere, M., Halazonetis, T., Sherman, N.E., Pagano, M. (2006): SCFbetaTrCP-mediated degradation of Claspin regulates recovery from the DNA replication checkpoint response. Mol. Cell 23: 319–329.

Pines, J., Rieder, C.L. (2001): Re-staging mitosis: a contemporary view of mitotic progression. Nat. Cell Biol. 3: E3–E6.

Raman, M., Earnest, S., Zhang, K., Zhao, Y., Cobb, M.H. (2007): TAO kinases mediate activation of p38 in response to DNA damage. EMBO J. 26: 2005–2014.

Rasband, W. (1997-2011.): ImageJ. http://imagej.nih.gov/ij/.

Reference.MD (2011): Medical information from National Library of Medicine 2007 Medical Subject Headings, National Institutes of Health Unified Medical Language System, Drugs@FDA, Federal Drug Administration Adverse Event Reporting System. http://www.reference.md.

Reinhardt, H.C., Aslanian, A.S., Lees, J.A., Yaffe, M.B. (2007): p53-deficient cells rely on ATM- and ATR-mediated checkpoint signaling through the p38MAPK/MK2 pathway for survival after DNA damage. Cancer Cell 11: 175–189.

Reinhardt, H.C., Hasskamp, P., Schmedding, I., Morandell, S., van Vugt, M.A.T.M., Wang, X., Linding, R., Ong, S.E., Weaver, D., Carr, S.A., Yaffe, M.B. (2010): DNA damage activates a spatially distinct late cytoplasmic cell-cycle checkpoint network controlled by MK2-mediated RNA stabilization. Mol. Cell 40: 34–49.

Reinhardt, H.C., Yaffe, M.B. (2009): Kinases that control the cell cycle in response to DNA damage: Chk1, Chk2, and MK2. Curr. Opin. Cell Biol. 21: 245–255.

Rieder, C.L., Salmon, E.D. (1998): The vertebrate cell kinetochore and its roles during mitosis. Trends Cell Biol. 8: 310–318.

Robles, S.J., Buehler, P.W., Negrusz, A., Adami, G.R. (1999): Permanent cell cycle arrest in asynchronously proliferating normal human fibroblasts treated with doxorubicin or etoposide but not camptothecin. Biochem. Pharmacol. 58: 675–685.

Ronai, Z. (2006): Balancing Mdm2 - a Daxx-HAUSP matter. Nat. Cell Biol. 8: 790–791.

Saito-Ohara, F., Imoto, I., Inoue, J., Hosoi, H., Nakagawara, A., Sugimoto, T., Inazawa, J. (2003): PPM1D is a potential target for 17q gain in neuroblastoma. Cancer Res. 63: 1876–1883.

Sanchez, Y., Wong, C., Thoma, R.S., Richman, R., Wu, Z., Piwnica-Worms, H., Elledge, S.J. (1997): Conservation of the Chk1 checkpoint pathway in mammals: linkage of DNA damage to Cdk regulation through Cdc25. Science 277: 1497–1501.

Sanchez-Prieto, R., Rojas, J.M., Taya, Y., Gutkind, J.S. (2000): A role for the p38 mitogen-acitvated protein kinase pathway in the transcriptional activation of p53 on genotoxic stress by chemotherapeutic agents. Cancer Res. 60: 2464–2472.

Sanders, S.L., Portoso, M., Mata, J., Bähler, J., Allshire, R.C., Kouzarides, T. (2004): Methylation of histone H4 lysine 20 controls recruitment of Crb2 to sites of DNA damage. Cell 119: 603–614.

Sartori, A.A., Lukas, C., Coates, J., Mistrik, M., Fu, S., Bartek, J., Baer, R., Lukas, J., Jackson, S.P. (2007): Human CtIP promotes DNA end resection. Nature 450: 509–514.

Schwartz, H.S. (1975): Dna breaks in p288 tumor cells in mice after treatment with daunorubicin and adriamycin. Res. Commun. Chem. Pathol. Pharmacol. 10: 51–64.

Schwarz, J.K., Lovly, C.M., Piwnica-Worms, H. (2003): Regulation of the Chk2 protein kinase by oligomerization-mediated cis- and trans-phosphorylation. Mol. Cancer Res. 1: 598–609.

Shieh, S.Y., Ahn, J., Tamai, K., Taya, Y., Prives, C. (2000): The human homologs of checkpoint kinases Chk1 and Cds1 (Chk2) phosphorylate p53 at multiple DNA damage-inducible sites. Genes Dev. 14: 289–300.

Shreeram, S., Demidov, O.N., Hee, W.K., Yamaguchi, H., Onishi, N., Kek, C., Timofeev, O.N., Dudgeon, C., Fornace, A.J., Anderson, C.W., Minami, Y., Appella, E., Bulavin, D.V. (2006): Wip1 phosphatase modulates ATM-dependent signaling pathways. Mol. Cell 23: 757–764.

Smith, A.J., Cawston, T.E., Hazleman, B.L. (1985): A rapid and reproducible method for the analysis of immune complexes using affinity chromatography and Western blotting. J. Immunol. Methods 84: 125–134.

Stiff, T., Walker, S.A., Cerosaletti, K., Goodarzi, A.A., Petermann, E., Concannon, P., O'Driscoll, M., Jeggo, P.A. (2006): ATR-dependent phosphorylation and activation of ATM in response to UV treatment or replication fork stalling. EMBO J. 25: 5775–5782.

Stommel, J.M., Wahl, G.M. (2004): Accelerated MDM2 auto-degradation induced by DNA-damage kinases is required for p53 activation. EMBO J. 23: 1547–1556.

Sun, H., Liu, J., Zhang, J., Shen, W., Huang, H., Xu, C., Dai, H., Wu, J., Shi, Y. (2007): Solution structure of BRD7 bromodomain and its interaction with acetylated peptides from histone H3 and H4. Biochem. Biophys. Res. Commun. 358: 435–441.

Sun, Y., Jiang, X., Chen, S., Fernandes, N., Price, B.D. (2005): A role for the Tip60 histone acetyltransferase in the acetylation and activation of ATM. Proc. Natl. Acad. Sci. U. S. A. 102: 13182–13187.

Sun, Y., Jiang, X., Xu, Y., Ayrapetov, M.K., Moreau, L.A., Whetstine, J.R., Price, B.D. (2009): Histone H3 methylation links DNA damage detection to activation of the tumour suppressor Tip60. Nat. Cell Biol. 11: 1376–1382.

Suzuki, M., Boothman, D.A. (2008): Stress-induced premature senescence (SIPS)–influence of SIPS on radiotherapy. J. Radiat. Res. (Tokyo) 49: 105–112.

Sørensen, C.S., Syljuåsen, R.G., Falck, J., Schroeder, T., Rönnstrand, L., Khanna, K.K., Zhou, B.B., Bartek, J., Lukas, J. (2003): Chk1 regulates the S phase checkpoint by coupling the physiological turnover and ionizing radiation-induced accelerated proteolysis of Cdc25A. Cancer Cell 3: 247–258.

Takai, H., Naka, K., Okada, Y., Watanabe, M., Harada, N., Saito, S., Anderson, C.W., Appella, E., Nakanishi, M., Suzuki, H., Nagashima, K., Sawa, H., Ikeda, K., Motoyama, N. (2002): Chk2-deficient mice exhibit radioresistance and defective p53-mediated transcription. EMBO J. 21: 5195–5205.

Takekawa, M., Adachi, M., Nakahata, A., Nakayama, I., Itoh, F., Tsukuda, H., Taya, Y., Imai, K. (2000): p53-inducible wip1 phosphatase mediates a negative feedback regulation of p38 MAPK-p53 signaling in response to UV radiation. EMBO J. 19: 6517–6526.

Tang, J., Qu, L.K., Zhang, J., Wang, W., Michaelson, J.S., Degenhardt, Y.Y., El-Deiry, W.S., Yang, X. (2006): Critical role for Daxx in regulating Mdm2. Nat. Cell Biol. 8: 855–862.

ter Haar, E., Prabhakar, P., Prabakhar, P., Liu, X., Lepre, C. (2007): Crystal structure of the p38 alpha-MAPKAP kinase 2 heterodimer. J. Biol. Chem. 282: 9733–9739.

thesignalinggateway (2011): The UCSD Signaling Gateway. http://www.signaling-gateway.org/.

Thrower, J.S., Hoffman, L., Rechsteiner, M., Pickart, C.M. (2000): Recognition of the polyubiquitin proteolytic signal. EMBO J. 19: 94–102.

Tian, B., Yang, Q., Mao, Z. (2009): Phosphorylation of ATM by Cdk5 mediates DNA damage signalling and regulates neuronal death. Nat. Cell Biol. 11: 211–218.

Tibbetts, R.S., Brumbaugh, K.M., Williams, J.M., Sarkaria, J.N., Cliby, W.A., Shieh, S.Y., Taya, Y., Prives, C., Abraham, R.T. (1999): A role for ATR in the DNA damage-induced phosphorylation of p53. Genes Dev. 13: 152–157.

Toettcher, J.E., Mock, C., Batchelor, E., Loewer, A., Lahav, G. (2010): A synthetic-natural hybrid oscillator in human cells. Proc. Natl. Acad. Sci. U. S. A. 107: 17047–17052.

Toyoshima-Morimoto, F., Taniguchi, E., Nishida, E. (2002): Plk1 promotes nuclear translocation of human Cdc25C during prophase. EMBO Rep. 3: 341–348.

Tsai, A.G., Lieber, M.R. (2010): Mechanisms of chromosomal rearrangement in the human genome. BMC Genomics 11 Suppl 1: S1.

Uchida, S., Watanabe, N., Kudo, Y., Yoshioka, K., Matsunaga, T., Ishizaka, Y., Nakagama, H., Poon, R.Y.C., Yamashita, K. (2011): SCF(beta)TrCP mediates stress-activated MAPK-induced Cdc25B degradation. J. Cell Sci. 124: 2816–2825.

Uetake, Y., Sluder, G. (2010): Prolonged prometaphase blocks daughter cell proliferation despite normal completion of mitosis. Curr. Biol. 20: 1666–1671.

UniProt (2011): UniProt: the Universal Protein Resource. www.uniprot.org.

van Vugt, M.A.T.M., Gardino, A.K., Linding, R., Ostheimer, G.J., Reinhardt, H.C., Ong, S.E., Tan, C.S., Miao, H., Keezer, S.M., Li, J., Pawson, T., Lewis, T.A., Carr, S.A., Smerdon, S.J., Brummelkamp, T.R., Yaffe, M.B. (2010): A mitotic phosphorylation feedback network connects Cdk1, Plk1, 53BP1, and Chk2 to inactivate the G(2)/M DNA damage checkpoint. PLoS Biol. 8: e1000287.

Vassilev, L.T. (2006): Cell cycle synchronization at the G2/M phase border by reversible inhibition of CDK1. Cell Cycle 5: 2555–2556.

Verkerk, A.J., Pieretti, M., Sutcliffe, J.S., Fu, Y.H., Kuhl, D.P., Pizzuti, A., Reiner, O., Richards, S., Victoria, M.F., Zhang, F.P. (1991): Identification of a gene (FMR-1) containing a CGG repeat coincident with a breakpoint cluster region exhibiting length variation in fragile X syndrome. Cell 65: 905–914.

von Zglinicki, T., Saretzki, G., Ladhoff, J., d'Adda di Fagagna, F., Jackson, S.P. (2005): Human cell senescence as a DNA damage response. Mech. Ageing Dev. 126: 111–117.

Wang, B., Matsuoka, S., Ballif, B.A., Zhang, D., Smogorzewska, A., Gygi, S.P., Elledge, S.J. (2007): Abraxas and RAP80 form a BRCA1 protein complex required for the DNA damage response. Science 316: 1194–1198.

Wang, J., Gong, Z., Chen, J. (2011): MDC1 collaborates with TopBP1 in DNA replication checkpoint control. J. Cell Biol. 193: 267–273.

Wang, X., Zou, L., Lu, T., Bao, S., Hurov, K.E., Hittelman, W.N., Elledge, S.J., Li, L. (2006): Rad17 phosphorylation is required for claspin recruitment and Chk1 activation in response to replication stress. Mol. Cell 23: 331–341.

Ward, I.M., Chen, J. (2001): Histone H2AX is phosphorylated in an ATR-dependent manner in response to replicational stress. J. Biol. Chem. 276: 47759–47762.

Watanabe, N., Arai, H., Nishihara, Y., Taniguchi, M., Watanabe, N., Hunter, T., Osada, H. (2004): M-phase kinases induce phospho-dependent ubiquitination of somatic Wee1 by SCFbeta-TrCP. Proc. Natl. Acad. Sci. U. S. A. 101: 4419–4424.

White, A., Pargellis, C.A., Studts, J.M., Werneburg, B.G., Farmer, B.T. (2007): Molecular basis of MAPK-activated protein kinase 2:p38 assembly. Proc. Natl. Acad. Sci. U. S. A. 104: 6353–6358.

Wold, M.S. (1997): Replication protein A: a heterotrimeric, single-stranded DNA-binding protein required for eukaryotic DNA metabolism. Annu. Rev. Biochem. 66: 61–92.

Xia, Y., Yang, Q., Gong, X., Ye, F., Liou, Y.C. (2011): Dose-dependent mutual regulation between Wip1 and p53 following UVC irradiation. Int. J. Biochem. Cell Biol. 43: 535–544.

Xiao, A., Li, H., Shechter, D., Ahn, S.H., Fabrizio, L.A., Erdjument-Bromage, H., Ishibe-Murakami, S., Wang, B., Tempst, P., Hofmann, K., Patel, D.J., Elledge, S.J., Allis, C.D. (2009): WSTF regulates the H2A.X DNA damage response via a novel tyrosine kinase activity. Nature 457: 57–62.

Yamaguchi, H., Durell, S.R., Chatterjee, D.K., Anderson, C.W., Appella, E. (2007): The Wip1 phosphatase PPM1D dephosphorylates SQ/TQ motifs in checkpoint substrates phosphorylated by PI3K-like kinases. Biochemistry (Mosc.) 46: 12594–12603.

Yang, J., Yu, Y., Hamrick, H.E., Duerksen-Hughes, P.J. (2003): ATM, ATR and DNA-PK: initiators of the cellular genotoxic stress responses. Carcinogenesis 24: 1571–1580.

Yoda, A., Xu, X.Z., Onishi, N., Toyoshima, K., Fujimoto, H., Kato, N., Oishi, I., Kondo, T., Minami, Y. (2006): Intrinsic kinase activity and SQ/TQ domain of Chk2 kinase as well as N-terminal domain of Wip1 phosphatase are required for regulation of Chk2 by Wip1. J. Biol. Chem. 281: 24847–24862.

Yong, W., Bao, S., Chen, H., Li, D., Sánchez, E.R., Shou, W. (2007): Mice lacking protein phosphatase 5 are defective in ataxia telangiectasia mutated (ATM)-mediated cell cycle arrest. J. Biol. Chem. 282: 14690–14694.

Yu, S., Mangelsdorf, M., Hewett, D., Hobson, L., Baker, E., Eyre, H.J., Lapsys, N., Paslier, D.L., Doggett, N.A., Sutherland, G.R., Richards, R.I. (1997): Human chromosomal fragile site FRA16B is an amplified at-rich minisatellite repeat. Cell 88: 367–374.

Zhang, X., Lin, L., Guo, H., Yang, J., Jones, S.N., Jochemsen, A., Lu, X. (2009): Phosphorylation and degradation of Mdmx is inhibited by Wip1 phosphatase in the DNA damage response. Cancer Res. 69: 7960–7968.

Zlotorynski, E., Rahat, A., Skaug, J., Ben-Porat, N., Ozeri, E., Hershberg, R., Levi, A., Scherer, S.W., Margalit, H., Kerem, B. (2003): Molecular basis for expression of common and rare fragile sites. Mol. Cell. Biol. 23: 7143–7151.

Zou, L., Cortez, D., Elledge, S.J. (2002): Regulation of ATR substrate selection by Rad17-dependent loading of Rad9 complexes onto chromatin. Genes Dev. 16: 198–208.

Zou, L., Elledge, S.J. (2003): Sensing DNA damage through ATRIP recognition of RPA-ssDNA complexes. Science 300: 1542–1548.